

Adaptive Bitrate Streaming Over Cellular Networks: Rate Adaptation and Data Savings Strategies

Yanyuan Qin, Ph.D.

University of Connecticut, 2021

ABSTRACT

Adaptive bitrate streaming (ABR) has become the *de facto* technique for video streaming over the Internet. Despite a flurry of techniques, achieving high quality ABR streaming over cellular networks remains a tremendous challenge. First, the design of an ABR scheme needs to balance conflicting Quality of Experience (QoE) metrics such as video quality, quality changes, stalls and startup performance, which is even harder under highly dynamic bandwidth in cellular network. Second, streaming providers have been moving towards using Variable Bitrate (VBR) encodings for the video content, which introduces new challenges for ABR streaming, whose nature and implications are little understood. Third, mobile video streaming consumes a lot of data. Although many video and network providers currently offer data saving options, the existing practices are suboptimal in QoE and resource usage. Last, when the audio and video tracks are stored separately, video and audio rate adaptation needs to be dynamically coordinated to achieve good overall streaming experience, which presents interesting challenges while, somewhat surprisingly, has received little attention by the research community. In this dissertation, we tackle each of the above four challenges.

Firstly, we design a framework called PIA (PID-control based ABR streaming) that strategically leverages PID control concepts and novel approaches to account for the various requirements of ABR streaming. The evaluation results demonstrate that

PIA outperforms state-of-the-art schemes in providing high average bitrate with significantly lower bitrate changes and stalls, while incurring very small runtime overhead. We further design PIA-E (PIA Enhanced), which improves the performance of PIA in the important initial playback phase.

Secondly, we identify distinguishing characteristics of VBR encodings that impact user QoE and should be factored in any ABR adaptation decision and find that traditional ABR adaptation strategies designed for the Constant Bitrate (CBR) encodings are not adequate for VBR. We develop novel best practice design principles to guide ABR rate adaptation for VBR encodings. As a proof of concept, we design a novel and practical control-theoretic rate adaptation scheme, CAVA (Control-theoretic Adaption for VBR-based ABR streaming), incorporating these concepts. Extensive evaluations show that CAVA substantially outperforms existing state-of-the-art adaptation techniques.

Thirdly, we analyze the underlying causes for suboptimal existing data saving practices and propose novel approaches to achieve better tradeoffs between video quality and data usage. The first approach is Chunk-Based Filtering (CBF), which can be retrofitted to any existing ABR scheme. The second approach is Quality-Aware Data-efficient streaming (QUAD), a holistic rate adaptation algorithm that is designed ground up. Our evaluations demonstrate that compared to the state of the art, the two proposed schemes achieve consistent video quality that is much closer to the user-specified target, lead to far more efficient data usage, and incur lower stalls.

For the fourth challenge, we shed light on a number of limitations in existing practices both in the protocols and the player implementations, which can cause undesirable behaviors such as stalls, selection of potentially undesirable combinations such as very low quality video with very high quality audio, etc. Based on our gained insights, we identify the underlying root causes of these issues, and propose a number of practical design best practices and principles whose collective adoption will help avoid these issues and lead to better QoE.

Adaptive Bitrate Streaming Over Cellular Networks: Rate Adaptation and Data Savings Strategies

Yanyuan Qin

M.S. University of Connecticut, 2019

M.E. Shanghai Jiao Tong University, 2014

B.E. Nanjing University of Aeronautics and Astronautics, 2011

A Dissertation

Submitted in Partial Fulfillment of the

Requirements for the Degree of

Doctor of Philosophy

at the

University of Connecticut

2021

Copyright by

Yanyuan Qin

2021

APPROVAL PAGE

Doctor of Philosophy Dissertation

Adaptive Bitrate Streaming Over Cellular Networks: Rate Adaptation and Data Savings Strategies

Presented by

Yanyuan Qin, B.E., M.E.

| | |
|-------------------|----------------------|
| Major Advisor | _____ |
| | Bing Wang |
| Associate Advisor | _____ |
| | Krishna R. Pattipati |
| Associate Advisor | _____ |
| | Song Han |
| Associate Advisor | _____ |
| | Subhabrata Sen |

University of Connecticut

2021

ACKNOWLEDGMENTS

I would like to express my gratitude and appreciation for my major advisor, Professor Bing Wang, whose guidance, support and encouragement has been invaluable throughout this study. I feel extremely lucky being a member of the team, and having her as a constant source of courage and wisdom. Her sharp insight and concise description of complicated research problems and her dedication have set an example of academic perfection, from which I will continue to benefit in my future career.

I would like to thank Dr. Shubho Sen and Dr. Shuai Hao from AT&T Lab Research, Professor Krishna R. Pattipati from ECE department of UCONN, Professor Feng Qian from University of Minnesota-Twin City, for their guidance on my researches.

I would also like to thank, Professor Alexander Russel, Professor Peng Zhang, Professor Song Han, Professor Wei Wei, Professor Suining He, Professor Mohammad Maifi Hasan Khan, Professor Fei Miao and Professor Peter B. Luh for their advice and broad knowledge. It was my great pleasure working with such intelligent and responsible professors.

I would like to extend my gratitude to my colleagues, Ruofan Jin, Yuexin Mao, Levon Nazaryan, Sixia Chen, Lingyu Ren, Yan Li, Bing Yan, Reynaldo Morillo, Chaogun Yue, Shweta Ware, Chinmaey Shende, Cheojin Park, Zefan Tang, Wenfeng Wan, Jiangwei Wang and Lizhi Wang for their discussions and comments in my research. My thanks also go to all my friends for their endless support whenever I needed. Last but not least, I give my deepest gratitude and love to my parents, who have been a constant source of happiness and motivation for me.

TABLE OF CONTENTS

| | |
|--|--------|
| 1. Introduction | 1 |
| 1.1 ABR streaming | 1 |
| 1.2 ABR streaming for VBR encodings | 3 |
| 1.3 Data Usage for ABR Streaming | 4 |
| 1.4 ABR Streaming with Separate Audio and Video Tracks | 6 |
| 1.5 Contribution of This Dissertation | 8 |
| 1.6 Dissertation Roadmap | 10 |
| 2. A Control Theoretic Approach to ABR Video Streaming: A Fresh Look at PID-based Rate Adaptation | 11 |
| 2.1 Introduction | 11 |
| 2.2 Motivation and Background | 13 |
| 2.2.1 ABR streaming as a control problem | 14 |
| 2.2.2 PID control | 16 |
| 2.3 Adapting PID Control for ABR Streaming | 18 |
| 2.3.1 PIA core component | 18 |
| 2.3.2 PIA performance enhancing techniques | 21 |
| 2.3.3 PIA parameter tuning | 24 |
| 2.3.4 Putting it all together | 24 |
| 2.4 Performance Evaluation | 25 |
| 2.4.1 Evaluation setup | 25 |
| 2.4.2 PIA: Choice of parameters | 28 |
| 2.4.3 Performance comparison | 32 |
| 2.4.4 Computational overhead | 39 |
| 2.5 Improving Startup Performance | 40 |
| 2.6 Evaluation using DASH Implementation | 42 |
| 2.7 Conclusion and Future work | 46 |

| | |
|--|-----------|
| 3. ABR Streaming of VBR-encoded Videos: Characterization, Challenges, and Solutions | 47 |
| 3.1 Introduction | 47 |
| 3.2 The VBR Video Dataset | 50 |
| 3.3 VBR Streaming: Challenges | 52 |
| 3.3.1 VBR Video Characteristics | 53 |
| 3.3.2 Implications for Rate Adaptation | 56 |
| 3.3.3 VBR with Larger Cap | 57 |
| 3.4 Design Principles | 58 |
| 3.5 CAVA Design and Implementation | 61 |
| 3.5.1 Overview of CAVA | 61 |
| 3.5.2 PID Feedback Control Block | 62 |
| 3.5.3 The Inner Controller | 63 |
| 3.5.4 The Outer Controller | 67 |
| 3.5.5 Implementation | 68 |
| 3.6 Performance Evaluation | 69 |
| 3.6.1 Evaluation Setup | 69 |
| 3.6.2 Choice of Parameters for CAVA | 73 |
| 3.6.3 Comparison with Other Schemes | 75 |
| 3.6.4 Impact of CAVA Design Principles | 77 |
| 3.6.5 Codec Impact | 79 |
| 3.6.6 Impact of Higher Bitrate Variability | 80 |
| 3.6.7 Impact of Bandwidth Prediction Error | 80 |
| 3.6.8 DASH Implementation Results | 81 |
| 3.7 Related Work | 82 |
| 3.8 Conclusions and Future Work | 84 |

| | |
|---|-----------|
| 4. Quality-aware Strategies for Optimizing ABR Video Streaming QoE and Reducing Data Usage | 85 |
| 4.1 Introduction | 85 |
| 4.2 Quality and Bitrate Tradeoffs | 88 |
| 4.2.1 Video Dataset | 88 |
| 4.2.2 Video Quality Metrics | 90 |
| 4.2.3 Perceptual Quality vs. Encoding Bitrate | 91 |
| 4.3 Reducing Data Usage | 93 |
| 4.3.1 Current Data Saving Practices | 94 |
| 4.3.2 Quality-aware Data Saving | 95 |
| 4.4 Chunk-based Filtering (CBF) | 96 |
| 4.4.1 CBF Approach | 96 |
| 4.4.2 CBF vs. TBF | 97 |
| 4.4.3 Deployment Scenarios | 98 |
| 4.5 Grounds-up Design: QUAD | 100 |
| 4.6 Implementation & Evaluation Setup | 104 |
| 4.7 Evaluation Existing ABR Schemes Enhanced with CBF | 107 |
| 4.7.1 Benefits of CBF | 107 |
| 4.7.2 CBF vs. Network Bandwidth Cap | 109 |
| 4.7.3 CBF vs. TBF | 111 |
| 4.8 Evaluation of QUAD | 112 |
| 4.8.1 QUAD vs. CBF | 112 |
| 4.8.2 dash.js based Evaluation | 113 |
| 4.8.3 ExoPlayer based Evaluation | 115 |
| 4.8.4 In-the-wild Tests | 117 |
| 4.9 Related work | 118 |
| 4.10 Summary | 119 |

| | |
|---|-----|
| 5. ABR Streaming with Separate Audio and Video Tracks: Measurements and Best Practices | 121 |
| 5.1 Introduction | 121 |
| 5.2 Motivation and Methodology | 122 |
| 5.2.1 Motivation | 122 |
| 5.2.2 High-level Methodology | 123 |
| 5.2.3 ABR Streaming Protocols | 124 |
| 5.2.4 Players | 125 |
| 5.3 Practice of Popular Players | 125 |
| 5.3.1 Experimental Setup | 125 |
| 5.3.2 ExoPlayer | 127 |
| 5.3.3 Shaka Player | 131 |
| 5.3.4 dash.js Player | 133 |
| 5.3.5 Summary of Findings | 133 |
| 5.4 Suggested Best Practices | 135 |
| 5.4.1 Server Side Manifest Specifications | 135 |
| 5.4.2 Player Side ABR Logic | 136 |
| 5.5 Summary | 137 |
| 6. Conclusion and Future Work | 140 |
| 7. List of Publications during My PhD Study | 142 |
| Bibliography | 147 |

LIST OF FIGURES

| | | |
|------|--|----|
| 1.1 | ABR streaming of demuxed audio and video (the different colors represent the chunks from different tracks). | 7 |
| 2.1 | ABR streaming based on open-loop control (a) and closed-loop control (b). | 15 |
| 2.2 | PIA main components. | 18 |
| 2.3 | Characteristics of the network bandwidth traces that are used in performance evaluation. | 26 |
| 2.4 | Region of K_p and K_i and the corresponding “heat” values in one setting (video bitrate set \mathcal{R}_3 , chunk duration 2 s, video length 20 min, startup latency 10 s, $\mu = 1$, $\lambda = 8.5$ (which is the same as the maximum bitrate (in Mbps) in \mathcal{R}_3). | 29 |
| 2.5 | Choosing β in PIA. In (b), the setting is the same as that used for Fig. 2.4. | 31 |
| 2.6 | Performance comparison in the default setting (chunk duration 2 s, video bitrate set \mathcal{R}_2 , video length 20 minutes, startup latency 10 s). | 32 |
| 2.7 | Comparison of different schemes for one trace under the default setting (chunk duration 2 s, video bitrate set \mathcal{R}_2 , video length 20 minutes, startup latency 10 s). The plot on buffer level shows the results until the end of the downloading. | 34 |
| 2.8 | Impact of the target buffer level on performance (video bitrate set \mathcal{R}_2 , chunk duration 2 s, video length 20 minutes, startup latency 10 s). | 35 |
| 2.9 | The distribution of buffer occupancy of PIA (under the default setting, i.e., chunk duration 2 s, video bitrate set \mathcal{R}_2 , video length 20 minutes, startup latency 10 s). | 38 |
| 2.10 | Impact of the maximum buffer size on the bitrate adaptation of PIA (under the default setting, i.e., chunk duration 2 s, video bitrate set \mathcal{R}_2 , video length 20 minutes, startup latency 10 s). | 38 |

| | | |
|------|--|----|
| 2.11 | An example that illustrates the impact of the maximum buffer size on the bitrate choice of PIA (under the default setting, i.e., chunk duration 2 s, video bitrate set \mathcal{R}_2 , video length 20 minutes, startup latency 10 s). . . . | 39 |
| 2.12 | Performance of PIA-E versus other schemes (chunk duration 2 s, video bitrate set \mathcal{R}_2 , startup latency 10 s). | 40 |
| 2.13 | Performance comparison in DASH (music show, chunk duration 2 s, video length 15 minutes, startup latency 10 s). | 43 |
| 2.14 | Performance comparison in DASH (BBB, chunk duration 5 s, video length 10 minutes, startup latency 10 s). | 44 |
| 3.1 | Bitrate of the chunks of a VBR video (Elephant Dream, H.264, YouTube encoded). | 52 |
| 3.2 | Chunk SI & TI (Elephant Dream, Track 3). | 54 |
| 3.3 | Quality of chunks in a VBR video (Elephant Dream, YouTube encoded, H.264). | 56 |
| 3.4 | Two myopic schemes and CAVA. | 59 |
| 3.5 | CAVA design diagram. | 61 |
| 3.6 | Illustration of (a) track selection, and (b) setting target buffer level. | 63 |
| 3.7 | Impact of inner controller window size. | 73 |
| 3.8 | Performance comparison for one video (Elephant Dream, FFmpeg encoded, H.264) under LTE traces. | 74 |
| 3.9 | Quality of Q1-Q3 chunks and all the chunks. | 76 |
| 3.10 | Impact of the design principles of CAVA. | 79 |
| 3.11 | Performance comparison in dash.js (Big Buck Bunny, YouTube encoded, H.264, LTE traces). | 79 |
| 4.1 | Quality vs. bitrate for one video (ED). | 91 |
| 4.2 | Quality vs. bitrate for track 4 (480p). | 92 |
| 4.3 | Illustration of CBF (ED, $Q_r = 80$). | 97 |

| | | |
|------|---|-----|
| 4.4 | CBF, TBF ⁻ , and TBF ⁺ (ED, $Q_r = 80$). | 97 |
| 4.5 | Illustration of CBF deployment. | 100 |
| 4.6 | Design diagram of QUAD. | 101 |
| 4.7 | Two existing ABR schemes with and without CBF (ED, YouTube encoded, target quality 80). | 108 |
| 4.8 | CBF versus capping network bandwidth (ED, YouTube encoded, target quality 80). | 109 |
| 4.9 | RobustMPC with CBF vs TBF (ToS, YouTube encoded, target quality 80). | 111 |
| 4.10 | QUAD vs. two existing schemes with CBF (ED, YouTube encoded, target quality 80). | 113 |
| 4.11 | QUAD vs. two existing schemes with CBF (ED, BBB, YouTube encoded, target quality 80). | 114 |
| 4.12 | QUAD vs. BOLA-E with and without CBF in dash.js (ED, YouTube encoded, target quality 80). | 115 |
| 4.13 | QUAD vs. Exo with and without CBF in ExoPlayer (ED, YouTube en- coded, target quality 80). | 116 |
| 5.1 | ExoPlayer results (DASH). | 129 |
| 5.2 | ExoPlayer results (HLS). | 130 |
| 5.3 | Shaka Player results (HLS). | 131 |
| 5.4 | dash.js results (DASH). | 134 |

LIST OF TABLES

| | | |
|-----|--|-----|
| 2.1 | Key notation. | 14 |
| 2.2 | Comparison of computational overhead. | 39 |
| 3.1 | Performance comparison (YouTube videos). | 77 |
| 3.2 | CAVA versus BOLA-E in dash.js. | 83 |
| 4.1 | Data saving options in Amazon Prime video. | 94 |
| 4.2 | RobustMPC vs. RobustMPC+CBF. | 110 |
| 4.3 | In-the-wild tests using ExoPlayer. | 117 |
| 5.1 | Video and audio of a YouTube drama show. | 126 |
| 5.2 | Bitrates of the full set of audio and video combinations (used in HLS manifest file H_{all}). | 138 |
| 5.3 | Bitrates of a subset of audio and video combinations (used in HLS manifest file H_{sub}). | 139 |

Chapter 1

Introduction

Video streaming has come to dominate mobile data consumption today. As per Cisco's Visual Network Index report [1], mobile video traffic now accounts for more than half of all mobile data traffic. Ensuring good viewing experience for this important application class is critical to content providers, content distribution networks, and mobile operators. Despite much effort, achieving good quality video streaming over cellular networks remains a tremendous challenge [2].

1.1 ABR streaming

Most video contents are currently streamed using Adaptive Bit-Rate (ABR) streaming over HTTP (specifically HLS [3] and DASH [4]), the *de facto* technology adopted by industry. In ABR streaming, a video is encoded into multiple resolutions/quality levels (or tracks). The encoding at each resolution/quality level is divided into equal-duration chunks, each containing data for a short interval's worth of playback (e.g., several seconds). A chunk at a higher resolutions/quality level requires more bits to encode, and is therefore larger in size. During playback, to fetch the content for a particular playpoint in the video, the video player dynamically determines what bitrate/quality chunk to download based on time-varying network conditions. The resulting playback involves showing different portions of the video using chunks selected from different tracks.

Various user engagement studies [5, 6, 7, 8] indicate that satisfactory ABR streaming needs to achieve three conflicting goals simultaneously: (1) maximize the playback

bitrate; (2) minimize the likelihood of stalls or rebuffering; and (3) minimize the variability of the selected video bitrates for a smooth viewing experience. Reaching any of the three goals alone is relatively easy – for instance, the player can simply stream at the highest bitrate to maximize the video quality; or it can stream at the lowest bitrate to minimize the stalls. The challenge lies in achieving all three goals simultaneously, especially over highly varying network conditions, typical of the last-mile scenarios in cellular networks.

Control theories have been applied to design the ABR algorithm. The studies [9, 10] directly use the standard PID controller, without adapting it to accommodate the special requirements of ABR streaming. The study in [11] shows that directly using PID control leads to worse performance than BOLA, while our proposed schemes (PIA and PIA-E) carefully adapt PID control for ABR streaming and outperform BOLA. The studies in [12, 13] conclude that PID control is not suitable for ABR streaming, and develop other control based approaches. MPC [13] uses another branch of control theory, model predictive control, to solve a QoE optimization problem. It, however, requires accurate future network bandwidth estimation and incurs significant computation overhead. BBA [14] selects video bitrates purely based on buffer occupancy. However, as we will discuss, BBA essentially uses a P-controller and does not consider the integral part, which affects its performance. BOLA [11] and an improved version BOLA-E [15] select the bitrate based on maximizing a utility function, considering both rebuffering and video quality. We showed in Section 2.6 that BOLA leads to significantly more rebuffering than our approach.

Another type of approach uses machine learning (e.g., reinforcement learning) to “learn” an ABR scheme from data. The study in [16] proposes a tabular Q-Learning based reinforcement learning approach for ABR streaming. This approach, however, does not scale to large state/action spaces. A more recent scheme, Pensieve [17], addresses the scalability issue using reinforcement learning based on neural networks. In [17], Pensieve is realized as a server-side ABR algorithm – the client feeds back

information to the server and the server makes the decisions on bitrate choices. For a given ABR algorithm, Oboe [18] pre-computes the best possible parameters for different network conditions and dynamically adapts these parameters at run-time. The study in [19] characterizes the VBR encoding characteristics, proposes design principles for VBR-based ABR streaming and a concrete scheme, CAVA, that instantiates these design principles.

Our study takes a fresh look at using PID control for ABR streaming and shows a somewhat surprising high-level finding: *by applying PID control in an explicit and adaptive manner, our ABR streaming algorithms substantially outperform the state-of-the-art video streaming schemes.* We will show that our proposed PIA [20, 21] scheme incurs much lower computational overhead and achieves a significantly better balance among the three performance metrics than MPC; PIA also outperforms RobustMPC [13] and BBA [14].

1.2 ABR streaming for VBR encodings

The video compression for a track can be (1) Constant Bitrate (CBR) – encodes the entire video at a relatively fixed bitrate, allocating the same bit budget to both *simple scenes* (i.e., low-motion or low-complexity scenes) and *complex scenes* (i.e., high-motion or high-complexity scenes), resulting in variable quality across scenes, or (2) Variable Bitrate (VBR) – encodes *simple scenes* with fewer bits and *complex scenes* with more bits, while maintaining a consistent quality throughout the track. VBR presents some key advantages over CBR [22], such as the ability to realize better video quality for the same average bitrate, or the same quality with a lower bitrate encoding than CBR. Traditionally, streaming services mainly deployed only CBR, partly due to various practical difficulties including the complex encoding pipelines for VBR, as well as the demanding storage, retrieval, and transport challenges posed by the multi-timescale bitrate burstiness of VBR videos. Most recently content providers have begun adopting VBR encoding [14, 23, 24, 25, 26], spurred by the promise of substantial

improvements in the quality-to-bits ratio compared to CBR, and by technological advancements in VBR encoding pipelines.

However, current commercial systems and ABR protocols do not fully make use of the characteristics of VBR videos; they typically assume a track's peak rate to be its bandwidth requirement when making rate adaptation decisions [24]. While content providers have recently begun adopting VBR encoding, their treatment to VBR videos is simplistic (e.g., by simply assuming that the bandwidth requirement of a chunk equals to the peak bitrate of the track) [24]. As we will see in §3.6.8, such simplistic treatment can lead to poor performance. Of the large number of existing studies, only a few targeted VBR videos [14, 27, 28]; most others were designed for and evaluated in the context of CBR encodings. While several schemes in the latter category can be applied for VBR videos by explicitly incorporating the actual bitrate of each chunk, they were not designed ground up to account for VBR characteristics, nor had their performance been evaluated for that case. We evaluate the performance of schemes from both categories (see §3.4 and §3.6), and show that they can suffer from a large amount of rebuffering and/or significant viewing quality impairments when used for VBR videos.

There exists little prior understanding of the issues and challenges involved in ABR streaming of VBR videos. Our study differs from all the above works in several important aspects, including developing insights based on analyzing content complexity, encoding quality, and encoding bitrates, identifying general design principles for VBR streaming, and developing a concrete, practical ABR scheme for VBR streaming that significantly outperforms the state-of-the-art schemes.

1.3 Data Usage for ABR Streaming

Video streaming is data intensive. An important question is how can we effectively reduce the bandwidth consumption for mobile video streaming while minimizing the impact on users' quality of experience (QoE)? This is a highly important and practical

research problem since cellular network bandwidth is a relatively scarce resource. The average data plan for a U.S. cellular customer is only 2.5 GB per month [29], while streaming just one-hour High Definition (HD) video on mobile Netflix can consume 3 GB data. Therefore, the capability to make more efficient use of data while still hitting quality targets is the key to enabling users to consume more content within their data budgets without adversely impacting QoE. In addition, downloading less data for a video session also translates to lower radio energy consumption, less thermal overhead on mobile devices, as well as potentially better QoE for other users sharing the same cellular RAN (radio access network) or base station.

Existing ABR adaptation schemes (§4.9) focus mainly on maximizing the video quality and user QoE. While some schemes do conservatively utilize the bandwidth, their decisions are primarily driven by QoE impairment concerns such as the possibility of stalls caused by the potentially inaccurate bandwidth estimation. For example, when selecting the next chunk, the default adaptation scheme in ExoPlayer [30] (a popular open-source player that is used in more than 10000 apps) only considers tracks whose declared bitrates are at least 25% lower than the estimated network bandwidth. Such a design saves data just by being conservative. As we show later, it can lead to significantly lower quality/QoE (§4.8.3). Existing ABR schemes do not explicitly consider bandwidth efficiency together with quality in making the track selection decisions.

Some mobile network operators and commercial video services provide users with certain “data saver” options. These options take either a service-based approach or a network-based approach. The former limits the highest level of quality/resolution/bitrate by, for example, streaming only standard definition (SD) content over cellular networks. A network-based approach instead limits the network bandwidth. We survey the “quality throttling” mechanisms used by today’s commercial video content providers for saving bandwidth for mobile devices, and pinpoint their inefficiencies (§4.2-§4.3). Despite their simplicity, we find such approaches often achieve tradeoffs between video quality and bandwidth usage that are far from what viewers desire. A key reason is that for

state-of-the-art encoders (e.g., H.264 [31], H.265 [32] and VP9 [33]), the actual perceived picture quality exhibits significant variability across different chunks within the same track, for both Constant Bitrate (CBR) and Variable Bitrate (VBR) encodings. Therefore, a data-saving approach that simply removes high tracks leads to quality variations. Such quality variability impairs user QoE, and makes suboptimal use of the network bandwidth.

1.4 ABR Streaming with Separate Audio and Video Tracks

On the server for Adaptive bitrate (ABR) streaming, a video track and its corresponding audio can be combined together as a single multiplexed track (in *muxed* mode), where each chunk in the track contains the associated video and audio content. Alternatively, the video and audio content can be maintained separately as demultiplexed tracks (in *demuxed* mode) on the server, as shown in Fig. 1.1. The demuxed approach offers a number of advantages for services that need to have more than one audio variant – e.g., to support multiple languages, or multiple audio quality levels or both. First, it requires significantly less storage at the origin server. To see this, consider a hypothetical service that uses M video and N audio tracks. The server only needs to store M video and N audio tracks for the demuxed mode, while it has to store a much larger set of $M \times N$ muxed tracks for the muxed mode. Second, *a subtle effect is that* the demuxed mode increases CDN cache hits. As an example, for a given chunk/playback position, suppose user A requests video track variant $V1$ and audio track variant $A2$, and at a later time, user B requests the same video track variant $V1$ and a different audio track variant $A1$. In muxed mode, B needs to download both $V1$ and $A1$ from the original server, while in demuxed mode, B can get the video chunk for $V1$ from the CDN cache (which cached it due to A 's earlier request), and only needs to get the audio chunk for $A1$ from the original server. Due to the above advantages, services are increasingly moving towards using demuxed audio and video tracks [24]. We focus on ABR streaming for demuxed video and audio tracks in this work.

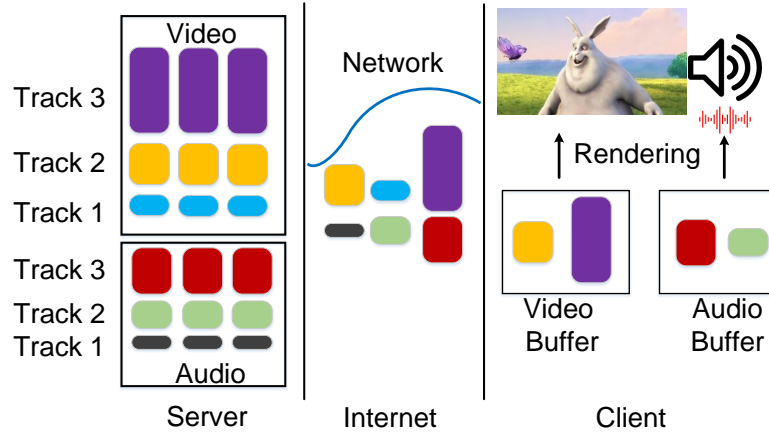


Fig. 1.1: ABR streaming of demuxed audio and video (the different colors represent the chunks from different tracks).

The literature on video rate adaptation is extensive [11, 13, 14, 34, 35, 36]. A common assumption regarding audio is that its bitrate is significantly lower than that of the video, and hence the decision on audio track selection has little impact on the video track selection [37]. The reality, however, is that increasingly an audio track can be of similar or even much higher bitrate than some of the video tracks. Based on the HLS authoring specification for Apple devices [38], the audio bitrate can be as high 384 Kbps for mobile devices, which can be much higher than the typical encoding bitrates of lower-rung video tracks in real services (e.g., the two lowest video tracks have peak rates around 100 and 250 Kbps respectively for one popular service). In addition, more and more devices support Dolby Atmos audio [39], for which the audio bitrate can be up to 768 Kbps [40]. As a result, audio can in reality consume a significant fraction of the available network bandwidth, and audio track selection can therefore significantly affect video selection and the overall viewing experience (see §5.3). Concurrently with the availability of higher bitrate audio tracks, the community has also realized the importance of selecting higher audio quality tracks when possible and appropriate. For example, Netflix very recently adopted audio adaptation at the player side to boost the overall video streaming experience [40, 41].

Little is known on how best to mesh together audio and video rate adaptation in ABR streaming. In fact, meshing together audio and video rate adaptation is a very challenging problem – it involves many pieces (in ABR protocols, server and player designs) and needs a holistic solution [42].

1.5 Contribution of This Dissertation

The contributions of this dissertation are as follows.

- we take a fresh look at PID-based control for ABR streaming. We design a framework called PIA (PID-control based ABR streaming) that strategically leverages PID control concepts and incorporates several novel strategies to account for the various requirements of ABR streaming. We evaluate PIA using simulation based on real LTE network traces [43], as well as using real DASH implementation. The results demonstrate that PIA outperforms state-of-the-art schemes in providing high average bitrate with significantly lower bitrate changes (reduction up to 40%) and stalls (reduction up to 85%), while incurring very small runtime overhead. We further design PIA-E (PIA Enhanced), which improves the performance of PIA in the important initial playback phase.
- We explore ABR streaming for VBR encodings across diverse video genres, encoding technologies, and platforms. We identify distinguishing characteristics of VBR encodings that impact user QoE and should be factored in any ABR adaptation decision. Traditional ABR adaptation strategies designed for the CBR case are not adequate for VBR. We develop novel best practice design principles to guide ABR rate adaptation for VBR encodings. As a proof of concept, we design a novel and practical control-theoretic rate adaptation scheme, CAVA (Control-theoretic Adaption for VBR-based ABR streaming), incorporating these concepts. Extensive evaluations show that CAVA substantially outperforms existing state-of-the-art adaptation techniques, validating the importance of these

design principles.

- Our study shows that existing data saving practices for Adaptive Bitrate (ABR) videos are suboptimal: they often lead to highly variable video quality and do not make the most effective use of the network bandwidth [44]. We identify underlying causes for this and propose two novel approaches to achieve better tradeoffs between video quality and data usage. The first approach is Chunk-Based Filtering (CBF), which can be retrofitted to any existing ABR scheme. The second approach is QQuality-Aware Data-efficient streaming (QUAD), a holistic rate adaptation algorithm that is designed ground up. We implement and integrate our solutions into two video player platforms (`dash.js` and ExoPlayer), and conduct thorough evaluations over emulated/commercial cellular networks using real videos. Our evaluations demonstrate that compared to the state of the art, the two proposed schemes achieve consistent video quality that is much closer to the user-specified target, lead to far more efficient data usage, and incur lower stalls.
- We examine the state of the art in the handling of demuxed audio and video tracks in predominant ABR protocols (DASH and HLS), as well as in real ABR client implementations in three popular players covering both browsers and mobile platforms. Combining experimental insights with code analysis, we shed light on a number of limitations in existing practices both in the protocols and the player implementations, which can cause undesirable behaviors such as stalls, selection of potentially undesirable combinations such as very low quality video with very high quality audio, etc. Based on our gained insights, we identify the underlying root causes of these issues, and propose a number of practical design best practices and principles whose collective adoption will help avoid these issues and lead to better QoE [42].

1.6 Dissertation Roadmap

The remainder of this dissertation is organized as follows.

In Chapter 2, we take a fresh look at PID-based bit rate adaptation and design novel ABR scheme that judiciously combines PID control and domain knowledge of ABR streaming. In Chapter 3, we first characterize VBR encodings and develop design principles. Then we design novel ABR scheme for VBR videos using the principles. In Chapter 4, quality-aware data saving strategies are designed, which provide data savings while allowing users' direct control of the video quality. In Chapter 5, we investigate the predominant ABR protocols and popular players and propose best practices for ABR Streaming with separate audio and video tracks. We draw the conclusion and highlight the future work in Chapter 6.

Chapter 2

A Control Theoretic Approach to ABR Video Streaming: A Fresh Look at PID-based Rate Adaptation

2.1 Introduction

Rate adaptation for ABR streaming can be naturally modeled as a control problem: the video player monitors the past network bandwidth and the amount of content in the playback buffer to decide the bitrate level for the current chunk; the decision will then affect the buffer level, which can be treated as feedback to adjust the decision for the next chunk. PID (named after its three correcting terms, namely “proportional”, “integral”, and “derivative” terms) is one of the most widely used feedback control techniques in practice [45]. It is conceptually easy to understand and computationally simple. There has been initial work on using PID control theory for ABR streaming. Specifically, the studies in [9, 10] directly apply the standard PID controller to ABR streaming with no modifications, which was shown to lead to significantly suboptimal performance [11]. The studies [12, 13] conclude that PID control is not suitable for ABR streaming.

In this section, we adopt a contrarian perspective and take a fresh look at the potential of PID control for ABR video streaming. We start by pointing out that a recent heuristic technique, BBA [14], can be shown to be, in effect, using a simplified form of PID control. We then conduct an in-depth study that explores using PID control for ABR streaming. Specifically, we design *PIA* (PID-control based ABR streaming),

a novel control-theoretic video streaming scheme that strategically incorporates PID control concepts and domain knowledge of ABR streaming. Our main contributions include the following.

- We take a fresh look at PID-based control for ABR streaming, and strategically leverage PID control concepts as the base framework for PIA. Specifically, the *core controller* in PIA differs from those in [9, 10] in that we define a control policy that makes the closed-loop control system linear, and easy to control and analyze. The core controller maintains the playback buffer to a target level, so as to reduce rebuffering.
- We add domain-specific enhancements to further improve the robustness and adaptiveness of ABR streaming. Specifically, PIA addresses two key additional requirements of ABR streaming, i.e., maximizing playback bitrate and reducing frequent bitrate changes. It also incorporates strategies to accelerate initial ramp-up and protect the system from saturation. We further develop *PIA-E* (PIA Enhanced) that improves the performance of PIA in the important initial playback phase, by dynamically adjusting the parameters used in the control loop.
- We explore parameter tuning. Specifically, the proportional gain K_p and the integral gain K_i are the two fundamental and most critical parameters that guide the PIA controller’s behavior. We develop a methodology that systematically examines a wide spectrum of network conditions and parameter settings to derive their (K_p, K_i) configurations that yield satisfactory quality of experience (QoE). Our results demonstrate that a common set of (K_p, K_i) values exist that have good performance across a wide range of network settings, indicating our schemes can be easily deployed in practice.

We conduct comprehensive evaluations of PIA using a large number of real cellular network traces with diverse network variability characteristics. The traces were

collected from two commercial LTE networks at diverse geographic locations, with a range of mobility conditions. Our key findings include the following.

- PIA achieves comparable bitrates as two state-of-the-art schemes, BBA [14] and MPC [13], while substantially reducing bitrate changes (49% and 40% lower, respectively) and rebuffering time (68% and 85% lower, respectively). Overall, PIA achieves the best balance among the three QoE metrics. Compared to PIA, the enhanced version, PIA-E, achieves higher bitrate for the beginning part of the video; for the entire video, PIA-E has similar rebuffering, average bitrate and bitrate changes as PIA.
- PIA and PIA-E have low computation overhead (e.g., comparable to BBA and only 0.5% of MPC based on our simulations). Our emulation results also show that their execution time is less than 2 seconds for a 15-minute video.

The rest of this chapter is organized as follows. Section 2.2 summarizes the background and motivations. Section 2.3 presents PIA, the PID based controller for ABR streaming. Section 2.4 evaluates the performance of PIA under a wide range of settings. Section 2.5 presents PIA-E, designed to improve the startup performance of PIA. Section 2.6 presents the implementation and evaluation of PIA and PIA-E using a real video player. Finally, Section 2.7 summarize this section.

2.2 Motivation and Background

ABR streaming has been used in many commercial systems [3, 46, 47]. For a satisfactory user-perceived QoE, ABR streaming needs to optimize several conflicting goals, including maximizing the average playback rate, minimizing stalls (or rebuffering), and reducing sudden and frequent quality variations [5, 6, 7, 8]. We next formulate ABR streaming as a control problem and describe the motivation for our study. Table 2.1 summarizes the main notation used in this chapter.

| | |
|-----------------|---|
| C_t | Network bandwidth at time t |
| \widehat{C}_t | Estimated network bandwidth at time t |
| x_t | Buffer level at time t (in seconds) |
| x_r | Target buffer level (in seconds) |
| R_t | Selected video bitrate for time t |
| Δ | Video chunk duration (in seconds) |
| δ | Startup latency (in seconds) |
| u_t | PID controller output |
| K_p, K_i, K_d | PID controller parameters |
| ζ | Damping ratio |
| ω_n | Natural frequency |
| β | Setpoint weighting parameter |

Table 2.1: Key notation.

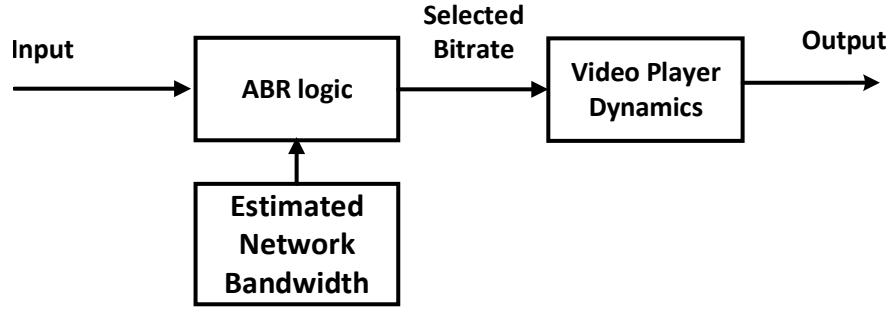
2.2.1 ABR streaming as a control problem

Deciding which level to choose in ABR streaming can be modeled as a control problem. Specifically, let x_t be the buffer level (in seconds) of the video player at time t , C_t the real-time network bandwidth at time t , and R_t the bitrate of the video chunk that is being downloaded at time t . Further, let Δ denote the video chunk duration (i.e., the duration of a chunk's playback time), δ denote the startup delay, i.e., how long it will take for the player to start playing. Then the player's buffer dynamics can be written as

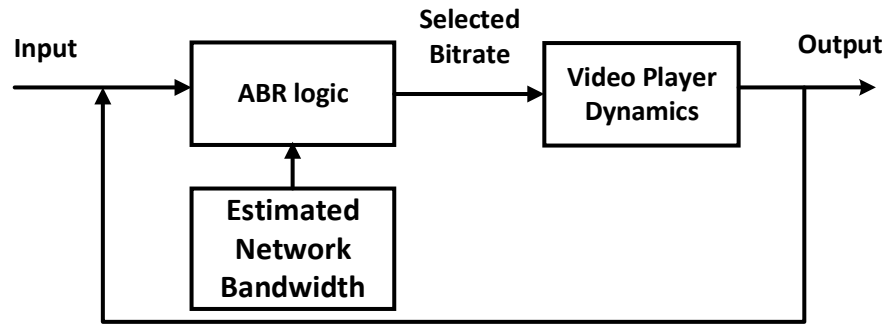
$$\dot{x}_t = \begin{cases} \frac{C_t}{R_t}, & \text{if } t \leq \delta \\ \frac{C_t}{R_t} - \mathbf{1}(x_t - \Delta), & \text{otherwise} \end{cases} \quad (2.1)$$

where $\mathbf{1}(x_t - \Delta) = 1$ if $x_t \geq \Delta$; otherwise, $\mathbf{1}(x_t - \Delta) = 0$ since in ABR streaming, a chunk has to be downloaded completely before any part of it can be played back.

In Eq. (2.1), \dot{x}_t is the rate of change of the buffer at time t . Here, C_t/R_t models the relative buffer filling rate. If $C_t > R_t$, i.e., the actual network bandwidth is larger



(a)



(b)

Fig. 2.1: ABR streaming based on open-loop control (a) and closed-loop control (b).

than the bitrate of the video chunk being downloaded, the buffer level will increase. Otherwise, the buffer level will be at the same level (if $C_t = R_t$) or decrease (if $C_t < R_t$).

One simple control strategy is to select the video bitrate for each chunk based on the prediction of real-time link bandwidth, \widehat{C}_t . Specifically, it simply chooses the highest bitrate that is less than \widehat{C}_t . This is an open-loop control strategy (illustrated in Fig. 2.1(a)), since the output (e.g., the buffer level) is not fed back to the system to assist the decision making. It is not robust against network link bandwidth estimation errors. As an example, it may choose a high video bitrate if the estimated bandwidth, \widehat{C}_t , is high, even if the current playback buffer level is very low. If it turns out that \widehat{C}_t is an overestimate of the actual network bandwidth, the buffer can be even further drained and become empty, causing stalls. Closed-loop or feedback control, as illus-

trated Fig. 2.1(b), is more effective in dealing with network link bandwidth estimation errors. We therefore focus on closed-loop/feedback control in this chapter.

2.2.2 PID control

As mentioned earlier, PID control is by far the most common way of using feedback in engineering systems. A PID controller works by continuously monitoring an “error value”, defined as the difference between the setpoint and measured process variable [45]. Specifically, let u_t represent the control signal, and e_t the error feedback at time t . Then

$$u_t = K_p e_t + K_i \int_0^t e_\tau d\tau + K_d \frac{de_t}{dt}, \quad (2.2)$$

where the three parameters K_p , K_i and K_d are all non-negative, and denote the coefficients for the proportional, integral and derivative terms, respectively. As defined above, a PID controller takes account of the present, past and future values of the errors through the three terms, respectively. Some applications may require using only one or two terms to provide the appropriate system control. This is achieved by setting the other parameters to zero. A PID controller is called a PI, PD, P or I controller in the absence of the respective control actions [45].

In the video streaming scenario, the real-time buffer level is the measured process variable, and the reference/target buffer level is the setpoint. We next show that a recent state-of-the-art buffer based scheme, BBA [14], can be mapped to a P-controller (though the paper does not claim any control-theoretic underpinnings). In BBA, the video player maintains a buffer level, and empirically sets two thresholds, $\theta_{\text{high}} > \theta_{\text{low}}$. If the buffer level is below θ_{low} , the video player always picks the lowest bitrate, R_{min} ; if the buffer level is above θ_{high} , the video player picks the highest bitrate, R_{max} ; otherwise, the video player picks the video bitrate proportionally to buffer level. The selected

bitrate, R_t , can therefore be represented as

$$R_t = \begin{cases} R_{\min}, & x_t < \theta_{\text{low}}, \\ \frac{R_{\max} - R_{\min}}{\theta_{\text{high}} - \theta_{\text{low}}} (x_t - \theta_{\text{low}}) + R_{\min}, & \theta_{\text{low}} \leq x_t \leq \theta_{\text{high}} \\ R_{\max}, & x_t > \theta_{\text{high}} \end{cases}$$

Comparing the above with Eq. (2.2), we see that it is equivalent to a P-controller when $x_t \in [\theta_{\text{low}}, \theta_{\text{high}}]$ with $K_p = \frac{R_{\max} - R_{\min}}{\theta_{\text{high}} - \theta_{\text{low}}}$, $K_i = 0$ and $K_d = 0$.

BBA has been tested successfully in a large-scale deployment [14], indicating that a PID-type control framework has the potential for ABR streaming. On the other hand, P-controller only considers the present error (i.e., the proportional term), and ignores the other two terms. It is well known that the absence of an integral term in a system may prevent the system from reaching its target value [45]. This is especially true for video streaming, where inaccurate network bandwidth estimation may cause the error to accumulate over time. Therefore, including the integral term can potentially further improve the performance of BBA. PID's ability to address accumulative errors is advantageous compared to model predictive control (MPC) based approach in [13], which does not consider accumulative errors (unless new state variables are added) and also requires accurate network bandwidth prediction. In addition, MPC is much more computation-intensive than PID (see Section 2.4.4).

We investigate PID-based control for ABR streaming in this chapter, motivated by the widespread adoption of PID control in various domains beyond video streaming (e.g., industrial control, process control) and BBA. Using PID for ABR streaming, however, has several challenges. First, the goal of PID control is to maintain a target buffer level that is only indirectly related to QoE. Indeed, while maintaining the buffer at a target level can help in preventing rebuffering, it does not help with the other two metrics on playback quality and bitrate variation. Second, PID is often used in continuous time and state space, while video streaming is a discrete-time system, where the decisions are made at chunk boundaries and the video bitrate levels are discrete.

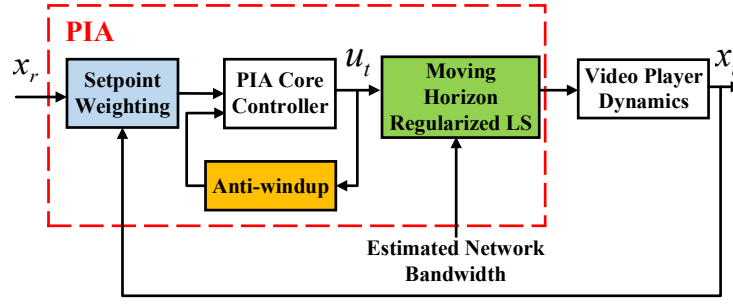


Fig. 2.2: PIA main components.

Finally, while PID is conceptually simple, the parameters (K_p , K_i and K_d) need to be tuned carefully. Here important questions are how to choose these parameters, and to determine whether there exists a parameter set that is applicable to a wide range of network and video settings. Some of the above challenges have been pointed out in [12, 13], which take the position that PID is not suitable for ABR streaming. As we shall show, none of the above challenges is a fundamental hurdle for using PID-based control for ABR streaming.

2.3 Adapting PID Control for ABR Streaming

We propose PIA, a PID based rate adaption algorithm for ABR streaming. As shown in Fig. 2.2, it contains a PI-based core control block as well as three mechanisms to address specific requirements for ABR streaming. We first describe the core component, and then the three performance enhancing mechanisms.

2.3.1 PIA core component

The core component of PIA adjusts the standard PID control policy in Eq. (2.2) so that the resultant closed-loop system is linear, and hence easier to control and analyze. We next define the controller output, analyze the system behavior, and provide insights into how to choose the various parameters.

Recall the dynamic video streaming model in Eq. (2.1), where x_t is the video player buffer level at t , C_t is the network bandwidth at time t , and R_t is the video bitrate chosen for time t . We define the controller output, u_t , as

$$u_t = \frac{C_t}{R_t}, \quad (2.3)$$

and set the control policy as

$$u_t = K_p(x_r - x_t) + K_i \int_0^t (x_r - x_\tau) d\tau + \mathbf{1}(x_t - \Delta) \quad (2.4)$$

where K_p and K_i denote, respectively, the parameters for proportional and integral control, x_r denotes target buffer level, and Δ is the chunk duration. The choice of x_r depends on system constraints, a point we will come back to in Section 2.4.

The above control policy differs from the standard PID control policy in Eq. (2.2) in the last term $\mathbf{1}(x_t - \Delta)$, which is a novel aspect of our design. As we shall see, it provides linearity, making the closed-loop control system easier to control and analyze. In our control policy, the parameter for derivative control $K_d = 0$ (hence strictly speaking, our controller is a PI controller). This is because derivative action is sensitive to measurement noise [45] and measuring network bandwidth in our context is prone to noise.

Intuitively, u_t defined in Eq. (2.3) is a unitless quantity representing the relative buffer filling rate. With u_t selected, based on Eq. (2.3), the player can select the corresponding bitrate as

$$R_t = \frac{\widehat{C}_t}{u_t}, \quad (2.5)$$

where \widehat{C}_t is the estimated link bandwidth at time t . Since video bitrate levels are discrete, we can choose the bitrate to be the highest that is below \widehat{C}_t/u_t . This choice of R_t can increase, decrease or maintain the buffer level.

We next analyze the system to provide insights into its behavior as well as providing guidelines in choosing the controller parameters. Combining equations (2.1) and (2.4) yields

$$\dot{x}_t = u_t - \mathbf{1}(x_t - \Delta) = K_p(x_r - x_t) + K_i \int_0^t (x_r - x_\tau) d\tau, \quad (2.6)$$

when the video starts playback (i.e., when $t \geq \delta$). We see that it is a linear system. Taking Laplace transform on both sides of Eq. (2.6) yields

$$sx(s) = K_p(x_r(s) - x(s)) + \frac{K_i}{s}(x_r(s) - x(s)), \quad (2.7)$$

where s is a complex Laplace transform variable. Let $T(s)$ be the system transfer function, which describes the relationship of the input and output of a linear time-invariant system. From Eq. (2.7), we have

$$T(s) = \frac{x(s)}{x_r(s)} = \frac{K_p s + K_i}{s^2 + K_p s + K_i}, \quad (2.8)$$

which is a second-order system. In the above transfer function, since $T(0) = 1$, the system can track step changes in the target buffer level, x_r , with zero error in the steady state [48], indicating that our system can maintain the preset target buffer level. From Eq. (2.8), we have

$$2\zeta\omega_n = K_p, \quad \omega_n^2 = K_i, \quad (2.9)$$

where ζ and ω_n are the *damping ratio* and the *natural frequency*, respectively, two important properties of the system. Solving the above two equations, we have

$$\zeta = \frac{K_p}{2\sqrt{K_i}}, \quad \omega_n = \sqrt{K_i}. \quad (2.10)$$

Damping ratio represents the system's ability for reducing its oscillations. In our context, it measures how the buffer will oscillate around the target buffer level – small damping will cause the buffer to change rapidly, while large damping will cause the buffer to change slowly in a sluggish manner. Natural frequency represents the frequency at which a system tends to oscillate in the absence of any driving or damping force. Empirically it has been found that ζ in the range $[0.6, 0.8]$ yields a very good system performance [49]. As a result, K_p and K_i should be chosen so that $\zeta \in [0.6, 0.8]$. We will discuss how to tune K_p and K_i in Section 2.4.2.

2.3.2 PIA performance enhancing techniques

Based on the core component of PIA, we now add three domain-specific enhancements to PIA to further improve its robustness and adaptiveness for ABR streaming.

Accelerating initial ramp-up. At the beginning of the video playback, the buffer level x_t can be much smaller than the target buffer level x_r . In this case, observe from Eq. (2.4) that u_t will be large. A large u_t will result in low video bitrate, R_t , and therefore a low quality at the beginning, which can adversely impact initial user experience. To address this issue, we include a setpoint weighting parameter [45], $\beta \in (0, 1]$, into the control policy as

$$u_t = K_p(\beta x_r - x_t) + K_i \int_0^t (x_r - x_\tau) d\tau + \mathbf{1}(x_t - \Delta). \quad (2.11)$$

Note that β is only included in the proportional term; it does not affect the steady-state behavior of the control system [45]. When $\beta = 1$, the above control policy reduces to (2.4). When $\beta < 1$, it can lead to smaller u_t , and hence faster initial ramp-up in video bitrate. However, very small β can lead to aggressive choice of video bitrate, and hence increase the chance of buffer emptying, causing rebuffering at the beginning of the playback. We explore how to set β in Section 2.4.2. The system transfer function corresponding to the above control policy is

$$T(s) = \frac{x(s)}{x_r(s)} = \frac{\beta K_p s + K_i}{s^2 + K_p s + K_i} = \frac{\beta K_p s + K_i}{s^2 + 2\zeta\omega_n s + \omega_n^2}. \quad (2.12)$$

Note that both damping ratio, ζ , and natural frequency, ω_n remain the same as those in Eq. (2.10).

Minimizing bitrate fluctuations. The simple choice of R_t in Eq. (2.5) mainly tracks the network bandwidth. It, however, may lead to frequent and/or abrupt bitrate (and hence quality) changes, adversely impacting viewing quality. To address the above issue, we develop a regularized least squares (LS) formulation that considers both video bitrate and the changes in video bitrate to achieve a balance between both of these

metrics. Specifically, it minimizes the following objective function

$$J(\ell_t) = \sum_{k=t}^{t+N-1} \left(u_k R(\ell_t) - \widehat{C}_k \right)^2 + \eta (R(\ell_t) - R(\ell_{t-1}))^2, \quad (2.13)$$

where ℓ_t and ℓ_{t-1} represent the tracks selected for chunks t (the current chunk) and $t - 1$ (i.e., the previous chunk), respectively¹, u_k is the controller output for the k -th chunk, \widehat{C}_k is the estimated link bandwidth for the k -th chunk, η is the weight factor for bitrate changes, and $R(\ell)$ represents the bitrate corresponding to track ℓ .

Let \mathcal{L} denote the set of all possible track levels. For every $\ell_t \in \mathcal{L}$, the formulation in Eq. (2.13) considers a moving horizon of N chunks in the future (represented as the sum of N terms, one for each of the N future chunks). The first term in the sum aims to minimize the difference between $u_k R(\ell_t)$ and the estimated network bandwidth \widehat{C}_k so as to maximize $R(\ell_t)$ (and hence quality) under the bandwidth constraint and the selected u_k . The second term aims to minimize the variability in bitrate for two adjacent chunks (i.e., the current and previous chunks) for a smooth viewing experience. The weight factor η can be set to reflect the relative importance of these two terms. We use $\eta = 1$ (i.e., equal importance) in the rest of the chapter since maximizing the video quality and reducing quality variation are both important for user QoE. To reduce the number of video bitrate changes, in Eq. (2.13), we assume that the same track is chosen for the next N chunks (this assumption is used only for determining the track/bitrate for chunk t ; the actual track/bitrate for the future chunks will be decided at later times, independent of the assumption made for the decision of chunk t). For Constant Bitrate (CBR) videos (which is the focus of this chapter), the chunks in the same track have the same bitrate. Therefore, in Eq. (2.13), the bitrate of the next N chunks are all equal to $R(\ell_t)$. For Variable Bitrate (VBR) videos, the formulation can be modified in a straightforward manner². Last, in Eq. (2.13), the control output, u_k , is updated according to the control policy in Eq. (2.11), based on the estimated buffer size, x_k ,

¹ Here we slightly abuse notation by using t to represent the index of the chunk chosen at time t , and using $t - 1$ to represent the index of the previous chunk.

² For VBR videos, even the chunks in the same track have variable bitrate. In that case, we can modify

over the moving horizon. The estimated buffer size, x_k , is updated through Eq. (2.1) using $R(\ell_t)$ as the video bitrate and the estimated network bandwidth \widehat{C}_k .

The optimal solution of Eq. (2.13) is

$$\ell_t^* = \arg \min_{\ell_t \in \mathcal{L}} J(\ell_t), \quad (2.14)$$

where \mathcal{L} denotes the set of all possible track levels. We can find ℓ_t^* easily by plugging in all possible values of ℓ_t , $\ell_t \in \mathcal{L}$, into Eq. (2.13), and select the value that provides the minimum objective function value in Eq. (2.13).

The complexity of the above formulation is as follows. For every $\ell_t \in \mathcal{L}$, obtaining $J(\ell_t)$ requires computation of N steps. Therefore, the total computational overhead is $O(|\mathcal{L}|N)$, significantly lower than the complexity of $O(|\mathcal{L}|^N)$ in [13].

Dealing with bitrate saturation. Following the control policy, u_t may become negative (e.g., when the current buffer level exceeds the target buffer level). In this case, solving Eq. (2.13) will lead R_t to be the minimum bitrate. During this time period, if we continue using the integral term, $I_{\text{out}} = K_i \int_0^t (x_r - x_\tau) d\tau$, u_t may remain negative for an extended period of time, causing R_t to stay at the minimum bitrate level for an extended period of time (so called system saturation [45]), and causing the buffer level to continue to grow.

Such system saturation is undesirable since it will cause the client to select low bitrate (and hence low quality) chunks that adversely impact user QoE, even though the network bandwidth is able to support higher quality streaming. To deal with the above scenario, we incorporate an anti-windup technique (to deal with integral windup, i.e., integral term accumulates a significant error) for negative u_t , or more specifically, when $u_t \leq \epsilon$, $0 < \epsilon \ll 1$. Many anti-windup techniques have been proposed in the literature. In the first term of (2.13), we replace $R(\ell_t)$ with $R_k(\ell_t)$ to reflect that the bitrate is time varying; in the second term, we replace $R(\ell_t)$ and $R(\ell_{t-1})$ with the average bitrate of the corresponding tracks, denoted as $\bar{R}(\ell_t)$ and $\bar{R}(\ell_{t-1})$, respectively, so that the penalty for quality variation is zero as long as the two adjacent chunks are in the same track.

literature [45]. We adopt a simple technique, which sets u_t to ϵ , chooses R_t as the maximum bitrate, and does not change I_{out} when $u_t \leq \epsilon$. This corresponds to turning off the integral control when u_t is below ϵ . We set ϵ to a small positive value, 10^{-10} , in the rest of this chapter.

2.3.3 PIA parameter tuning

Three important parameters in PIA are K_p , K_i and β , where K_p and K_i determine the system behavior and β is used for faster initial ramp-up. For a given network setting (e.g., cellular networks), since β does not affect the steady-state behavior [45], we can first assume a fixed β (e.g., $\beta = 1$) and tune K_p and K_i to achieve a desirable steady-state behavior (i.e., jointly maximize the three metrics in QoE). Once K_p and K_i are fixed, we then tune β for the initial stage of the video playback. The values of K_p and K_i need to be tuned so that the resultant system behavior is compatible with the network setting. Taking cellular networks as an example, since the bandwidth is highly dynamic, it is reasonable to tune the system so that the buffer level does not fluctuate drastically. Otherwise, the buffer can suddenly become very low, making the system vulnerable to stalls. We describe this approach using a set of network traces from commercial cellular networks in Section 2.4.2.

2.3.4 Putting it all together

We now summarize the workflow of PIA depicted in Fig. 2.2. PIA takes the target buffer level x_r , the current buffer level x_t , and the estimated network bandwidth as input, and computes the selected track level ℓ_t^* , which is then fed into the Video Player Dynamics block to update the buffer level. PIA considers both present and past estimation errors, as well as incorporates all the three QoE metrics in the control loop. PIA also includes an anti-windup mechanism to deal with bitrate saturation, and a setpoint weighting technique to provide faster initial ramp-up.

2.4 Performance Evaluation

In this section, we evaluate the performance of PIA using simulation; evaluation through real implementation on a video player is deferred to Section 2.6. Simulation allows us to evaluate a large set of parameters in a scalable manner, while real implementation provides insights under various system constraints. In both cases, the network conditions are driven by a set of traces captured from commercial LTE networks that allow reproducible runs, as well as apple-to-apple comparison of different schemes. We first describe the evaluation setup, choice of parameters for PIA, and then compare PIA against several state-of-the-art schemes.

2.4.1 Evaluation setup

Network bandwidth traces. We focus on LTE networks that dominate today’s cellular access technology. For evaluation under realistic LTE network environments, we collected 50 network bandwidth traces from two large commercial LTE networks in the US. These traces were collected under a wide range of settings, including different times of day, different locations (in three U.S. states, CT, NJ and NY), and different movement speed (stationary, walking, local driving, and highway driving).

Each trace contains 30 minutes of one-second measurement of network bandwidth. The bandwidth was measured on a mobile device, as the throughput of a large file downloading from a well provisioned server to the device. Fig. 2.3(a) is a boxplot that shows the minimum, first quartile, median, third quartile, and maximum bandwidth of each trace, where the traces are sorted by the median bandwidth. We see that the network bandwidth is indeed highly dynamic. For some traces, the maximum bandwidth is tens of Mbps, while the minimum bandwidth is less than 10 Kbps.

These network traces, by capturing the bandwidth variability over time, accurately reflect the impact of lower level network characteristics (e.g., signal strength, loss, and RTT) on the network bandwidth perceived by an application. Using the net-

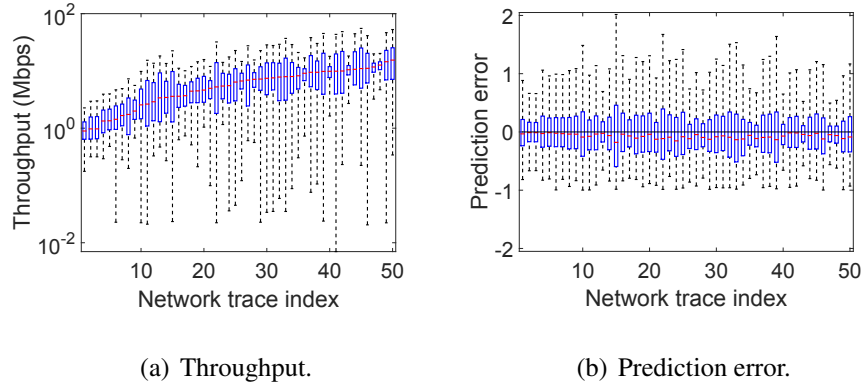


Fig. 2.3: Characteristics of the network bandwidth traces that are used in performance evaluation.

work traces is sufficient when evaluating ABR schemes; there is no need to explicitly incorporate lower level network characteristics since ABR adaptation operates at the application level, using application-level estimation of the network bandwidth.

Video parameters. We use three video bitrate sets, all being Constant Bitrate (CBR) videos: $\mathcal{R}_1 = [0.35, 0.6, 1, 2, 3]$ Mbps, $\mathcal{R}_2 = [0.35, 0.6, 1, 2, 3, 5]$ Mbps and $\mathcal{R}_3 = [0.2, 0.4, 0.6, 1.2, 3.5, 5, 6.5, 8.5]$ Mbps. The first set is based on the reference for YouTube video bitrate levels (corresponding to 240p, 360p, 480p, 720p and 1080p respectively) [50]. The second set adds a higher bitrate level of 5 Mbps to the first set. The third set is based on Apple’s HTTP Live Streaming standard [51]. For each bitrate set, we further consider three variants with chunk duration of 2, 4, and 8 s.

ABR Schemes. We compare PIA against four other schemes; in Section 2.6, we further compare the performance of PIA and BOLA [11], another state-of-the-art ABR scheme, using DASH implementation.

- **RB:** The bitrate is picked as the maximum possible bitrate that is below the predicted network bandwidth. This is a simple open-loop controller (see Section 2.2), serving as a baseline.
- **BBA [14]:** It is a state-of-the-art buffer based scheme. We use BBA-0, which is

the BBA variant for CBR streaming, the focus of this work. We set the lower and upper buffer thresholds as $\theta_{\text{low}} = 10$ s and $\theta_{\text{high}} = 60$ s, respectively, and empirically verified that the above thresholds work well on our dataset.

- **MPC and RobustMPC [13]:** Both are state-of-the-art ABR schemes based on model predictive control. RobustMPC is more conservative in estimating network bandwidth, and has been shown to outperform MPC [17] in more dynamic network settings (e.g., cellular networks). Both schemes use a look-ahead horizon of 5 chunks (as suggested by the paper).
- **PIA:** Unless otherwise stated, the target buffer level $x_r = 60$ s that is compatible with the setting of BBA. In Section 2.4.3, we vary the target buffer level and explore its impact on performance. The look-ahead horizon is set to 5 chunks, i.e., $N = 5$ in Eq. (2.13).

For all the schemes, unless otherwise stated, the startup playback latency (i.e., the latency from when requesting the first chunk of the video to starting the playback of the video), δ , is set to 5, 10 or 15 s. For BBA and MPC, their parameters are either selected based on the original papers, or configured by us based on the properties of the videos (e.g., chunk duration and encoding rates) as justified above.

Network bandwidth prediction. For the schemes that require network bandwidth estimation, it is set as the harmonic mean of the network bandwidth of the past 20 s. Harmonic mean has been shown to be robust to measurement outliers [34]. Fig. 2.3(b) shows the boxplots of the bandwidth prediction errors (the difference of the predicted and actual bandwidths divided by the actual bandwidth) of the network bandwidth traces used in our evaluations. Each box in the plot corresponds to the distribution of all prediction instances within a particular trace. The prediction is at the beginning of every second. As shown, the median prediction error is 20% to 40%, highlighting the challenges of accurate bandwidth prediction in LTE networks. As we shall show

later in Section 2.4.3, our PIA scheme is very robust to such levels of inaccuracy in network bandwidth estimation.

2.4.2 PIA: Choice of parameters

Following the methodology outlined in Section 2.3.3, we first tune K_p and K_i , and then tune β for PIA. One question we aim to answer is whether there exists a set of K_p and K_i values that works well in a wide range of settings. This is an important issue related to the practicality of PIA – because if the choice of K_p and K_i were too sensitive to the settings, then tuning and/or adapting them for different settings would require more effort.

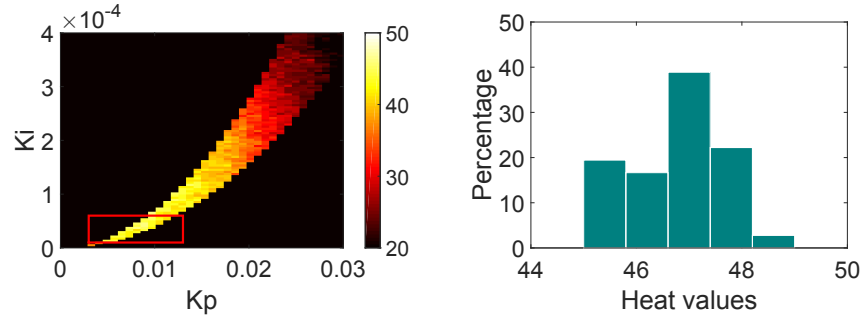
Tuning K_p and K_i

We use a single combined performance metric when tuning K_p and K_i . This is because, while as described earlier, the QoE is affected by three metrics (average video bitrate, the amount of bitrate changes and rebuffering) jointly, comparing the QoE under different choices of K_p and K_i is much simpler when using a single combined metric. Currently there is no consensus in the field around the form of such a metric. One approach is using a weighted sum of the three metrics as in [13]. Specifically, for a video of M chunks,

$$\text{QoE} = \sum_{t=1}^M R_t - \mu \sum_{t=1}^{M-1} |R_{t+1} - R_t| - \lambda \sum_{t=1}^M S_t. \quad (2.15)$$

where R_t is the bitrate of the t -th chunk and S_t is the amount of stalls for the t -th chunk, and μ and λ are weights that represent, respectively, the importance of the middle and last terms (i.e., bitrate changes and rebuffering) relative to the first term (i.e., average bitrate) in the sum. There is no well agreed-upon settings for μ and λ ; we therefore vary μ and λ over multiple values to assess sensitivity.

The trace-driven simulation allows us to consider a very wide range of settings by varying a number of parameters: the video bitrate set, video length, chunk size, startup



(a) Heatmap.

(b) Histogram of “heat” values.

Fig. 2.4: Region of K_p and K_i and the corresponding “heat” values in one setting (video bitrate set \mathcal{R}_3 , chunk duration 2 s, video length 20 min, startup latency 10 s, $\mu = 1$, $\lambda = 8.5$ (which is the same as the maximum bitrate (in Mbps) in \mathcal{R}_3).

latency, and μ and λ in (2.15). Specifically, the video bitrate set is either \mathcal{R}_1 , \mathcal{R}_2 , or \mathcal{R}_3 (see Section 2.4.1), video length is 5, 10 or 20 minutes, chunk duration is 2, 4 or 8 s, startup latency is 5, 10 or 15 s, and μ is 1 or 2, and λ is the maximum bitrate level of a video (e.g., 3 Mbps in \mathcal{R}_1) or twice as much. The choice of μ and λ is based on the settings in [13]. In each setting (i.e., after fixing the above parameters), we consider each of the 50 network bandwidth traces individually. For the k -th network trace, we vary the values of K_p and K_i in a wide range to find a pair of K_p and K_i that maximizes the QoE (note that as described in Section 2.3, we only consider valid combinations of K_p and K_i values, i.e., those so that the damping ratio is in $[0.6, 0.8]$). Once the maximum QoE, denoted as Q_k^* , is determined, the QoE under each valid (K_p, K_i) pair is compared to Q_k^* to see whether it is within 90% of Q_k^* . Specifically, we define a binary function $f_k(K_p, K_i)$ for the k -th network bandwidth trace, where $f_k(K_p, K_i) = 1$ if the resulting QoE under K_p and K_i is within 90% of Q_k^* , otherwise, $f_k(K_p, K_i) = 0$. We then consider all the network bandwidth traces, and create a heat map with the “heat” for each valid pair of K_p and K_i values as $\sum_k f_k(K_p, K_i)$. Clearly, a larger “heat” value for a K_p and K_i pair means that it leads to good performance for more network bandwidth traces.

Fig. 2.4(a) shows an example heat map for one setting (details of the setting described in the caption of the figure). The black region represents invalid K_p and K_i pairs (i.e., those causing the damping ratio out of the desired range $[0.6, 0.8]$). For the valid K_p and K_i pairs, the “heat” value varies, with the highest values in the bottom left region, marked by the rectangle (brighter color represents higher “heat” values). Fig. 2.4(b) is the histogram of the “heat” values in the rectangle area (excluding those corresponding to invalid K_p and K_i pairs). It shows that majority of the values are close to 50 (i.e., the maximum “heat”), indicating that the valid K_p and K_i pairs marked by the rectangle provide good performance across almost all network traces.

We repeat the above procedure for all the settings, and find the following region of K_p and K_i values leads to good performance for all the settings

$$\begin{aligned} K_p &\in [1 \times 10^{-3}, 14 \times 10^{-3}] \\ K_i &\in [1 \times 10^{-5}, 6 \times 10^{-5}] \\ \text{s.t. } \zeta(K_p, K_i) &\in [0.6, 0.8]. \end{aligned} \tag{2.16}$$

Specifically, under the above range of values, the average “heat” for the different settings varies from 31 to 50, and the standard deviation varies from 0.25 to 3.45. The results in the rest of the chapter use $K_p = 8.8 \times 10^{-3}$, approximately the middle of the range of K_p in (2.16), and $K_i = 3.6 \times 10^{-5}$ so that the damping ratio is $1/\sqrt{2}$, a widely recommended value for damping ratio [49, 52].

The finding that a set of K_p and K_i values works well under a wide range of settings is encouraging. Considering that the network traces were collected under a wide range of settings and that they exhibit significantly different characteristics (see Fig. 2.3), our results show that K_p and K_i can be tuned to accommodate the large variations among individual traces. The above results indicate that we can find a range of K_p and K_i values to make the system capable of dealing with the rapid bandwidth variations (one of the predominant characteristics of cellular networks), despite the differences across individual network conditions.

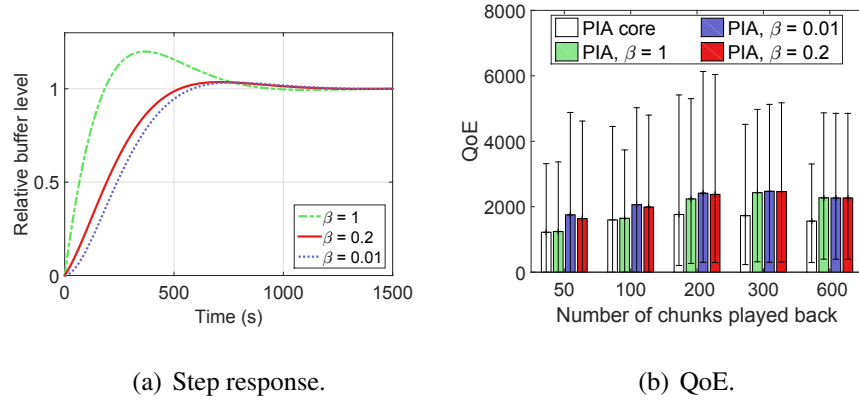


Fig. 2.5: Choosing β in PIA. In (b), the setting is the same as that used for Fig. 2.4.

Tuning β

Once K_p and K_i are determined, we tune β for the initial stage of the video playback. Specifically, we set β to 0.01, 0.2, 0.4, 0.6, 0.8, and 1.0. Fig. 2.5(a) shows the step response of the control policy (only the results for $\beta = 0.01$, 0.2 and 1 are shown for better clarity). When $\beta = 1$, the buffer becomes full much more quickly than when $\beta = 0.2$ and 0.01. This is because, as explained in Section 2.3.2, lower bitrate tends to be selected when $\beta = 1$, causing the buffer to fill up more quickly.

To examine the three QoE metrics jointly, Fig. 2.5(b) plots the QoE when playing up to the i -th chunk of a video of 600 chunks when $\beta = 0.01$, 0.2 or 1. The results are averaged over all the network traces; the 95% confidence intervals are plotted in the figure as well. We see that β indeed affects the QoE for the initial playback, and $\beta = 1$ leads to lower QoE compared to $\beta = 0.01$ and 0.2. Further investigation reveals that $\beta = 0.01$ leads to more rebuffering than $\beta = 0.2$. The above results are for the setting used for Fig. 2.4. Results in other settings show similar trends. Since rebuffering has very detrimental effects on viewing quality, we use $\beta = 0.2$ in the rest of the chapter.

Last, the results of PIA core (i.e., without the three enhancing techniques) are also shown in Fig. 2.5(b). We see that PIA core indeed leads to lower QoE compared to the full-fledged PIA, demonstrating the benefits of our three enhancing techniques.

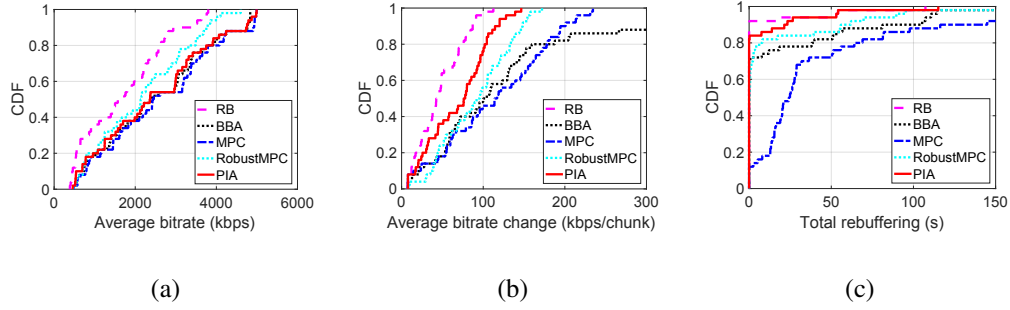


Fig. 2.6: Performance comparison in the default setting (chunk duration 2 s, video bitrate set \mathcal{R}_2 , video length 20 minutes, startup latency 10 s).

2.4.3 Performance comparison

In the following, we first present the performance of PIA in the default setting, i.e., chunk duration of 2 s, video bitrate set \mathcal{R}_2 , video length of 20 minutes, and startup latency of 10 s. After that, we evaluate the impact of the various parameters on the performance of PIA.

Fig. 2.6 plots the CDF of the three QoE metrics over all network bandwidth traces in the default setting. The performance of four schemes, RB, BBA, MPC, RobustMPC and PIA, are plotted. We see that, while the amount of bitrate change and rebuffering is low under RB, its average bitrate is significantly lower than those of the other schemes. PIA achieves comparable average bitrate as BBA and MPC, with significantly less bitrate changes and rebuffering. Specifically, the average bitrate of PIA is 98% and 96% of that of BBA and MPC, respectively, while the average amount of bitrate change is 49% and 40% lower, and the average amount of rebuffering is 68% and 85% lower than BBA and MPC, respectively. RobustMPC has significantly lower rebuffering than MPC, but its rebuffering is still higher than that under PIA. In addition, RobustMPC leads to significantly lower average bitrate than MPC, PIA and BBA.

Overall, *PIA achieves the best balance among the three conflicting QoE metrics*. As described earlier, the inferior performance of RB is because it uses an open-loop control without any feedback. The superior performance of PIA compared to BBA is

because BBA implicitly uses one form of P-control (Section 2.2) that only takes the present error into account, while PIA considers both the present and past errors. PIA's approach of applying PID in an explicit and adaptive manner further facilitates the design and improves the performance. The performance of MPC is sensitive to network bandwidth estimation errors [13]: it solves a discrete optimization problem at each step; when network bandwidth estimation is inaccurate, the input to the optimization problem is correspondingly inaccurate, leading to suboptimal performance. RobustMPC leads to lower rebuffering than MPC due to its more conservative network bandwidth estimation. It, however, also leads to significantly lower bitrate choices.

To provide further insights, Fig. 2.7 plots the bitrate selection and the buffer level over time for BBA, MPC and PIA when using one network trace. For reference, it also plots the network bandwidth of the trace. We clearly see that BBA has significantly more bitrate changes; MPC tends to be more aggressive in choosing higher bitrates, which can lead to excessive rebuffering. The bitrate selection under PIA matches well with the network bandwidth without frequent bitrate changes. In terms of the buffer level/occupancy (i.e., the duration of the video content that has been brought in and has not yet been played back) shown in the bottom plot in Fig. 2.7, the buffer level of MPC is lower than that of BBA and PIA due to its aggressive choice of bitrate; the buffer level of PIA reaches the target level of 60 s at around 300 s, and then stays around the target level; the buffer level of BBA is in between that of MPC and PIA.

Impact of target buffer level. We vary the target buffer level, x_r , from 30 to 200 seconds, and evaluate its impact on the various performance metrics. We observe that larger target buffer levels lead to lower bitrate choices (to reach the larger target buffer levels during buffer ramp-up periods, e.g., at the beginning of the playback or after stall events). A large target buffer level also has the drawback that it may lead to more waste of resources when a user abandons watching a video in the middle of the playback. Using a small target buffer level, however, can lead to higher rebuffering. Fig. 2.8 plots the average bitrate and the amount of rebuffering for different x_r values. We observe no-

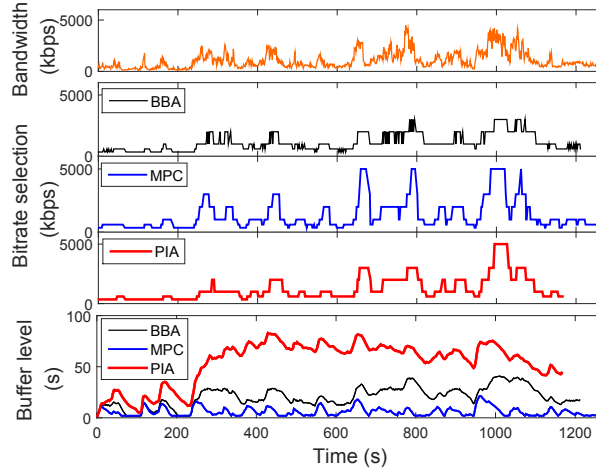


Fig. 2.7: Comparison of different schemes for one trace under the default setting (chunk duration 2 s, video bitrate set \mathcal{R}_2 , video length 20 minutes, startup latency 10 s). The plot on buffer level shows the results until the end of the downloading.

ticeably lower bitrate when $x_r = 150$ seconds, and noticeably higher rebuffering when $x_r = 30$ seconds. Setting x_r to 50 to 120 seconds leads to similarly good performance in all three performance metrics (the average bitrate change between two consecutive chunks across the x_r values is similar, and is not shown in the figure).

Impact of video length. The above results are for video length of 20 mins. We vary the ending time of the video to investigate PIA’s performance for shorter videos. When the ending time is larger than 5 mins (i.e., video length longer than 5 mins), we observe similar results as before; for much shorter videos, PIA has lower average bitrate compared to MPC (the average bitrate of PIA is 81% of MPC when the video length is 2 minutes, and 90% of MPC when the video length is 5 minutes), but still outperforms BBA and MPC on the other two metrics. We investigate how to improve the bitrate of PIA in the startup phase in Section 2.5.

Impact of video bitrate sets. Recall that the video bitrate set \mathcal{R}_2 has one higher bitrate level of 5 Mbps compared to \mathcal{R}_1 . We further investigate two more video bitrate sets $\mathcal{R}_4 = [0.2, 0.35, 0.6, 1, 2, 3]$ Mbps, which has one lower bitrate of 0.2 Mbps compared

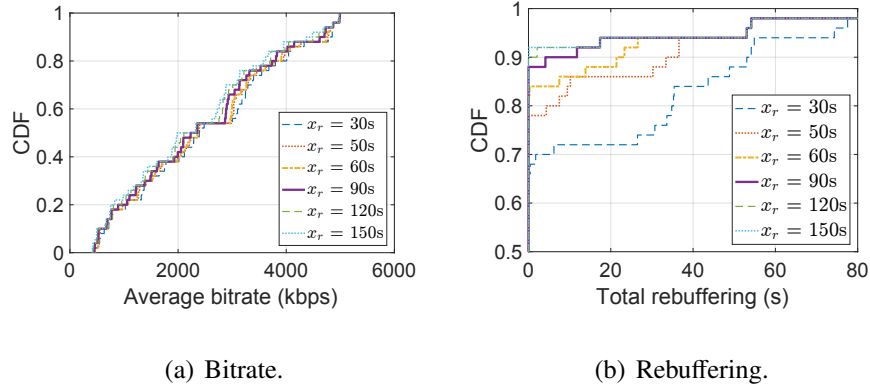


Fig. 2.8: Impact of the target buffer level on performance (video bitrate set \mathcal{R}_2 , chunk duration 2 s, video length 20 minutes, startup latency 10 s).

to \mathcal{R}_1 ; and $\mathcal{R}_5 = [0.2, 0.35, 0.6, 1, 2, 3, 5]$ Mbps, which has one lower and one higher video bitrate levels (of 0.2 and 5 Mbps) compared to \mathcal{R}_1 . We observe consistent trend for all the schemes under the above three video bitrate sets. Comparing the results under \mathcal{R}_1 and \mathcal{R}_2 , we see that adding one higher bitrate level leads to higher average video bitrate, more bitrate changes, and more rebuffering; comparing the results under \mathcal{R}_1 and \mathcal{R}_4 , we see that adding one lower bitrate level maintains the average video bitrate while reducing bitrate changes and rebuffering; comparing \mathcal{R}_1 and \mathcal{R}_5 , we see that adding both one lower and higher bitrate levels increases the average video bitrate and bitrate changes, while reducing the rebuffering. In general, adding more bitrate levels helps improve at least one of the three metrics. Across the settings, PIA has the lowest bitrate switches, the lowest rebuffering, and similar average bitrate compared to BBA and MPC.

Impact of video chunk duration. We vary the video chunk duration by setting it to 2, 4, or 8 s. We found that, for all chunk durations, PIA consistently outperforms MPC and BBA in balancing the tradeoffs incurred by the three metrics. For example, for chunk duration of 8 s, PIA's average playback bitrate differs from BBA and MPC only by 0.1% and 3.2%, respectively, while PIA reduces the rebuffering duration by 67%

and 68% compared to those of BBA and MPC, respectively.

Buffer occupancy and impact of maximum buffer size. In the evaluations so far, we assume that all data downloaded ahead of the current playback point is stored in the client buffer until it is played back. Fig. 2.9 plots the distribution of the buffer occupancy (i.e., all the chunks brought in that have not yet been played back) under PIA in the default setting across all the network traces, where we record the buffer occupancy after downloading each chunk. We observe that 52% of the time, the buffer occupancy is below the target buffer size (60 s), 85% of the time it is below 100 s, and 95% of the time it is below 200 s. The above results indicate that, while there is no explicit constraint on buffer size, the amount of video stored at the client under PIA is not large (200 s of video corresponds to at most 125 MB even if we consider buffering the maximum bitrate track in \mathcal{R}_2).

In practice, a player may impose a maximum buffer size, B_{\max} , so that the amount of video downloaded before its playback time does not exceed this limit. We explore a simple strategy for this case. Specifically, the client stops downloading video when the buffer is full, and resumes downloading when there is space in the buffer. We set $B_{\max} = 90, 120, 150, 180$ or 210 s, motivated by the practice of commercial players, which set the maximum buffer limit to tens to hundreds of seconds [14, 24, 30, 53]. In the following, in the interest of space, we only report the results when $B_{\max} = 90$ or 210 s.

When imposing the maximum buffer limit, not surprisingly, the average bitrate of all the schemes is reduced. On the other hand, the reduction under PIA when $B_{\max} = 90$ s is only slightly more than that $B_{\max} = 200$ s (consistent with the observation in Fig. 2.9 that 82% and 96% of the time, the buffer size is less than 90 s and 210 s, respectively). PIA still achieves the best balance among the three conflicting performance metrics. Fig. 2.10 plots the distribution of the tracks selected by PIA under the default setting across all the network traces (the video bitrate set \mathcal{R}_2 has six tracks with increasing bitrate). For comparison, the bitrate choices when there is no maximum buffer limit

are also plotted in the figure. We observe that, when imposing a maximum buffer limit, the probability of choosing the highest track is reduced (particularly when $B_{\max} = 90$ s), while the probability of choosing the lower tracks is increased. This is because, with the maximum buffer limit, the amount of video in the buffer is limited (and hence tends to be less than the amount when there is no buffer limit); the player thus has less cushion for preventing buffer underruns, and is less likely to choose the highest track (which takes longer to download compared to lower tracks, causing more buffer drainage). Fig. 2.11 shows an example. We see from 150 to 260 seconds, the buffer level is significantly lower under $B_{\max} = 90$ s than that when $B_{\max} = 210$ s. As a result, the player chooses lower tracks for the former, while choosing the highest track for the latter.

In the above, we use a simple strategy that stops downloading when the buffer is full, which does not fully leverage the network bandwidth. This simple strategy can be improved in two directions. The first direction is segment replacement, i.e., the player can leverage the bandwidth to preempt some earlier downloaded chunks that are of lower bitrate (i.e., replace them with chunks with higher bitrate and hence quality). While segment replacement has been used in commercial systems, the performance of existing commercial implementation is not satisfactory [24]. The key decision of segment replacement is to select which chunks to preempt and which bitrate levels to replace them with, which we will investigate in future studies. The second direction is designing bitrate selection strategies to download higher bitrate chunks proactively, instead of filling in the buffer with lower bitrate chunks. Further exploration along this direction is also left as future work.

Impact of startup delay. So far we have set the startup delay to be 10 s, i.e., waiting for 10 s after requesting the first chunk of the video before starting the playback of the video. We next vary the startup delay. Specifically, we assume the chunk duration is 2 or 6 s and the startup delay is 6 or 12 s, equivalent to 3 or 6 chunks for chunk duration of 2 s, and 1 or 2 chunks for chunk duration of 6 s. Our results show that

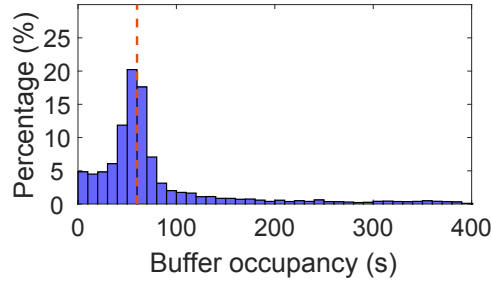


Fig. 2.9: The distribution of buffer occupancy of PIA (under the default setting, i.e., chunk duration 2 s, video bitrate set \mathcal{R}_2 , video length 20 minutes, startup latency 10 s).

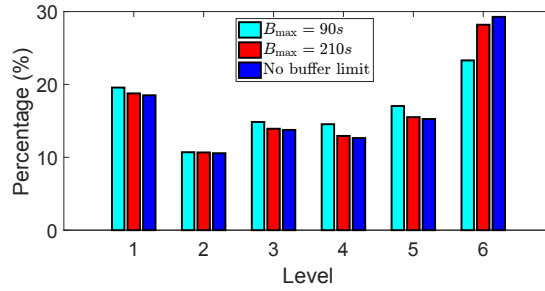


Fig. 2.10: Impact of the maximum buffer size on the bitrate adaptation of PIA (under the default setting, i.e., chunk duration 2 s, video bitrate set \mathcal{R}_2 , video length 20 minutes, startup latency 10 s).

the amount of rebuffering depends more on the number of chunks that is downloaded during the startup delay, and is less sensitive to the length of the startup delay. For the same amount of startup delay (in seconds), using a smaller chunk duration leads to less rebuffering than using a larger chunk duration. In addition, having at least 2 or 3 chunks in buffer before playback starts leads to significantly less rebuffering than having a single chunk. The above findings are consistent with those in [24].

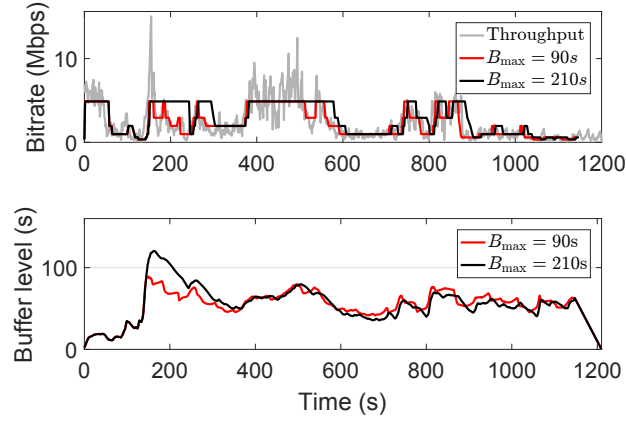


Fig. 2.11: An example that illustrates the impact of the maximum buffer size on the bitrate choice of PIA (under the default setting, i.e., chunk duration 2 s, video bitrate set \mathcal{R}_2 , video length 20 minutes, startup latency 10 s).

2.4.4 Computational overhead

As described earlier, the computational overhead of PIA is much lower than that of MPC: for $|\mathcal{L}|$ bitrate levels and horizon N , the complexity of MPC is $O(|\mathcal{L}|^N)$, while the complexity of PIA is $O(|\mathcal{L}|N)$. Table 2.2 compares the average execution time of running MPC, BBA and PIA for a 600-chunk video (2-second chunk with bitrate set \mathcal{R}_2) on a commodity laptop with Intel i5 2.6 GHz CPU and 16 GB RAM. The CPU time for PIA is 0.17 s, comparable to that of BBA. The CPU time for MPC is more than 200 times higher than that for PIA.

Table 2.2: Comparison of computational overhead.

| | MPC | BBA | PIA |
|--------------|-------|------|------|
| CPU time (s) | 36.04 | 0.08 | 0.17 |

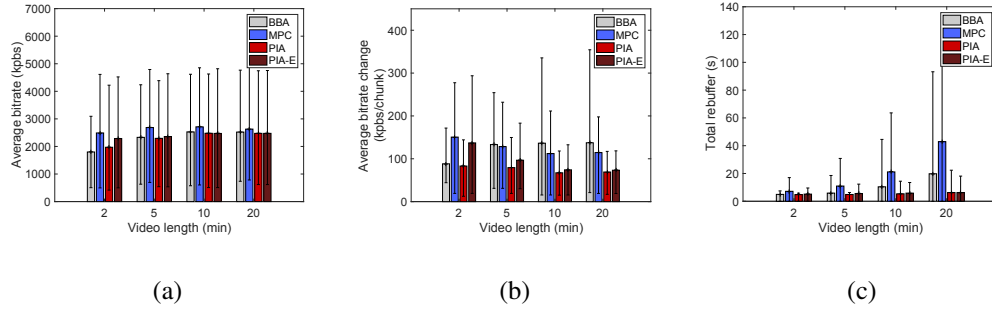


Fig. 2.12: Performance of PIA-E versus other schemes (chunk duration 2 s, video bitrate set \mathcal{R}_2 , startup latency 10 s).

2.5 Improving Startup Performance

As shown in Section 2.4, the average bitrate under PIA in the startup phase (up to 5 minutes into the playback) can be 20% lower than that of MPC. We next present a variant of PIA, PIA-E (PIA Enhanced), that improves PIA's startup performance. The bitrate selection during the startup phase needs to balance two aspects: the quality of the video and the accumulation of the video content. The quality of the early part of the video (the chunks downloaded during the startup phase) is important, since low quality may prompt a user to stop watching the video. On the other hand, the startup phase also plays an important role in building up the video content in the buffer to reduce the likelihood of rebuffering in the future; choosing lower bitrate chunks helps to accumulate more content in the buffer. A good strategy for the startup phase thus needs to account for these two conflicting aspects.

Our goal of designing PIA-E is to increase the bitrate for the early part of the video, without increasing the amount of rebuffering during the later part of the playback. We achieve this goal by dynamically adjusting a selective set of parameters over time. Specifically, observe from Eq. (2.13) that the bitrate for the early part of the video can be increased by decreasing the controller output, u_t , which can be achieved by adjusting the parameters, K_p , β , x_r , and K_i , based on Eq. (2.11). Let $K_p(t)$, $\beta(t)$, $x_r(t)$, and $K_i(t)$ denote the values of these parameters at time t . We next describe one

design of PIA-E that adjusts $K_p(t)$ and $x_r(t)$ overtime. At the end of this section, we discuss other design options.

Adjusting $K_p(t)$ and $x_r(t)$. This design keeps $\beta(t) = \beta$ and $K_i(t) = K_i$, and dynamically adjusts $K_p(t)$ and $x_r(t)$ over time, starting with initial values that are selected for the startup phase, and ending with the values that have been tuned for the steady state. Specifically, we set $K_p(t)$ as a decreasing function of t that decreases from an initial value αK_p , $\alpha > 1$, to K_p over a time interval, and set $x_r(t)$ as an increasing function of t that increases from a small value to x_r over a time interval. As a result, the first term in Eq. (2.11) is a non-negligible negative value at the beginning of the playback, leading to lower u_t and hence larger bitrate choices. Specifically, let τ denote the time interval. We set

$$K_p(t) = \begin{cases} \alpha K_p - \frac{(\alpha K_p - K_p)t}{\tau}, & 0 \leq t \leq \tau \\ K_p, & t > \tau \end{cases} \quad (2.17)$$

Similarly, we set $x_r(t)$ as a linear function with the minimum value of 2Δ initially (which is twice of the chunk duration; the target buffer level cannot be zero, and the value 2Δ is chosen empirically).

$$x_r(t) = \begin{cases} \max\left(2\Delta, \frac{x_r t}{\tau}\right), & 0 \leq t \leq \tau \\ x_r, & t > \tau \end{cases} \quad (2.18)$$

In the above design, $x_r(t)$ follows a ramp change. For such a ramp change, the system in Eq. (2.11) can track x_r with the error proportional to the inverse of the so-called velocity constant K_v in the steady state [48]. From the transfer function Eq. (2.12), we derive K_v as $1/K_v = K_p(1 - \beta)/K_i$. Evidently, when $\beta = 1$, the steady state error is zero, and is non-zero when $\beta < 1$. Therefore, we choose $\beta = 1$ for the above choice of $x_r(t)$.

We explored the choice of α (as 2 or 4) and τ (as 2, 5, or 10 minutes). Fig. 2.12 plots the performance of PIA-E versus other schemes, $\alpha = 4$ and $\tau = 5$ minutes (which

achieves the best tradeoff). The results when playing up to 2, 5, 10 or 20 minutes of the video are shown in the figure. We observe that for the first 2 minutes, PIA-E indeed leads to significantly higher bitrate: the average bitrate is 14% higher than that of PIA, 27% higher than that of BBA and only 8% lower than that of MPC. On the other hand, the average bitrate change for PIA-E is higher than that of PIA, but still 9% less compared to MPC on average. The amount of rebuffering of PIA-E is similar to that of PIA. When the ending time is larger (i.e., 5, 10 or 20 minutes), the performance of PIA-E is very close to PIA, confirming that the more aggressive bitrate choice of PIA-E for the early part of the video does not adversely affect the performance for the later part of the video.

Other designs. In the above design, we set $K_p(t)$ and $x_r(t)$ as piece-wise linear functions. We also explored setting them as exponential functions, and observed that the resultant design can achieve similar performance. In addition, we have explored dynamically adjusting $K_p(t)$ and $\beta(t)$, and observed similar performance³. Last, we explored dynamically adjusting a single parameter (e.g., $x_r(t)$), and observed that the resultant performance is inferior to that when adjusting two parameters simultaneously.

2.6 Evaluation using DASH Implementation

We have implemented PIA and PIA-E using `dash.js` (version 2.2.0) [53], a production quality open source framework provided by DASH Industry Forum [54]. To evaluate the performance of PIA and PIA-E under realistic network settings, we create an emulation environment as follows. We use a Linux machine running Apache `httpd` as the video server and a Windows laptop (with i7-5700HQ 3.50 GHz CPU and 16 GB memory) as the client. The server and client are connected by a 100 Mbps Ethernet link. We apply the Linux `tc` tool at the server to emulate the downlink bandwidth using the LTE bandwidth traces that we collected. The latency between the server and client is set to

³ Note that in Eq. (2.11), since u_t is affected by the product of β and x_r , it is sufficient to vary either $\beta(t)$ or $x_r(t)$; there is no need to vary them simultaneously.

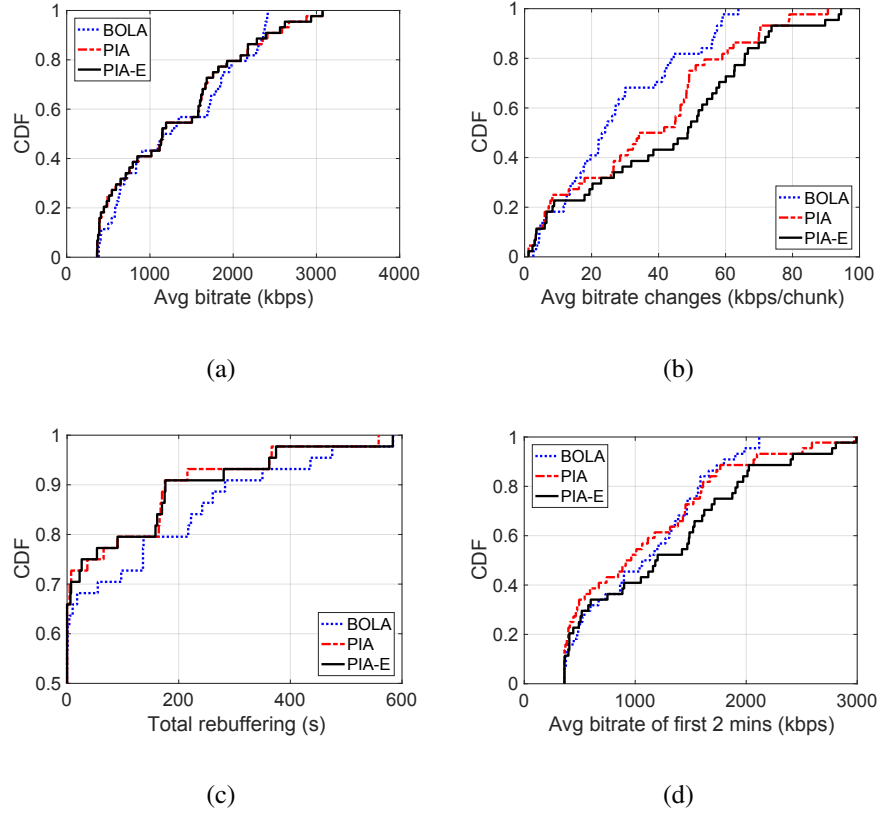


Fig. 2.13: Performance comparison in DASH (music show, chunk duration 2 s, video length 15 minutes, startup latency 10 s).

70 ms as it is the average latency reported by OpenSignal’s latency report. The client uses Chrome browser to run `dash.js`.

Implementation of PIA and PIA-E in `dash.js`. We implemented two new ABR streaming rules (each about 400 LoC) in `dash.js` to realize PIA and PIA-E. The parameters used for PIA and PIA-E are as those used in Sections 2.4 and 2.5, respectively. The bandwidth estimation requires knowing the past throughput per second (we use the harmonic mean of the throughput of the past 20 seconds). We therefore further developed a bandwidth estimation module that uses progress events in `dash.js` to obtain the past throughput per second. Specifically, when receiving one progress event, we calculate the number of bytes downloaded since the last event.

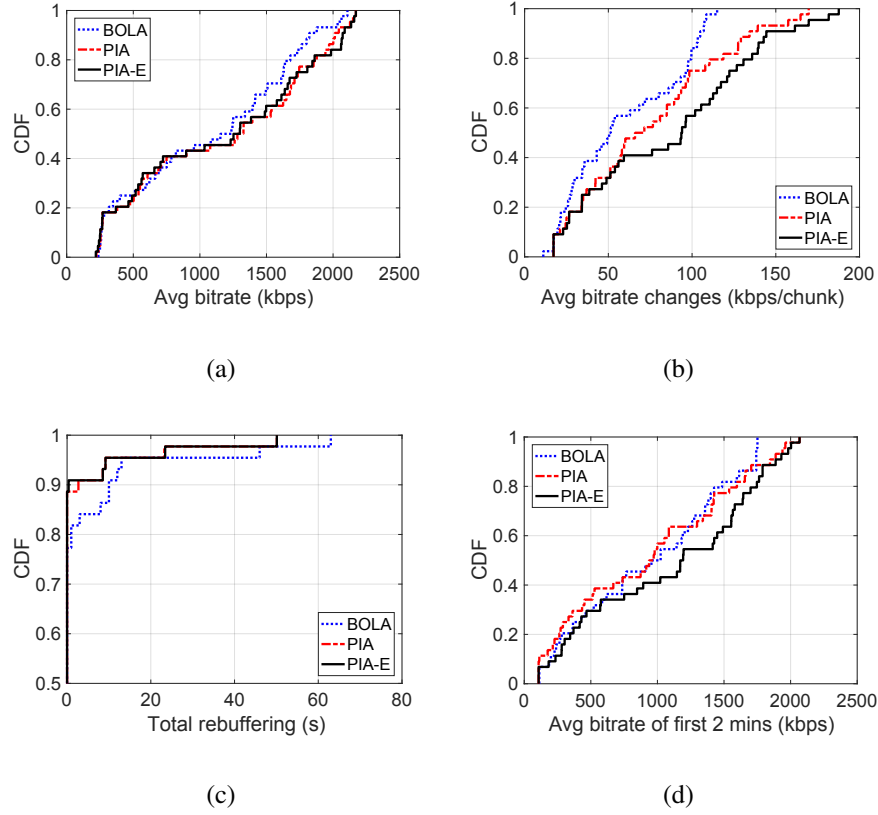


Fig. 2.14: Performance comparison in DASH (BBB, chunk duration 5 s, video length 10 minutes, startup latency 10 s).

Videos. We use three CBR videos encoded using FFmpeg [55]. The first video is a music show, around 15 minutes long, with five tracks of resolution 240p, 360p, 480p, 720p and 1080p, respectively (the bitrate of the tracks varies from 0.36 to 3.09 Mbps); the chunk duration is 2 s. The other two videos are Big Buck Bunny (BBB) and Tears of Steel (ToS), both around 10 minutes long, with chunk duration of 5 s. ToS has five tracks, with the same resolutions and slightly lower bitrate (0.32 to 2.84 Mbps across the tracks) compared to the music show. BBB has one additional lower track (144p resolution) and the bitrate of the six tracks varies from 0.11 to 2.20 Mbps.

Comparing simulation and implementation results. We compare the results obtained from our `dash.js` implementation with those from the simulations, and con-

firm that the results are consistent. Specifically, for the music show, under PIA, 90% of the relative differences between implementation and simulation results are within 6.5% for average bitrate; for bitrate changes and rebuffering duration, 90% of the absolute differences are within 15 Kbps/chunk and 3 s, respectively. The results for PIA-E are similar. The performance differences between implementation and simulation results are due to multiple reasons. First, the simulation assumes a perfect CBR video where all the chunks in the same track have exactly the same bitrate; the video used in the implementation, while encoded as CBR, has bitrate variability across the chunks. Second, the implementation results are affected by various practical factors (e.g., server response time, client computational and response time, network RTT and TCP window size), which are not accounted for in the simulations.

Performance comparison. We compare the performance of PIA and PIA-E with a state-of-the-art scheme, BOLA [11], that was implemented in `dash.js` version 2.2.0. BOLA selects the bitrate to maximize a utility function considering both rebuffering and delivered bitrate. The upper threshold of BOLA is set to 60 s (the default value is 30 s) to be compatible with the target buffer level of 60 s in PIA. Fig. 2.13 plots the QoE metrics of PIA, PIA-E and BOLA for the music show video. We observe that PIA-E achieves higher average bitrate than PIA and BOLA for the first 2 minutes of the video. For the entire video, PIA-E leads to comparable performance as PIA: PIA-E leads to slightly more rebuffering, and similar average bitrate and bitrate changes. BOLA has higher rebuffering and lower bitrate changes than PIA and PIA-E. Fig. 2.14 plots the results for the BBB video. We observe similar results as those for the music show except that (i) the average bitrate change per chunk for all the three schemes is larger, which is due to the larger chunk duration in BBB (5 versus 2 s), and (ii) the amount of rebuffering is significantly lower due to the much lower bitrate of the lowest track in BBB (0.11 versus 0.36 Mbps). For ToS, the average bitrate change per chunk is similar to that for BBB due to the same chunk duration of 5 s of these two videos, and the amount of rebuffering is similar to that of the music show due to the similar bitrate of

the lowest track of these two videos (the figures are omitted in the interest of space).

Runtime overhead. We record the CPU execution time of the ABR logic in the JavaScript code when a video is being played. The execution time of the default ABR logic in the `dash.js` player is 1.2 s for the entire 15-min music show video. The execution time of our PIA logic is 1.9 s, only slightly larger than that of the default ABR logic. For PIA-E, the execution time is 2.0 s (compared to PIA, it has additional calculation of $K_p(t)$ and $\beta(t)$). The execution time PIA-E and for the other two videos is similar. The above results indicate that PIA incurs very small runtime overhead, despite its non-trivial decision process shown in Fig. 2.2.

2.7 Conclusion and Future work

In this chapter, we have explored using feedback control theory for creating the adaptation logic component critical to ABR video streaming. By strategically applying a PID controller in an explicit and adaptive manner, PIA considerably outperforms the state-of-the-art video streaming schemes in balancing the complex tradeoffs associated with the key QoE metrics, as demonstrated by extensive evaluations. PIA is also lightweight and easy to deploy. We believe the same high-level principle can be applied to other multimedia applications with content quality adaptation, such as live video conferencing. In our future work, we plan to port our implementation to mobile devices to better assess PIA's performance in the wild, and also conduct deeper exploration of other network and streaming settings (e.g., live streaming).

Chapter 3

ABR Streaming of VBR-encoded Videos: Characterization, Challenges, and Solutions

3.1 Introduction

Adaptive Bitrate (ABR) streaming (specifically HLS [3] and DASH [4]) has emerged as the *de facto* video streaming technology in industry for dynamically adapting the video streaming quality based on varying network conditions. A video is compressed into multiple independent *streams* (or *tracks*), each specifying the same content but encoded with different bitrate/quality. A track is further divided into a series of *chunks*, each containing data for a few seconds' worth of playback. During streaming playback, to fetch the content for a particular play point in the video, the adaptation logic at the client player dynamically determines what bitrate/quality chunk to download.

The video compression for a track can be (1) Constant Bitrate (CBR) – encodes the entire video at a relatively fixed bitrate, allocating the same bit budget to both *simple scenes* (i.e., low-motion or low-complexity scenes) and *complex scenes* (i.e., high-motion or high-complexity scenes), resulting in variable quality across scenes, or (2) Variable Bitrate (VBR) – encodes *simple scenes* with fewer bits and *complex scenes* with more bits, while maintaining a consistent quality throughout the track.

VBR presents some key advantages over CBR [22], such as the ability to realize better video quality for the same average bitrate, or the same quality with a lower bitrate encoding than CBR. Traditionally, streaming services mainly deployed only CBR,

partly due to various practical difficulties including the complex encoding pipelines for VBR, as well as the demanding storage, retrieval, and transport challenges posed by the multi-timescale bitrate burstiness of VBR videos. Most recently content providers have begun adopting VBR encoding [14, 23, 24], spurred by the promise of substantial improvements in the quality-to-bits ratio compared to CBR, and by technological advancements in VBR encoding pipelines. Current commercial systems and ABR protocols do not fully make use of the characteristics of VBR videos; they typically assume a track’s peak rate to be its bandwidth requirement when making rate adaptation decisions [24]. Existing ABR streaming research centered mostly on CBR encoding, and very little on the VBR case (see §3.7). Therefore there exists little prior understanding of the issues and challenges involved in ABR streaming of VBR videos.

In this chapter, we explore a number of important open research questions around ABR streaming for VBR-encoded video. We make the following main contributions:

- We analyze the characteristics of VBR videos (§3.3) using a rich set of videos spanning diverse content genres, predominant encoding technologies (H264 [31] and HEVC (H.265) [32]) and platforms (§3.2). Jointly examining content complexity, encoding quality, and encoding bitrates, we identify distinguishing characteristics of VBR encodings that impact user QoE, and their implications for ABR rate adaptation and QoE metrics. We find that, for real-world VBR encoding settings, complex scenes, although encoded with more bits, have inferior encoding quality compared to other scenes in the same track, across a range of video quality metrics. We also find that different chunk sizes across the video can be used to identify relative scene complexity with high accuracy. These two key observations (i) suggest the need to provide complex scenes with *differential treatment* during streaming, as improving the quality of complex scenes brings more QoE enhancement compared to improving simple scenes [27], and (ii) provide us a practical pathway towards achieving this differential treatment in the context of today’s *de facto* ABR protocols where the scene complexity or quality information is typically unavailable to the ABR logic.

- Based on our analysis, we enunciate three key design principles (*non-myopic*, *differential treatment*, and *proactive*) for ABR rate adaptation for VBR videos (§3.4). These principles explicitly account for the characteristics of VBR videos (including scene complexity, quality, and bitrate variability across the video). Specifically, the *non-myopic* principle dictates considering multiple future chunks when making rate adaptation decisions, leading to better usage of the available network bandwidth; the *differential treatment* principle strategically favors complex scenes over simple scenes for better user QoE; the last principle proactively reacts to chunks' variable sizes/bitrates by, for example, pre-adjusting the target buffer level, thus further facilitating the smoothness and adaptiveness of VBR streaming.
- We design CAVA (Control-theoretic Adaption for VBR-based ABR streaming), a novel, practical ABR rate adaptation algorithm based on concrete instantiations of these principles (§3.5). CAVA uses control theory that has shown promise in adapting to dynamic network bandwidth such as that in cellular networks [13, 56]. Its design involves two tightly coupled controller loops that work in synergy using easy-to-obtain information such as VBR chunk sizes and historically observed network bandwidth. Specifically, CAVA improves the QoE by (i) using Proportional-Integral-Derivative (PID) control concepts [45] to maintain a dynamic target buffer level to limit stalls, (ii) judiciously selecting track levels to maximize the quality while minimizing quality changes, and (iii) strategically favoring chunks for complex scenes by saving bandwidth for such chunks.
- We evaluate the performance of CAVA for a wide range of real-world network scenarios, covering both LTE and broadband (§3.6). Our results show that CAVA considerably outperforms existing state-of-the-art ABR schemes across several important dimensions. It provides significantly enhanced quality for complex scenes while not sacrificing the quality of other scenes. Depending on the video, the percentage of low-quality chunks under CAVA is up to 75% lower than that of other schemes. CAVA also leads to substantially lower rebuffering (up to 95%) and quality variation (up to 48%).

The network data usage under CAVA is in the same ballpark or slightly lower than most of the other schemes. The above results demonstrate that CAVA achieves a much better balance in the multiple-dimension design space than other schemes.

The performance improvements hold across a wide spectrum of settings, indicating that the three design principles hold broadly. Our implementation of CAVA in the open source `dash.js` [53] player further demonstrates that CAVA is lightweight and practical.

3.2 The VBR Video Dataset

Our video dataset includes 16 videos: 8 encoded by YouTube, and 8 encoded by us using FFmpeg [55], following specifications in [57]. Each video is around 10 minutes, and includes 6 tracks/levels (we use the terms *track* and *level* interchangeably) for ABR streaming, with resolutions of 144p, 240p, 360p, 480p, 720p, and 1080p, respectively.

Our use of YouTube and FFmpeg encodings complement each other. YouTube represents the state-of-the-art practice of VBR encoding from a popular commercial streaming service. With FFmpeg, we explore state-of-the-art VBR encoding recommendations from another commercial streaming service, Netflix [57]. We also use FFmpeg to explore a variety of other settings (e.g., 4x-capped video (§3.3.3), H.265 encoding) beyond the above cases. We next explain in detail how we obtain our dataset.

Videos Encoded by FFmpeg. We select 4 publicly available *raw* videos from [58]. These videos include Elephant Dream (ED), Big Buck Bunny (BBB), Tears of Steel (ToS), and Sintel, in the categories of animation and science fiction. We encode these 4 raw videos into 4 H.264 and 4 H.265 videos using FFmpeg (8 encoded videos in total). For each video, we choose the aforementioned six tracks (144p to 1080p), consistent with [59]. To encode each track, we follow the per-title “three-pass” encoding procedure from Netflix [57]. In the first pass, a video clip is encoded using a fixed constant rate factor (CRF) value, which accounts for motion and has been shown to outperform other methods such as constant quantization parameter (QP) [60]. In the second

and third passes, we use the output bitrates of the first step to drive a two-pass VBR encoder to avoid over-allocating bits for simple scenes and under-allocating bits for complex scenes. In practice, *capped VBR* (i.e., the chunk bitrate is capped at a certain high limit) is often used to limit the amount of bitrate variability and enable the player to estimate the incoming chunk sizes [24]. Following the latest recommendations from HLS [38], we encode the videos to be 2× capped (i.e., the peak bitrate is limited to 200% of the average) using `-maxrate` and `-bufsize`, two options in FFmpeg. After a track is encoded, we segment it into 2-sec chunks.

Our encoding uses both the widely adopted H.264, and a more recent and efficient codec, H.265 [32]. We use CRF value of 25, which provides good viewing quality [57, 60].

For an encoded video, we assess its quality relative to a *reference video* (§3.3.1), which is its corresponding raw video footage.

Videos Encoded by YouTube. We upload the aforementioned 4 raw videos to YouTube and download the encoded videos using `youtube-dl` [61]. We also downloaded 4 other videos from YouTube, in the categories of sports, animal, nature and action movies.

The highest quality track of these 4 videos has a resolution of 2160p, with average bitrate of 14 – 18 Mbps, significantly higher than lower tracks. To be consistent with the other videos which were 6-track with top track at 1080p, for these 4 videos, we use the bottom six tracks between 144p and 1080p as the set of tracks for ABR adaptation. We use the top track (2160p) as the reference video to measure the video quality of the lower tracks, as we do not have the raw source for these videos. All YouTube videos are encoded using H.264 codec [31], with chunk duration around 5 seconds, consistent with that in [62].

Chunk Duration and Bitrate Variability. Overall, our dataset includes two chunk durations: 2 (FFmpeg encodings) and 5 seconds (YouTube encodings). They are consistent with the range of chunk durations (2 to 10 seconds) that are used in

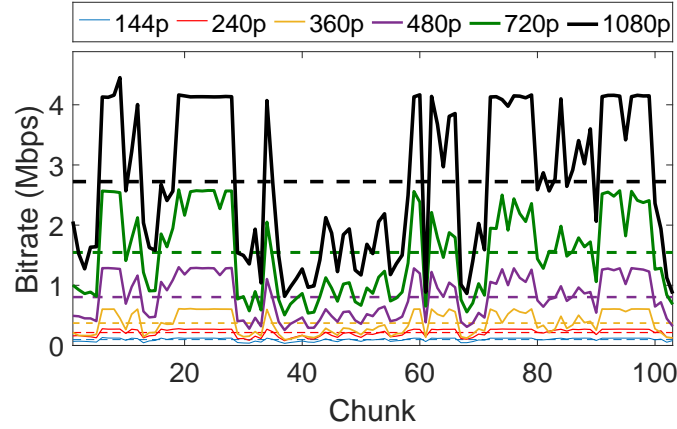


Fig. 3.1: Bitrate of the chunks of a VBR video (Elephant Dream, H.264, YouTube encoded).

commercial services [24], and allow us to investigate the impact of chunk duration on the performance of ABR streaming in §3.6. All encoded videos exhibit significant bitrate variability: the coefficient of variation of the bitrate in a track varies from 0.3 to 0.6. Fig. 3.1 shows an example YouTube video; the six horizontal dashed lines mark the average bitrate of the six tracks. All encodings are capped VBR: for YouTube videos, the maximum bitrate of a track ranges between $1.1\times$ to $2.3\times$ the average bitrate; for the FFmpeg videos, the corresponding range is $1.4\times$ to $2.4\times$. Note that although we set the cap to $2\times$ explicitly for FFmpeg, the resulting videos can exceed the cap slightly to achieve the specified quality. For all videos, the two lowest tracks have the lowest variability, since the low bitrate limits the amount of variability that can be introduced in VBR encoding; for all the other tracks, the ratio is 1.4 to 2.4.

3.3 VBR Streaming: Challenges

We now analyze our video dataset described in §3.2: we first present the characteristics of VBR encoding, and then show its implications for ABR streaming, highlighting challenges of streaming VBR videos.

3.3.1 VBR Video Characteristics

Scene Complexity and Chunk Size

Classifying chunks by scene complexity is useful for ABR streaming since the knowledge of scene complexity can be used for rate adaptation. For instance, since complex scenes in a video play a particularly important role in viewing quality [27], the player may choose higher tracks for complex scenes to bring more enhancement to viewing experience.

One way of determining scene complexity is through Spatial information (SI) and Temporal Information (TI) [63], two commonly used metrics for quantifying the spatial and temporal complexity of the scenes. This approach, however, requires computation-heavy content-level analysis. More importantly, such scene complexity information is not available in the complex ABR streaming pipeline in today’s commercial services, and would involve non-trivial changes to realize, including resources to compute the complexity information and new features to the ABR streaming standard specifications. Below, we propose a simple and lightweight method that uses relative chunk size to approximate scene complexity, and can be readily used for ABR streaming (§3.3.2).

Our approach is motivated by the following two properties. (1) Since the VBR encoding principles dictate that simple scenes are encoded with fewer bits and complex scenes with more bits [64], we expect that the relative size of a chunk (in bytes) can be used as a proxy for the relative scene complexity. (2) Since the scene complexity is a function of the content itself (e.g., motion, details in the scene), we expect that the scene complexity at a given playback point in a video is consistent among different tracks. Combining with the property that the relative size of a chunk is correlated with the scene complexity, we expect that a chunk that is relatively large/small in one track (compared to other chunks in that track) is also relatively large/small in another track.

We verify the above two properties as follows. To verify Property (1), we calculate the SI and TI values (recall that SI and TI are two commonly used complexity

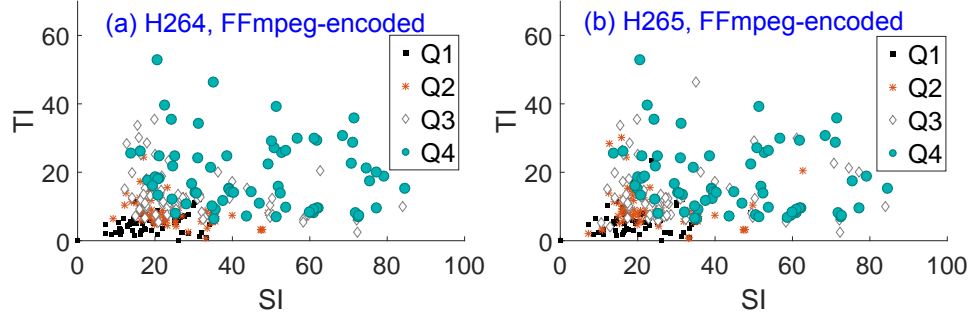


Fig. 3.2: Chunk SI & TI (Elephant Dream, Track 3).

metrics) for each chunk in a video. Specifically, we obtain SI and TI values from the raw video, which is not affected by encoding distortion, and hence the SI and TI values thus obtained reflect the inherent scene complexity more accurately. We then consider an encoded video, for each track, we classify the chunks into four categories, based on their size distribution. Specifically, a chunk with a size falling into the first quartile is called a Q1 chunk, and a chunk with a size falling into the second quartile is called a Q2 chunk, and so on. We observe that indeed chunks in lower quartiles have lower SI and TI values, while the Q4 chunks tend to have the largest SI and TI values. Fig. 3.2 shows an example. For the H.264 encoding, Fig. 3.2(a) shows that 78% of Q4 chunks have SI and TI larger than 25 and 7, respectively, while only 11% of Q1 chunks and 14% of Q2 chunks have SI and TI larger than these thresholds. For H.265 (Fig. 3.2(b)), 75% of Q4 chunks have SI and TI larger than 25 and 7, respectively, while only 5% of Q1 chunks and 14% of Q2 chunks have SI and TI larger than these thresholds. To verify Property (2), let $\{c_{\ell,1}, \dots, c_{\ell,n}\}$ denote the sequence of the chunk categories for track/level ℓ , where $c_{\ell,i} \in \{1, 2, 3, 4\}$ represents the category of the i th chunk in track ℓ , and n is the number of chunks in a track. We then calculate the correlation between each pair of tracks. Our results confirm that all the correlation values are close to 1, indicating that chunks with the same index (i.e., at the same playback position) are indeed in consistent categories across tracks.

The above two properties together suggest that we can classify chunks into differ-

ent categories of scene complexity simply based on chunk size. For consistent classification across tracks, we can leverage the consistent relative sizes across tracks, use one track as the reference track, and classify chunks at different playback positions based on their chunk sizes in that track (so that chunks with the same index will be in the same class). Specifically, we choose a reference track (e.g., a middle track), and classify the chunks at different playback positions into four categories, Q1, Q2, Q3, and Q4 chunks, based on which quartile that the size of a chunk falls into. After that, all chunks in the same playback positions are placed into the same category, regardless of the tracks.

The above classification method is based on quartiles. Other methods can also be used (e.g., using five classes instead of four classes); our design principles (§3.4) and rate adaptation scheme (§3.5) are independent of this specific classification method.

Scene Complexity and Encoding Quality

After classifying chunks into the four categories as above, we now analyze the encoding quality of the chunks in each category. VBR encoding allocates fewer bits to simple scenes and more bits to complex scenes so as to maintain a constant quality across the scenes [64]. We show below, however, the quality across the scenes is not constant in a specific track. Specifically, we use three quality metrics, Peak Signal-to-Noise Ratio (PSNR), Structural Similarity Index (SSIM) [65], and Video Multimethod Assessment Fusion (VMAF) [66, 67, 68]. PSNR is a traditional image quality metric. The PSNR of a chunk is represented as the median PSNR of all frames in that chunk. SSIM is a widely used perceptual quality metric; it utilizes local luminance, contrast and structure measures to predict quality. VMAF is a recently proposed perceptual quality metric that correlates quality strongly with subjective scores and has been validated independently in [69]. There are two VMAF models: *TV model* for larger screens (TV, laptop, tablet), and *phone model* for smaller screens (phones). The aggregate VMAF of a chunk can be calculated in multiple ways [70]. We use the median VMAF value of all frames in a chunk as the VMAF value for the chunk (using mean leads to similar values for the

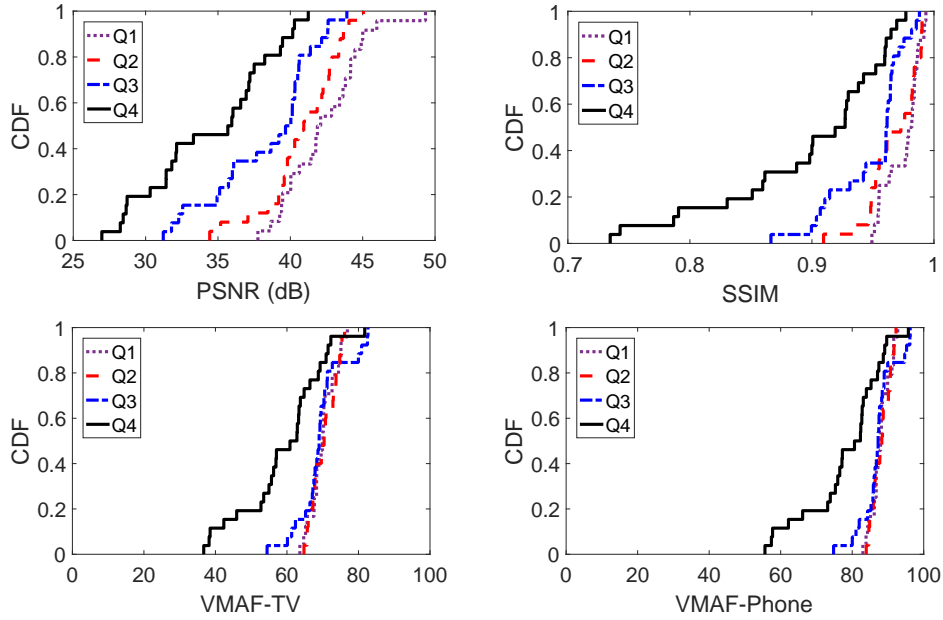


Fig. 3.3: Quality of chunks in a VBR video (Elephant Dream, YouTube encoded, H.264).

videos in our dataset).

Fig. 3.3 plots the CDF of the quality, measured in PSNR, SSIM, VMAF TV, and VMAF phone model, for a YouTube-encoded video. For each quality metric, the results of a middle track (480p) are shown in the figure. We observe that, while Q1 to Q4 chunks have increasing sizes (in bits), they have decreasing quality. In addition, the quality gap between Q4 and Q1–Q3 chunks is particularly large, despite that Q4 chunks have the most bits. This is because it is challenging to encode complex scenes to have the same quality of simple scenes. We make similar observations for videos encoded using FFmpeg and H.265 encoded videos (figures omitted).

3.3.2 Implications for Rate Adaptation

As described above, we have identified two important characteristics of VBR encoding: (1) *the relative size of a chunk (relative to the other chunks in the same track) is a good indication of the scene complexity*, and (2) *complex scenes, despite being encoded with more bits, have inferior qualities compared to other scenes in the same track, across*

a range of quality metrics. They both have important implications on rate adaption during VBR streaming process.

In particular, the second observation is opposite to what one would like to achieve during playback, where having higher quality for complex scenes is more important [27]. It indicates that complex scenes need to receive differential treatment to achieve a higher quality,

which requires (i) inferring the scene complexity, and (ii) carefully designing ABR streaming algorithms. The first requirement can be achieved based on our first observation, by using chunk sizes to infer scene complexity. It has two advantages compared to using those based on video content (e.g., SI and TI). First, it is simple to compute. Second, chunk sizes are already known at the client in current dominant ABR standards¹.

Achieving the second requirement is very challenging.

Given that complex scenes are already encoded with more bits than other scenes in the same track, choosing higher tracks for complex scenes indicates that a significant amount of network bandwidth needs to be allocated to stream complex scenes, which may come at the cost of lower tracks for simple scenes. We therefore need to design ABR streaming schemes to judiciously use network bandwidth, favoring Q4 chunks while not degrading the quality of other chunks too drastically (§3.4, §3.5).

3.3.3 VBR with Larger Cap

In this chapter, we mainly use 2× capped VBR videos. The bitrate cap, while limits the amount of bitrate variability and makes it easier to stream VBR videos over the Internet, also limits the quality of the videos, particularly for complex scenes. The recommendation on VBR encoding has been evolving. The original recommendation was to set the cap to 1.1× [3], and has now evolved to 2× [38]. It is conceivable that

¹ Chunk size information is included in the manifest file sent from server to client in DASH, and more recently HLS has added this feature [24].

the cap will be even larger in the future. For this reason, we further encode one of the publicly available videos to be $4\times$ capped.

We observe that the characteristics described in §3.3 still hold for this video. Specifically, Q4 chunks, even under $4\times$ cap, are still of significantly lower quality than other chunks.

As an example, for the middle track (480p), the median VMAF value (phone model) for the Q4 chunks is 79, significantly lower than the values of 88, 88, and 85 for Q1 to Q3 chunks. This might be because it is inherently very difficult to encode complex scenes to reach the same quality as simple scenes [71]. Therefore, for VBR videos of larger caps, we still need to incorporate these characteristics when designing ABR schemes (§3.6.6).

3.4 Design Principles

We believe that a good rate adaptation scheme for VBR videos must (i) take the per-chunk bitrate information into consideration (also suggested by [24]), which is available to the clients in dominant ABR standards (see §3.3.2), and (ii) use per-chunk bitrate information properly, by incorporating the characteristics of VBR videos. We next propose three design principles for VBR video rate adaptation.

Be Non-myopic (P1). This requires considering not only the bitrate of the immediate next chunk, but also the bitrate of multiple future chunks. A myopic scheme only considers the bitrate of the immediate next chunk, leading to level selections that only match the current resource (in terms of network bandwidth or player buffer level). As a result, a myopic scheme oftentimes mechanically selects very high (low) levels for chunks with small (large) sizes – exactly the opposite to what is desirable for VBR videos (§3.3). We illustrate this using two myopic schemes: (i) BBA-1 [14], a buffer-based scheme, and (ii) a rate-based scheme [28], referred to as RBA henceforth. Both schemes are myopic: when selecting the track for the next chunk, BBA-1 selects the highest track based on a *chunk map*, which defines the allowed chunk sizes as a range

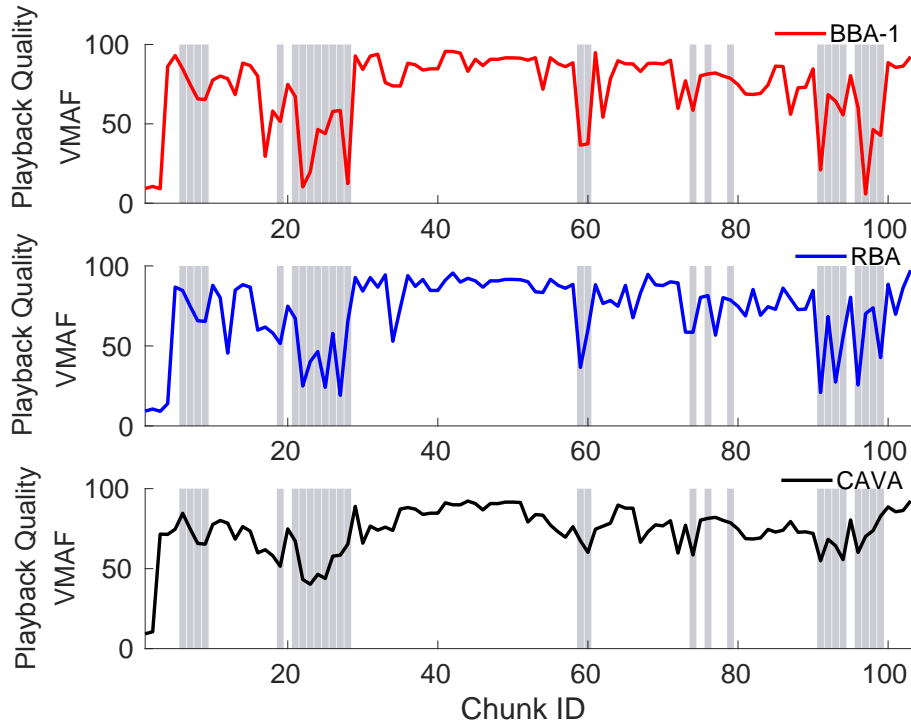


Fig. 3.4: Two myopic schemes and CAVA.

from the average chunk size of the lowest track to that of the highest track; RBA selects the highest track so that after downloading the corresponding chunk, the player buffer will still contain at least four chunks, where the downloading time of a chunk is obtained as its size divided by the estimated network bandwidth. Fig. 3.4 shows an example that illustrates the performance of BBA-1 and RBA (the top two plots), where the shaded bars mark the playback positions of Q4 chunks. We observe that indeed BBA-1 and RBA tend to lead to low qualities for Q4 chunks (recall that these tend to correspond to complex scenes) and high qualities for Q1-Q3 chunks (with simpler scenes). For comparison, we also plot our scheme CAVA (to be described in §3.5) in Fig. 3.4. In this example, for BBA-1 and RBA, the average VMAF quality of Q4 chunks is 49 and 52, and the amount of rebuffering is 6s and 4s, respectively; both are significantly worse than our scheme CAVA, under which the average VMAF quality of Q4 chunks is 65 with no rebuffering.

Offer Differential Treatment (P2). This principle favors more complex scenes

by explicitly accounting for the chunk size and quality characteristics of VBR videos (§3.3.2). The differential treatment can be achieved by using resources saved from simple scenes for complex scenes. While this suggests potentially lower quality for simple scenes, a good VBR rate adaptation scheme needs to achieve a balance: improve the quality of complex scenes while not degrading too much the quality of simple scenes. This principle is particularly important when complex scenes have lower quality than simple scenes in the same track, as we have observed in §3.3.1, since in this case, it is preferable to choose a higher track for complex scenes to achieve comparable quality as simple scenes. Even in an ideal VBR encoding, where complex scenes have similar quality as simple scenes in the same track, this principle is still important, since complex scenes, being of larger sizes, naturally need more resources than simple scenes in the same track. Offering differential treatment thus helps the VBR algorithm make judicious rate adaptation decisions when the network bandwidth is limited.

Be Proactive (P3). Since VBR videos have high bitrate variability and the size/bitrate of future chunks is known beforehand, it is desirable to account for the variability proactively. This is especially true for complex scenes corresponding to large chunks. Suppose when making a decision at time t , the player notices that consecutive positions after t contain complex scenes. If the playback buffer is low and the network bandwidth is low, then rebuffering will inevitably occur. Fortunately, with the known chunk size information, the rate adaptation algorithm can, instead, react to the cluster of large chunks *early*—before time t instead of right at t —by, for example, pre-adjusting the target buffer level for buffer-related approaches.

Discussion. Several existing schemes [13, 27, 56] use a window-based approach that considers multiple future chunks in bitrate adaptation, which differs from our non-myopic principle that is motivated specifically by the dynamic chunk bitrates/sizes of VBR videos (§3.5.3). Note that **P1** and **P3** share in common that they both require considering future chunks. But they differ mainly in the timescale: the non-myopic principle considers a small number of future chunks to account for the variability of

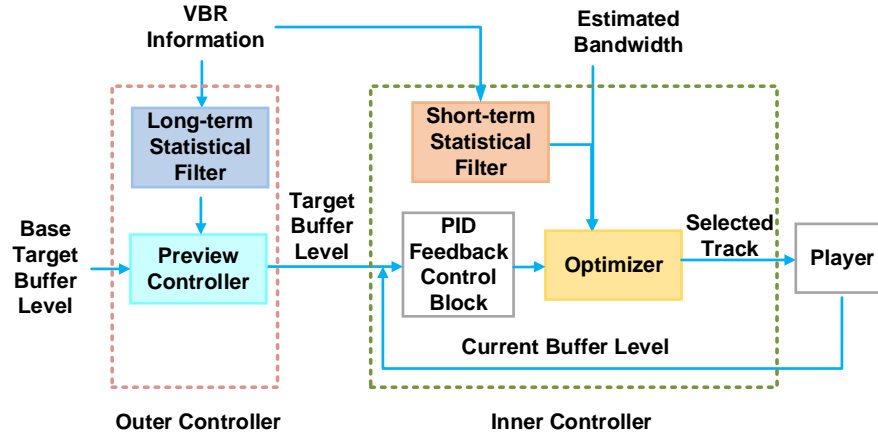


Fig. 3.5: CAVA design diagram.

VBR videos in the short timescale, in order to facilitate the *current* decision; the proactive principle, on the other hand, considers chunks further away in future to benefit *future* decisions in a proactive manner.

3.5 CAVA Design and Implementation

We now instantiate the three principles (§3.4) and design a control-theoretic rate adaptation scheme, CAVA, for VBR streaming. The reason for adopting a control-theoretic approach is because it has shown promise in adapting to dynamic network bandwidth [13, 56]. The design of CAVA is compatible with the current dominant ABR standards (DASH and HLS), and can be readily used in practice.

3.5.1 Overview of CAVA

We design CAVA to address both chunk size variability, an inherent feature of VBR videos, and quality variability in VBR videos, a characteristic that we identified in today’s VBR encodings (§3.3.1). Even under an ideal VBR encoding where complex scenes have similar quality as other scenes in the same track, CAVA still has its value in addressing the inherent chunk size variability of VBR videos.

Fig. 3.5 shows the design diagram for CAVA, which builds on the basic feedback

control framework [56]. CAVA introduces significant innovations by (i) generalizing the control framework from plain CBR to VBR, (ii) designing an inner controller that reacts in short timescale, and incorporates the *non-myopic* and *differential treatment principles*, and (iii) designing an outer controller that reacts over a longer timescale, and incorporates the *proactive principle*.

The control framework uses PID control [45], a widely used feedback control technique. The reason for using PID control is its good performance and robustness [56]. As shown in Fig. 3.5, CAVA consists of two controllers that work in synergy to realize the aforementioned three principles.

- The *inner controller* is responsible for selecting the appropriate track level. It employs a PID feedback control block that maintains the target buffer level by properly adjusting the control signals (§3.5.2). Then based on the controller’s output, together with the estimated bandwidth and a short-term average of future chunks’ bitrate, CAVA invokes an optimization algorithm that incorporates non-myopic (**P1**) and differential treatment (**P2**) principles to perform VBR-aware track level selection (§3.5.3).
- The *outer controller*’s job is to determine the target buffer level that is used by the inner controller. When doing so, CAVA exercises proactive principle (**P3**) to adjust the target buffer level proactively based on dynamics of future chunks (§3.5.4).

3.5.2 PID Feedback Control Block

The PID feedback control continuously monitors an “error value”, i.e., the difference between the target and current buffer levels of the player, and adjusts the control signal to maintain the target buffer level. To account for the characteristics of VBR videos, it considers per-chunk size information and uses a dynamic target buffer level. This differs from the PID controller design for CBR [56], which uses a fixed target buffer level and a fixed average bitrate for each track.

Specifically, let C_t denote the network bandwidth at time t . Let ℓ_t denote the track number selected at time t , with the corresponding bitrate of the chunk denoted as

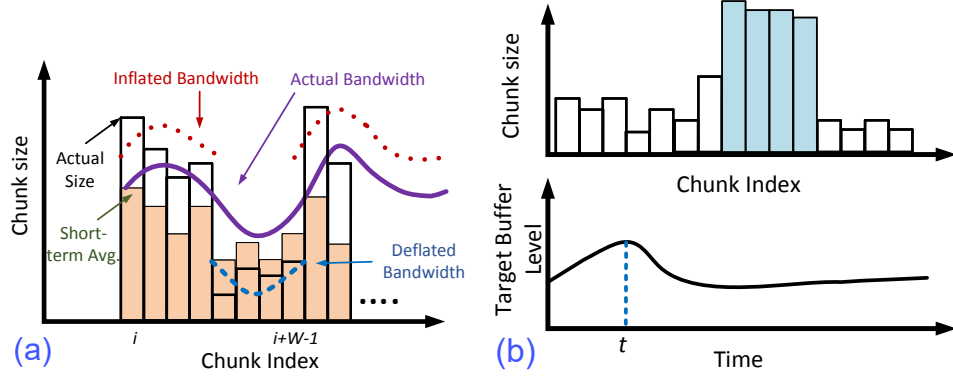


Fig. 3.6: Illustration of (a) track selection, and (b) setting target buffer level.

$R_t(\ell_t)$. We use $R_t(\ell_t)$ instead of $R(\ell_t)$ to reflect that it is a function of time t since for VBR videos, the bitrate varies significantly even inside a track. The controller output, u_t , is defined as

$$u_t = \frac{C_t}{R_t(\ell_t)}, \quad (3.1)$$

which is a unitless quantity representing the relative buffer filling rate. The control policy is defined as

$$u_t = K_p(x_r(t) - x_t) + K_i \int_0^t (x_r(t) - x_\tau) d\tau + \mathbf{1}(x_t - \Delta) \quad (3.2)$$

where K_p and K_i denote respectively the parameters for proportional and integral control (two key parameters in PID control), x_t and $x_r(t)$ denote respectively the current and target buffer level at time t (both in seconds), Δ denotes the playback duration of a chunk, and the last term, $\mathbf{1}(x_t - \Delta)$, is an indicator function (it is 1 when $x_t \geq \Delta$ and 0 otherwise), which makes the feedback control system linear, and hence easier to control and analyze. The target buffer level is dynamic, set by the outer controller (§3.5.4).

3.5.3 The Inner Controller

The inner controller determines ℓ_t , the track at time t . Based on the definition in Eq. (3.1), once the controller output u_t is determined using Eq. (3.2), we can simply determine ℓ_t so that the corresponding bitrate $R_t(\ell_t)$ is the maximum bitrate that is below \widehat{C}_t/u_t , where \widehat{C}_t is the estimated network bandwidth at time t . This approach is,

however, myopic (only considering the next chunk), and is thus undesirable for VBR videos.

We next formulate an optimization problem that accounts for both the non-myopic and differential treatment principles (§3.4) to determine ℓ_t . Fig. 3.6(a) illustrates the approach. Suppose at time t , we need to select the track number for chunk i . Following the non-myopic principle (**P1**), we consider a window of W chunks, from i to $i + W - 1$, and use the average bitrate of these W chunks to represent the bandwidth requirement of chunk i . This is handled by the “Short-term Statistical Filter” in Fig. 3.5. Using the average bitrate of W chunks (instead of the bitrate of chunk i) leads to smoother bandwidth requirement from the chunks, avoiding mechanically choosing very high (low) levels for chunks with small (large) bitrates.

To provide differential treatment (**P2**) to chunks with different complexities, we assume either *inflated* or *deflated* network bandwidth, depending on whether chunk i contains complex or simple scenes. For complex scenes, we assume inflated network bandwidth, allowing a higher track to be chosen, while for simple scenes, we assume deflated bandwidth so as to save bandwidth for complex scenes. The track selection algorithm maximizes the quality level to match the assumed network bandwidth, while minimizing the number of quality level changes between two adjacent chunks. In the example in Fig. 3.6(a), chunk i is a Q4 chunk, and hence we assume inflated bandwidth, which allows a higher level track to be selected.

Optimization Formulation. We next describe our optimization formulation. Our current design uses track level to approximate the quality since this is currently the only available quality information in predominant ABR standards; using such information only allows CAVA to be easily deployable. In our performance evaluation (§3.6), we use a perceptual quality metric (VMAF) to evaluate CAVA, and show that it achieves good perceptual quality although the formulation does not explicitly use a perceptual quality metric.

The optimization aims to minimize a weighted sum of two penalty terms: the

first term represents the deviation of the selected bitrate from the estimated network bandwidth, and the second term represents the track change relative to the previous chunk. Other formulations might also be possible; our empirical results show that this formulation works well in practice. Specifically, we aim to minimize

$$Q(\ell_t) = \sum_{k=t}^{t+N-1} \left(u_k \bar{R}_t(\ell_t) - \alpha_t \widehat{C}_k \right)^2 + \eta_t (r(\ell_t) - r(\ell_{t-1}))^2, \quad (3.3)$$

where u_k and \widehat{C}_k are respectively the controller output and the estimated link bandwidth for the k -th chunk, $\eta_t \geq 0$ is a parameter that represents the weight of the second term, $\bar{R}_t(\ell_t)$ is the average bitrate over a window of W chunks (according to **P1**), from t to $t + W$, at track ℓ_t (here we slightly abuse the notation to use t to represent the chunk index for time t), and $r(\ell)$ denotes the average bitrate of track ℓ .

Penalty on deviation from estimated bandwidth. The first term in Eq. (3.3) represents the penalty based on how much the required bandwidth deviates from the estimated network bandwidth. Specifically, minimizing this penalty term aims at selecting the largest ℓ_t (and hence the highest quality) so that the difference between the required bandwidth, $u_k \bar{R}_t(\ell_t)$, and the assumed bandwidth, $\alpha_t \widehat{C}_k$, is minimized (α_t is a factor that deflates or inflates the estimated bandwidth; see details later on). Following the non-myopic principle (**P1**), we use $\bar{R}_t(\ell_t)$ (instead of $R_t(\ell_t)$), which is the average bitrate of W future chunks, to represent the bandwidth requirement of chunk t . We refer to W as the *inner controller window size* and explore its configuration in §3.6.2.

When operating online, CAVA only has a limited view towards future network conditions. Therefore, the penalty term on deviation from estimated bandwidth considers the bandwidth needed to download a finite horizon of N future chunks. We assume that these N chunks are all from the same track, ℓ_t , to reduce the number of quality level changes. In the rest of the chapter, we set N to 5 chunks, a relatively short horizon to accommodate network bandwidth dynamics.

Note that several existing schemes [13, 27, 56] also examine a finite horizon of chunks in their online algorithms (controlled by N in CAVA). But none of them utilizes

concepts like our non-myopic principle in computing the bandwidth requirement from multiple future chunks (controlled by W in CAVA), whose sizes may vary significantly in VBR, for rate adaptation.

Penalty on track change. The second term in Eq. (3.3) represents the penalty on track change. Specifically, minimizing the second term aims at selecting ℓ_t so that its difference from ℓ_{t-1} , i.e., the track of the previous chunk, is minimized. We consider two categories of chunks, Q4 and non-Q4 chunks when setting η_t , a weight factor. If the current and previous chunks fall in different categories, we set η_t to 0; otherwise we set η_t to 1 (so as to give equal weight to the two terms in Eq. (3.3) since both are important for QoE). That is, we do not penalize quality change if two consecutive chunk positions are in different categories (and hence of different importance in viewing quality).

Recall that $r(\ell)$ denotes the average bitrate of track ℓ . The penalty term on track change uses $r(\ell_t) - r(\ell_{t-1})$, instead of $\ell_t - \ell_{t-1}$ or $R_t(\ell_t) - R_t(\ell_{t-1})$. This is because $r(\ell_t) - r(\ell_{t-1})$ reflects track change, and yet is in the unit of bitrate, which is the same as that of the first term in Eq. (3.3). The expression $\ell_t - \ell_{t-1}$ represents track change directly, whose unit is however different from that of the first term in Eq. (3.3); the expression $R_t(\ell_t) - R_t(\ell_{t-1})$ represents bitrate change on a per chunk level, which is not meaningful for VBR videos since even chunks in the same track can have highly dynamic bitrate.

Deflating/inflating network bandwidth estimate. In Eq. (3.3), $\alpha_t \widehat{C}_k$ represents the assumed network bandwidth for chunk k . As mentioned earlier, according to differential treatment principle (P2), we set $\alpha_t > 1$ for complex scenes to inflate the bandwidth, and set $\alpha_t < 1$ for simple scenes to deflate the bandwidth. Determining the value of α_t presents a tradeoff: a large value for complex scenes can lead to higher quality level, at the cost of potential stalls; similarly, a small α_t value for simple scenes, while can save bandwidth and eventually benefit complex scenes, may degrade the quality of simple scenes too much. We have varied α_t for complex scenes from 1.1 to 1.5, and varied α_t for simple scenes from 0.6 to 0.9. In the rest of the chapter, we set $\alpha_t = 1.1$

for Q4 chunks and $\alpha_t = 0.8$ for Q1-Q3 chunks, which lead to a good tradeoff observed empirically.

In addition, we use the following heuristic for Q1-Q3 chunks: if the current chunk is a Q1-Q3 chunk and the selected level is very low (i.e., level 1 or 2) under the above strategy, while the buffer level is above a threshold (chosen as 10 seconds in §3.6) indicating low risk of stalls, we do not deflate network bandwidth, and instead use $\alpha_t = 1$. This heuristic avoids choosing unnecessarily low levels for Q1-Q3 chunks. Similarly, we can use a heuristic for Q4 chunks: if the current chunk is a Q4 chunk and the buffer level is below a threshold indicating high risk of stalls, we can also set α_t to 1 (i.e., do not inflate network bandwidth). This heuristic can lead to lower stalls at the cost of potentially reducing the quality of Q4 chunks. Our evaluations show that in the settings that we explore, the number of stalls in CAVA is already very low even without using this heuristic. Therefore, in §3.6, we only report the results when this heuristic is disabled.

Time complexity. Let \mathcal{L} be the set of all track levels. The optimal track is

$$\ell_t^* = \arg \min_{\ell_t \in \mathcal{L}} Q(\ell_t). \quad (3.4)$$

We can find ℓ_t^* easily by evaluating (3.3) using all possible values of $\ell_t \in \mathcal{L}$, and selecting the value that minimizes the objective function. For every $\ell_t \in \mathcal{L}$, obtaining $Q(\ell_t)$ requires computation of N steps. Therefore, the total computational overhead of solving (3.4) is $O(N|\mathcal{L}|)$.

3.5.4 The Outer Controller

When using the inner controller alone, we observe that rebuffering sometimes happens when the network bandwidth is very low and the buffer level is also low (due to relatively large chunks downloaded earlier). While the inner controller reacts by selecting the track with the lowest bitrate, the reaction appears to be too late. To deal with such cases, we incorporate the proactive principle (**P3**) by adopting the concept of *preview control* from control theory [72] to adjust the target buffer level proactively.

Fig. 3.6(b) illustrates our approach. The target buffer level is set to the base target buffer level, added by a term that is determined by future chunk size variability. Specifically, when there are large chunks in the future, and hence a higher chance of longer downloading time and slower buffer filling rate that can lead to buffer underrun, the target buffer level is adjusted to a higher level to react proactively (handled by the “Long-term Statistical Filter” in Fig. 3.5), as illustrated in the region around t in Fig. 3.6(b). This adjustment will reduce rebuffering because the controller aims to reach a higher target buffer level.

Specifically, let x_r denote a base target buffer level (we set it to 60 seconds in §3.6; setting it to 40 seconds leads to similar results). The target buffer level at time t , $x_r(t)$, is set to be x_r added by a term that accounts for the future chunk size variability. We use a track $\tilde{\ell}$ (e.g., a middle track) as the reference track. If the average size of the future chunks in that track is above the mean value of that track, we proactively increase the target buffer level as:

$$x_r(t) = x_r + \max\left(\frac{\sum_{k=t}^{t+W'} R_k(\tilde{\ell})\Delta - r(\tilde{\ell})W'\Delta}{r(\tilde{\ell})}, 0\right), \quad (3.5)$$

where W' is referred to as *outer controller window size* that represents how much to look ahead, Δ is the chunk duration, $r(\tilde{\ell})$ is the average bitrate of the reference track $\tilde{\ell}$, and $R_t(\tilde{\ell})$ represents the bitrate of the chunk at time t (again we slightly abuse the notation to use t to represent chunk index). In the second term in Eq. (3.5), the numerator represents how much (in bits) the sum of the next W' chunks deviates from the average value; dividing the numerator by $r(\tilde{\ell})$ converts the unit of the deviation to seconds, compatible with how we represent buffer level. To avoid pathological scenarios where $x_r(t)$ becomes too large, we limit its value to $2x_r$, which is chosen empirically. The choice of W' is explored in §3.6.2.

3.5.5 Implementation

We have implemented CAVA in `dash.js`, a production quality open-source web-based DASH video player [53] (version v2.7.0). Under the `dash.js` framework, we imple-

mented a new ABR streaming rule `CAVARule.js` (consisting of 520 LoC) to realize CAVA. In addition, the interface of `dash.js` only exposes limited information including the track format, buffer occupancy level, bandwidth estimation, and declared bitrate. The segment size information, however, is not accessible by default. We therefore add a new `LoadSegmentSize` class to expose such information to the ABR logic. We further develop a bandwidth estimation module that responds to playback progress events to estimate throughput using a harmonic mean of the past 5 chunks.

3.6 Performance Evaluation

We explore CAVA and its parameter settings across a broad spectrum of real-world scenarios (covering both LTE and broadband), using 16 video clips (§3.2). Each video is around 10 minutes long. The length is much longer than network RTT and the timescale of ABR rate adaptation. In addition, it allows the player to go beyond the start-up phase, allowing us to understand both start-up and longer-term behaviors. These videos cover different content genres (i.e., animation, science fiction, sports, animal, nature and action), track encodings (Youtube and FFmpeg [55]), codecs (H.264 [31] and H.265 [32]), and chunk durations (2 and 5 seconds).

3.6.1 Evaluation Setup

To ensure repeatable experimentations and evaluate different schemes under identical settings, we use real-world network trace-driven replay experiments. To make the large state space exploration scalable and tractable, we use both trace-driven simulations, and experiments with our prototype implementation in `dash.js`.

We use two sets of network traces. The first set, *LTE*, contains 200 cellular network traces we captured in commercial LTE networks with a collaborator driving coast-to-coast across the US. The LTE traces were represented as per-second network throughput, recorded when downloading a large file from a well-provisioned server to a mobile phone. The second set, *FCC*, contains 200 broadband traces, randomly chosen

from the set of traces collected by the FCC [73], represented as per-5 second network throughput. Each trace contains at least 18 minutes of bandwidth measurements.

ABR logic operates at the application level, using application-level estimation of the network bandwidth (based on the throughput for recently downloaded chunks) as part of the decision process to determine the quality of the next chunk to download [14, 24, 34]. The impact of lower level network characteristics such as signal strength, loss, and RTT on ABR adaptation behavior is reflected through their impact on the network throughput. Therefore, our evaluation is through replaying the network traces that capture the network bandwidth variability over time.

ABR Schemes. We compare CAVA with the following state-of-the-art rate adaptation schemes:

- MPC and RobustMPC [13], which are based on model predictive control. RobustMPC is shown to outperform MPC under more dynamic network bandwidth settings [35].
- PANDA/CQ [27], which incorporates video quality information to optimize the performance of ABR streaming using dynamic programming. Specifically, it considers a window of N future chunks while making decisions. We investigate two variants, (i) *max-sum* that maximizes the sum of the quality of the next N chunks, and (ii) *max-min* that maximizes the minimum quality of the next N chunks.
- BOLA-E [37], which selects the bitrate to maximize a utility function considering both rebuffering and delivered bitrate. It is an improved version of BOLA [11].
- BBA-1 [14] and RBA [28]. Both are myopic schemes (§3.4). Through extensive evaluation, we find that, consistent with the example in §3.4, CAVA significantly outperforms these two schemes in all cases. In the interest of space, we omit the results for these two schemes.

Since our focus is VBR-encoded videos, following the recommendation of each scheme described above, we use the actual size of a video chunk in making rate adaptation decisions. Note that, of all the schemes, only PANDA/CQ relies on using video

quality information. Such information, however, is not available in the dominant ABR protocols used today (i.e., HLS and DASH), limiting the practical applicability and deployability of such a scheme. Still, using video quality information as part of the adaptation decision process can be potentially valuable, and for that reason, we include PANDA/CQ in our evaluations. As we shall see later in §3.6.3, while CAVA does not use such video quality information and relies only on information available in ABR streaming protocols, it still outperforms PANDA/CQ. Learning based approaches such as [35] require extensive training on a large corpus of data, and are not included for comparison since our focus is on pure client-side based schemes that are more easily deployable.

ABR Configurations. An important parameter in all schemes is the playback startup latency, i.e., the minimum number of seconds worth of video data that needs to be downloaded before the client begins playback. We explore a range of values for this parameter, guided by commercial production players [24], and report results for one setting – 10 seconds (results for other practical settings were similar). A startup delay of 10 seconds corresponds to having two chunks in the buffer for chunk length of 5 seconds (as the case for YouTube videos), consistent with the recommendation of having at least two to three chunks before starting playback [24]. Another important factor is the network bandwidth estimation technique used by the ABR logic. For a fair comparison, for all the schemes that need bandwidth estimation, we use the harmonic mean of the past 5 chunks as the bandwidth prediction approach, as the technique has been shown to be robust to measurement outliers [13, 34]. We evaluate the impact of inaccurate bandwidth estimation on performance in §3.6.7. Unless otherwise stated, the maximum buffer size is set to 100 seconds for all the schemes for apple-to-apple comparison. The client does not download the next chunk when the maximum buffer size is reached.

For CAVA, the base target buffer level, x_r , is set to 60 seconds. The controller parameters, K_p and K_i , are selected adopting the methodology outlined in [56]. Specif-

ically, we varied K_p and K_i , and confirmed that, similar to [56], a wide range of K_p and K_i values lead to good performance.

Performance Metrics. We use five metrics: four for measuring different aspects of user QoE and one for measuring resource efficiency, i.e., network data usage. All metrics are computed with respect to the delivered video, i.e., considering the chunks that have been downloaded and played back. We measure the video quality using VMAF (a recently proposed perceptual quality metric from Netflix, see §3.3.1). Specifically, we use the VMAF phone model (covers typical smartphone viewing settings) for the evaluations with the cellular traces, and the VMAF TV model (covers typical larger screen TV viewing settings) for the evaluations with the FCC traces, based on the typical device types and viewing conditions prevalent in cellular and home networks, respectively.

The performance metrics are (i) *quality of Q4 chunks*: captures the video quality for the most complex scenes. (ii) *low-quality chunk percentage*: among all the chunks played back in a given streaming session, this measures the proportion of chunks that were selected with low video quality. For the experiments, we identify VMAF values below 40 (representing poor or unacceptable quality [66]) as low quality. (iii) *rebuffering duration*: measures the total rebuffering/stall time in a video session. (iv) *average quality change per chunk*: is defined as the average quality difference of two consecutive chunks in playback order (since human eyes are more sensitive to level changes in adjacent chunks) for a session, i.e., $\sum_i |q_{i+1} - q_i|/n$, where q_i denotes the quality of i^{th} chunk (in terms of playback order), and n is the number of chunks. (v) *data usage*: captures the total amount of data downloaded (i.e., the total network resource usage) for a session. While comparing two schemes, for each of the last 4 metrics, a lower value is preferable; the only exception is the first metric (quality of Q4 chunks), where a higher value is preferable.

In the above performance metrics, we use perceptual quality metrics since they quantify the viewing quality more accurately compared to bitrate that is commonly

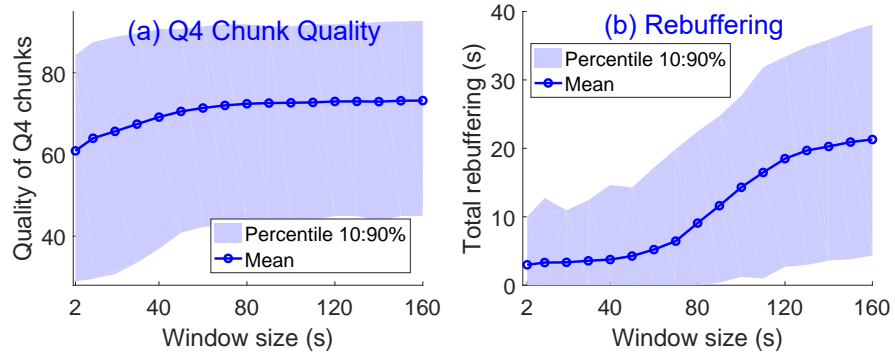


Fig. 3.7: Impact of inner controller window size.

used in the literature. As an example, the average bitrate of the delivered video, which is commonly used to quantify the quality of a streaming session, is an especially poor metric for VBR videos. To see this, consider two cases with the same average bitrate. In the first case, the lowest track is selected for Q4 chunks, while higher tracks are selected for Q1-Q3 chunks; in the second case, a medium track is selected for Q4 chunks, while low or medium tracks are selected for Q1-Q3 chunks. These two cases clearly lead to different viewing quality, while will be classified as being the same quality based on the average bitrate. In addition, we use metrics to capture both the average and tail behaviors. Specifically, the percentage of low quality chunks is an important metric on tail behavior since it has been reported that human eyes are particularly sensitive to bad quality chunks [70].

3.6.2 Choice of Parameters for CAVA

Inner controller window size. Recall that the inner controller in CAVA uses the average bitrate over a window of W future chunks to represent the bandwidth requirement of the current chunk. We investigate the impact of W on the performance of CAVA. Fig. 3.7 shows an example (Elephant Dream, FFmpeg encoded, H.264, LTE traces); the solid lines represent the average values, and the top and bottom of the shaded region represent the 90th and 10th percentile across the network traces, respectively. When in-

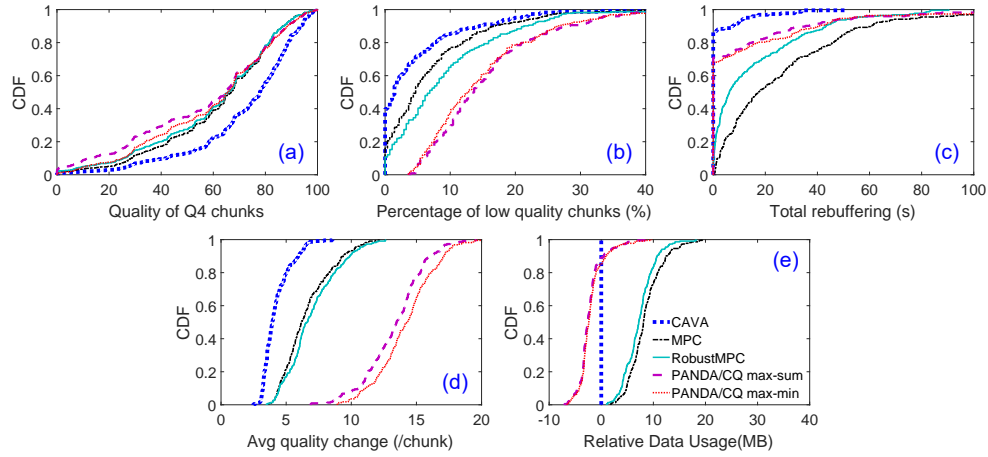


Fig. 3.8: Performance comparison for one video (Elephant Dream, FFmpeg encoded, H.264) under LTE traces.

creasing W , (i) the quality of the Q4 chunks first improves significantly and then flattens out, and (ii) the amount of rebuffering increases slightly and then sharply. Increasing W at the beginning is beneficial because even averaging over a few chunks can smooth out the bitrate of the chunks, which allows higher levels to be chosen for Q4 chunks (since the smoothed bitrate for a Q4 chunk tends to be lower than its actual bitrate). The impact on smoothing the bitrate diminishes after W becomes sufficiently large, leading to diminishing gains for Q4 chunks. The increase in rebuffering when W is large is because CAVA becomes less sensitive to the bitrate changes in that case. We set W to 40 seconds (i.e., 20 and 8 chunks for 2 and 5 seconds chunk durations, respectively) as this leads to a good tradeoff between quality and rebuffering.

Outer controller window size. The outer controller in CAVA uses a window of W' future chunks to adjust the target buffer level. We vary W' to explore its impact. In general, the amount of rebuffering decreases as W' increases since the controller reacts more proactively with larger W' . For some videos, however, the amount of rebuffering may start to increase as W' increases further. This is because using very large W' smoothes out the effect of the variability of the video (i.e., the average bitrate of the future W' chunks becomes closer to the average bitrate of the track, causing little incre-

ment in the target buffer level as shown in Eq. (3.5)). We set W' to 200 seconds (i.e., 100 and 40 chunks for 2 and 5 seconds chunk durations, respectively), which leads to good results in reducing rebuffering.

3.6.3 Comparison with Other Schemes

We compare CAVA with other ABR schemes using all the videos under both LTE and FCC traces (the comparison with BOLA-E is deferred to §3.6.8). Fig. 3.8(a)-(e) compare the performance of CAVA with other schemes for one FFmpeg encoded video under the LTE traces. Our results below focus on CAVA versus RobustMPC and PANDA/CQ max-min; MPC can have significantly more rebuffering than RobustMPC, and PANDA/CQ max-sum can have significantly lower quality for Q4 chunks than PANDA/CQ max-min. We observe that CAVA significantly outperforms RobustMPC and PANDA/CQ max-min. (i) With CAVA, a much larger proportion (79%) of the Q4 chunks are delivered at a quality higher than 60 (considered as good quality [66]), compared to only 59% and 57% for RobustMPC and PANDA/CQ max-min, respectively. The median VMAF value across Q4 chunks is 78 under CAVA, 11 and 12 larger than the corresponding values for RobustMPC and PANDA/CQ max-min, respectively, indicating noticeable perceptual improvements (It has been reported that a difference of 6 or more in VMAF would be noticeable to a viewer [74]). (ii) For the percentage of low-quality chunks, under CAVA, 40% of the traces have no low-quality chunks (VMAF score ≤ 40); and 82% of the traces have less than 10% low-quality chunks, significantly larger than the corresponding values 65% and 40% for RobustMPC and PANDA/CQ max-min, respectively. (iii) CAVA has no rebuffering for 85% of the traces, compared to only 20% and 68% of traces under RobustMPC and PANDA/CQ max-min, respectively. (iv) For average quality change per chunk, CAVA realizes substantially lower changes than the other schemes (on average, 67% and 29% of the values of RobustMPC and PANDA/CQ max-min, respectively), resulting in less variability in playback quality, and therefore more consistent and smoother playback experience. (v) CAVA has 5% to

40% lower data usage than RobustMPC. PANDA/CQ max-min has slightly lower data usage than CAVA (10% at most), at the cost of lower Q4 quality and overall quality (see below). Figures 3.9(a) and (b) show the quality of Q1-Q3 chunks and all the chunks, respectively. We observe that while CAVA does not lead to very high quality for Q1-Q3 chunks, it does not choose low quality for these chunks either. Overall, CAVA leads to a desired tradeoff in choosing less low-quality chunks compared to other schemes.

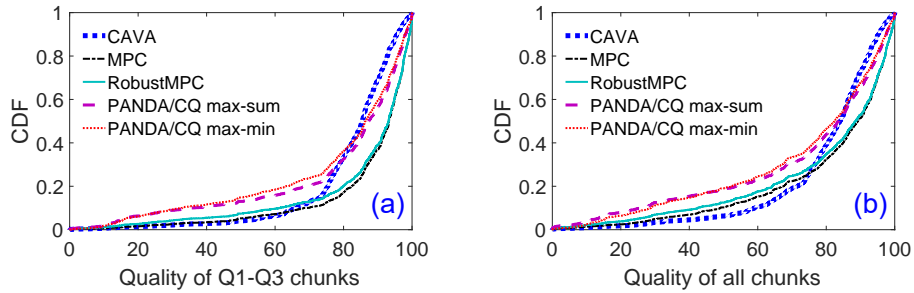


Fig. 3.9: Quality of Q1-Q3 chunks and all the chunks.

The above results are for one FFmpeg video under LTE traces. Table 3.1 shows the results for several YouTube videos under both LTE and FCC traces. For Q4 chunk quality, we show two values: the metric value (averaged over all the runs) obtained by CAVA subtracted by that of RobustMPC and PANDA/CQ max-min, respectively. For each of the other four performance metrics, we show two percentage values, (i) the difference in the metric value (averaged over all runs) for CAVA subtracted by that for RobustMPC, as a percentage of the latter value, and (ii) the corresponding value for CAVA vs. PANDA/CQ max-min. In Table 3.1, \uparrow indicates that CAVA has a higher value; while \downarrow indicates that CAVA has a lower value. The first part of Table 3.1 shows the results under LTE traces. We observe that CAVA leads to average quality improvement for Q4 chunks in the range of 8-18 VMAF points compared to RobustMPC, and 3-9 VMAF points compared to PANDA/CQ max-min. Also CAVA substantially reduces the average stall/rebuffering duration by 62%-95%, reduces the quality change per chunk by 25%-48%, and reduces the percentage of low-quality chunks by 4%-61%.

Table 3.1: Performance comparison (YouTube videos).

| | Video | Q4 chunk quality | Low-qual. chunks (%) | Stall duration (%) | Quality changes (%) | Data usage (%) |
|-----|--------|------------------------|----------------------------|--------------------------|---------------------------|----------------------|
| LTE | BBB | ↑13, ↑4 | ↓61, ↓31 | ↓62, ↓64 | ↓48, ↓37 | ↓11, ↓5 |
| | ED | ↑10, ↑4 | ↓54, ↓37 | ↓73, ↓77 | ↓38, ↓36 | ↓9, ↓4 |
| | Sintel | ↑8, ↑4 | ↓75, ↓42 | ↓83, ↓77 | ↓37, ↓32 | ↓8, ↓3 |
| | ToS | ↑9, ↑6 | ↓72, ↓55 | ↓84, ↓81 | ↓39, ↓40 | ↓9, ↓3 |
| | Animal | ↑15, ↑3 | ↓4, ↓7 | ↓83, ↓95 | ↓43, ↓38 | ↓11, ↓10 |
| | Nature | ↑10, ↑3 | ↓17, ↓11 | ↓80, ↓97 | ↓40, ↓41 | ↓7, ↓10 |
| | Sports | ↑18, ↑9 | ↓30, ↓2 | ↓83, ↓83 | ↓35, ↓31 | ↓8, ↓2 |
| | Action | ↑14, ↑6 | ↓49, ↓27 | ↓79, ↓74 | ↓38, ↓25 | ↓8, ↓3 |
| FCC | BBB | ↑11, ↑4 | ↓70, ↓28 | ↓26, ↓51 | ↓48, ↓32 | ↓8, ↓4 |
| | ED | ↑8, ↑3 | ↓33, ↓11 | ↓79, ↓34 | ↓36, ↓31 | ↓7, ↓2 |
| | Sintel | ↑7, ↑4 | ↓87, ↓70 | ↓94, ↓85 | ↓35, ↓26 | ↓6, ↓2 |
| | ToS | ↑6, ↑6 | ↓69, ↓62 | ↓90, ↓6 | ↓40, ↓38 | ↓7, ↓1 |
| | | ↑ better | ↓ better | ↓ better | ↓ better | ↓ better |

* The two numbers in each cell represents the changes by CAVA relative to RobustMPC and PANDA/CQ max-min, respectively.

Last, the data usage of CAVA is 7%-11% lower than RobustMPC, and 2%-10% lower than PANDA/CQ max-min.

The second part of Table 3.1 shows the results for FCC traces. Compared to the LTE trace results, the rebuffering for all the schemes becomes lower due to smoother network bandwidth profiles; CAVA still leads to lower rebuffering and better performance in all the performance metrics.

3.6.4 Impact of CAVA Design Principles

Recall CAVA incorporates three key design principles (§3.4). In the following, we investigate the contribution of each principle to the performance of CAVA. As detailed in

§3.4, the first (i.e., non-myopic) principle is used in the inner controller of CAVA: it uses the average bitrate of multiple future chunks to represent the bandwidth requirement of the current chunk when deciding the track level for the current chunk. The second (i.e., differential treatment) principle favors Q4 chunks over Q1-Q3 chunks. The third (i.e., proactive) principle is used in the outer controller: it considers long-term future (within tens of chunks) and increases the target buffer level to be prepared for incoming large chunks in the future. Of the three principles, the first principle is the basic principle, while the other two principles are used on top of the basic principle. In the following, we consider three variants of CAVA, referred to as CAVA-p1, CAVA-p12 and CAVA-p123, which includes the first principle, the first two principles, and all three principles, respectively.

Our evaluation confirms that the three principles indeed successfully play their individual roles. Specifically, CAVA-p1 already leads to fast responses to dynamic network bandwidths, consistent playback quality and low rebuffering; CAVA-p12 leads to higher Q4 chunk quality, while CAVA-p123 leads to lower rebuffering. Fig. 3.10 shows an example for one video (ED, FFmpeg encoded, H.264) under LTE traces. Fig. 3.10(a) plots the Q4 chunk quality under the two variants with the differential treatment principle (i.e., CAVA-p12 and CAVA-p123) relative to CAVA-p1. Specifically, it shows the distribution of the metric value under CAVA-p12 and CAVA-p123 minus the value under CAVA-p1 across all runs. We observe that for around 40% of the Q4 chunks, CAVA-p12 and CAVA-p123 lead to higher Q4 chunk quality. For only around 5% of the Q4 chunks, the quality under CAVA-p12 and CAVA-p123 is lower than CAVA-p1. Fig. 3.10(b) shows the total rebuffering of CAVA-p123 relative to CAVA-p12 for traces that lead to rebuffering under either of these two variants (35 out of 200 traces fall into this category). Specifically, it shows the metric value under each variant minus the value under CAVA-p12. We see that CAVA-p123 leads to lower rebuffering than CAVA-p12 in 55% of these traces and the reduction is up to 20 seconds.

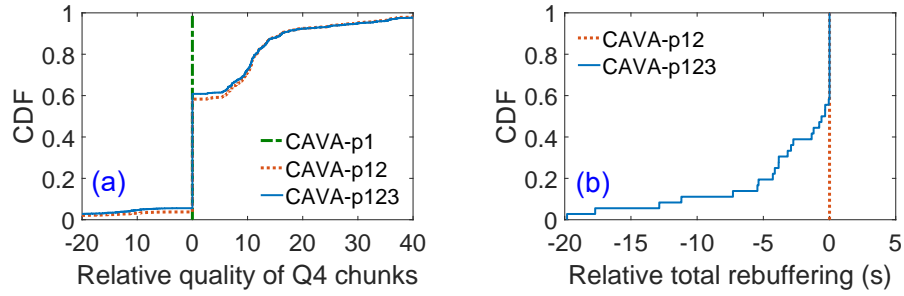


Fig. 3.10: Impact of the design principles of CAVA.

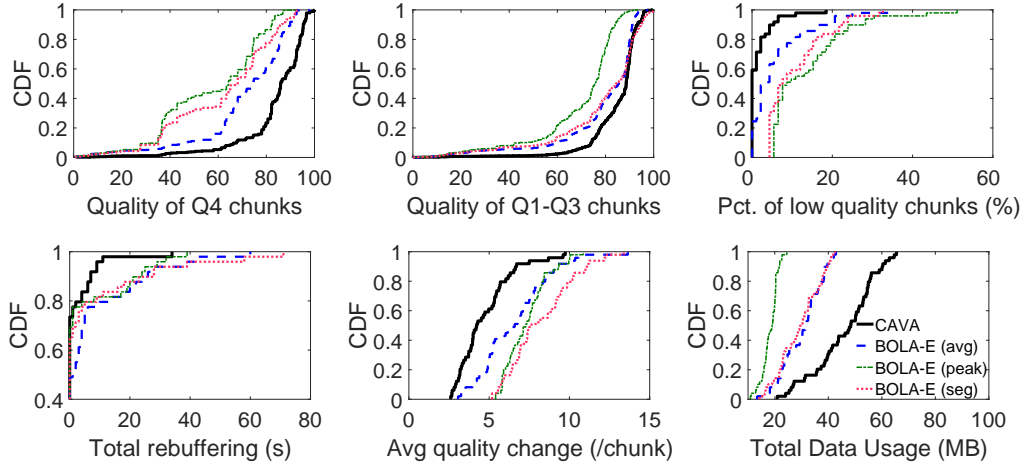


Fig. 3.11: Performance comparison in dash.js (Big Buck Bunny, YouTube encoded, H.264, LTE traces).

3.6.5 Codec Impact

For each video, the performance of all the schemes under H.265 encoding is better than that under H.264 encoding (figures omitted). This is due to the significantly lower bitrate requirement of H.265 encoding. We observe that CAVA also significantly outperforms all the other schemes under H.265 encoding. Compared to RobustMPC and PANDA/CQ max-min, on average, Q4 chunk quality under CAVA is 7-12 higher, the percentage of low-quality chunks is 51%-82% lower, rebuffering is 52%-91% lower, and average quality change is 27%-72% lower. Also CAVA has similar data usage compared to other schemes.

3.6.6 Impact of Higher Bitrate Variability

We further use the 4× capped VBR-encoded video (Elephant Dream FFmpeg encoded, in H.264) to explore the impact of higher bitrate variability. In this case, we observe similar trends as the earlier results. For CAVA, the average Q4 chunk quality is 65 across the LTE traces, 8 and 7 larger than RobustMPC and PANDA/CQ max-min, respectively. The average quality change is 42% and 68% lower, the rebuffering is 90% and 89% lower, and the average percentage of low-quality chunks is 39% and 57% lower.

3.6.7 Impact of Bandwidth Prediction Error

So far, we have used a particular bandwidth estimation algorithm (harmonic mean of past 5 chunks) to predict available network bandwidth. We next investigate the impact of bandwidth prediction errors on different schemes in a controlled manner as follows. We assume the bandwidth prediction error is err . That is, if the actual network bandwidth at time t is C_t , we assume that the predicted network bandwidth is uniformly randomly distributed in $C_t(1 \pm err)$. We vary err from 0 to 50% with a step of 25%. We observe that CAVA is insensitive to bandwidth prediction errors: the quality of Q4 chunks, the amount of rebuffering and the percentage of low quality chunks when $err=50\%$ are similar to those when $err=0$ (i.e., perfect prediction), demonstrating that CAVA is adaptive and tolerant to relatively significant bandwidth prediction errors (due to the control-theoretical underpinning). In comparison, MPC leads to significantly more rebuffering and data usage when $err=50\%$, compared to those when $err=0$. PANDA/CQ max-min leads to noticeably more rebuffering when err is increased from 0 to 50%. The reason why CAVA is resilient to bandwidth estimation errors is because it is a principled approach based on control theory – it continuously monitors the “errors” in the system, namely the difference between the target and current buffer levels of the player, and adjusts the control signal to correct “errors” caused by inaccurate bandwidth estimation.

3.6.8 DASH Implementation Results

We evaluate CAVA using the `dash.js` implementation (§3.5.5), and compare its performance with that of BOLA-E [37] implemented in `dash.js` version 2.7.0, which contains a stable release of BOLA-E. Our evaluations below use two computers (Ubuntu 12.04 LTS, CPU Intel Core 2 Duo, memory 4GB) with a 100 Mbps direct network connection to emulate the video server (Apache httpd) and client. At the client, we use Selenium [75] to programmatically run a Google Chrome web browser and use `dash.js` APIs to collect the streaming performance data. We use `tc` [76] to emulate real-world variable network conditions by programmatically “replaying” the network traces (§3.6.1).

We find that CAVA is very light-weight – even with the current prototype implementation, the runtime overhead (from profiling) is only around 56ms for a 10-minute video.

We compare the performance of CAVA with three versions of BOLA-E. Two versions are based on the original BOLA-E implementation, which takes a single bitrate value from each track (i.e., the declared bitrate from the manifest file). Specifically, we consider BOLA-E (peak), where the declared bitrate for a track is the peak bitrate of the track, and BOLA-E (avg), where the declared bitrate for a track is the average bitrate of the track. In the third version, referred to as BOLA-E (seg), we modified the original BOLA-E implementation to use the actual chunk size for each chunk, as suggested by the paper [11] for VBR encodings. All the three versions use the default parameters in BOLA-E. Fig. 3.11 shows the performance of CAVA and the three versions of BOLA-E for one Youtube video. We observe that CAVA outperforms the three versions of BOLA-E in having higher Q4 chunk quality, lower percentage of low-quality chunks, lower rebuffering, and lower quality changes. While the data usage of BOLA-E (all three variants) is lower than that of CAVA, it comes at the cost of worse performance in other performance metrics. The lower data usage of BOLA-E could be because it sometimes pauses before fetching the next chunk under various scenarios. In addition,

the implementation uses bitrate capping when switching to a higher bitrate to avoid bitrate oscillations.

Of the three BOLA-E variants, not surprisingly, BOLA-E (peak) is the most conservative variant in choosing bitrate, since it uses the peak bitrate of a track as the bitrate of every chunk in the track, and hence overestimates the bandwidth requirements of the individual chunks. In comparison, BOLA-E (avg) is the most aggressive, and BOLA-E (seg) is between BOLA-E (peak) and BOLA-E (avg). We see that for Q1-Q3 chunks, BOLA-E (seg) can choose even higher tracks than BOLA-E (avg), since BOLA-E (seg) uses the actual chunk size and can choose higher quality for some small chunks (that fall into Q1-Q3). We further see that using the actual chunk size in BOLA-E (seg) leads to more significant quality changes compared to BOLA-E (peak) and BOLA-E (avg). The above behaviors demonstrate once again that while it is important to consider individual chunk sizes to handle ABR streaming of VBR videos, the actual decision logic needs to be developed with VBR characteristics in mind; simply plugging in the individual chunk sizes is insufficient.

Table 3.2 compares the performance of CAVA and BOLA-E (seg) for four YouTube videos, all under LTE traces. We observe that while the data usage of BOLA-E (seg) is lower, CAVA outperforms BOLA-E (seg) in all the other metrics: on average, Q4 chunk quality under CAVA is 10-21 higher, the percentage of low-quality chunks is 73%-87% lower, rebuffering is 15%-65% lower, and quality changes is 24%-45% lower.

3.7 Related Work

There is a large body of existing work on ABR streaming [9, 11, 12, 13, 14, 18, 27, 28, 34, 35, 56, 77, 78, 79, 80]. Rate-based (e.g., [28, 34, 81]) ABR schemes select bitrate simply based on network bandwidth estimates. Buffer-based schemes, e.g., BBA [14], BOLA [11], and BOLA-E [37], select bitrate only based on buffer occupancy. Most recent schemes combine both rate-based and buffer-based techniques. For instance, MPC [13] and PIA [56] use control-theoretic approaches to design rate adaptation based

Table 3.2: CAVA versus BOLA-E in dash.js.

| Video | Q4 chunk quality | Low-qual. chunks (%) | Stall duration (%) | Quality changes (%) | Data usage (%) |
|--------|------------------------|----------------------------|--------------------------|---------------------------|----------------------|
| BBB | ↑21 | ↓87 | ↓65 | ↓45 | ↑56 |
| ED | ↑20 | ↓73 | ↓15 | ↓35 | ↑50 |
| Sports | ↑10 | ↓75 | ↓29 | ↓40 | ↑25 |
| ToS | ↑12 | ↓76 | ↓19 | ↓24 | ↑45 |

on both network bandwidth estimates and buffer status. Oboe [18] dynamically adjusts the parameters of an ABR logic to adapt to various network conditions. Another group of related studies [16, 35] uses machine learning based approaches, which “learns” ABR schemes from data.

While content providers have recently begun adopting VBR encoding, their treatment to VBR videos is simplistic (e.g., by simply assuming that the bandwidth requirement of a chunk equals to the peak bitrate of the track) [24]. As we have seen in §3.6.8, such simplistic treatment can lead to poor performance. Of the large number of existing studies, only a few targeted VBR videos [14, 27, 28]; most others were designed for and evaluated in the context of CBR encodings. While several schemes in the latter category can be applied for VBR videos by explicitly incorporating the actual bitrate of each chunk, they were not designed ground up to account for VBR characteristics, nor had their performance been evaluated for that case. We evaluate the performance of schemes from both categories in this chapter (see §3.4 and §3.6), and show that they can suffer from a large amount of rebuffering and/or significant viewing quality impairments when used for VBR videos.

Our study differs from all the above works in several important aspects, including developing insights based on analyzing content complexity, encoding quality, and encoding bitrates, identifying general design principles for VBR streaming, and develop-

ing a concrete, practical ABR scheme for VBR streaming that significantly outperforms the state-of-the-art schemes.

3.8 Conclusions and Future Work

Through analyzing a number of VBR-encoded videos from a variety of genres, we identified a number of characteristics related to scene complexities, bandwidth variability, and quality levels, that are relevant to ABR streaming and QoE. Based on these insights, we proposed 3 key principles to guide rate adaptation for VBR streaming. We also designed CAVA, a practical control-theoretic rate adaptation scheme that explicitly leverages our proposed principles. Extensive evaluations demonstrate that CAVA substantially outperforms existing ABR schemes even in challenging network conditions common in cellular networks. The results demonstrate the importance of utilizing these design principles in developing ABR adaptation schemes for VBR encodings. In this chapter, we primarily focused on the VoD setting. As future work, we will explore extending CAVA and its concepts to ABR streaming of live VBR encoded videos.

Chapter 4

Quality-aware Strategies for Optimizing ABR Video Streaming QoE and Reducing Data Usage

4.1 Introduction

This chapter attempts to answer the following question: how can we effectively reduce the bandwidth consumption for mobile video streaming while minimizing the impact on users' quality of experience (QoE)? This is a highly important and practical research problem since cellular network bandwidth is a relatively scarce resource. The average data plan for a U.S. cellular customer is only 2.5 GB per month [29], while streaming just one-hour High Definition (HD) video on mobile Netflix can consume 3 GB data. Therefore, the capability to make more efficient use of data while still hitting quality targets is the key to enabling users to consume more content within their data budgets without adversely impacting QoE. In addition, downloading less data for a video session also translates to lower radio energy consumption [82], less thermal overhead on mobile devices, as well as potentially better QoE for other users sharing the same cellular RAN (radio access network) or base station.

Existing ABR adaptation schemes (§4.9) focus mainly on maximizing the video quality and user QoE. While some schemes do conservatively utilize the bandwidth, their decisions are primarily driven by QoE impairment concerns such as the possibility of stalls caused by the potentially inaccurate bandwidth estimation. For example, when selecting the next chunk, the default adaptation scheme in ExoPlayer [30] (a popular open-source player that is used in more than 10000 apps) only considers tracks whose

declared bitrates are at least 25% lower than the estimated network bandwidth. Such a design saves data just by being conservative. As we show later, it can lead to significantly lower quality/QoE (§4.8.3). Existing ABR schemes do not explicitly consider bandwidth efficiency together with quality in making the track selection decisions.

Some mobile network operators and commercial video services provide users with certain “data saver” options. These options take either a service-based approach or a network-based approach. The former limits the highest level of quality/resolution/bitrate by, for example, streaming only standard definition (SD) content over cellular networks. A network-based approach instead limits the network bandwidth. We survey the “quality throttling” mechanisms used by today’s commercial video content providers for saving bandwidth for mobile devices, and pinpoint their inefficiencies (§4.2-§4.3). Despite their simplicity, we find such approaches often achieve tradeoffs between video quality and bandwidth usage that are far from what viewers desire. A key reason is that for state-of-the-art encoders (e.g., H.264 [31], H.265 [32] and VP9 [33]), the actual perceived picture quality exhibits significant variability across different chunks within the same track, for both Constant Bitrate (CBR) and Variable Bitrate (VBR) encodings. Therefore, a data-saving approach that simply removes high tracks leads to quality variations. Such quality variability impairs user QoE, and makes suboptimal use of the network bandwidth.

To address the drawbacks of the existing practices, we propose a *quality-aware data saving* strategy [83], which provides data savings while allowing users’ direct control of the video quality. Specifically, a user selects from multiple quality options (e.g., good, better, best), and the player will map the selection to a *target quality* (§4.3). Within this strategy, we propose two new schemes that explicitly consider the bandwidth efficiency by matching the fetched content quality against a target quality. In this way, the player will avoid fetching chunks whose qualities are beyond the target quality, leading to bandwidth savings. Specifically, the two new schemes are:

- *Chunk-Based Filtering (CBF)*. We propose a novel, quality-variability aware scheme

called Chunk-Based Filtering (CBF) (§4.4) that can be retro-fitted into existing ABR adaptation schemes [84]. Its high-level idea is as follows. For every chunk position in the video, CBF limits the choice of the highest quality chunk for ABR rate adaptation to the chunk whose quality is closest to the target quality. CBF thereby steers an ABR adaptation scheme to the set of more desirable choices (from the perspective of balancing the tradeoff between the video quality and bandwidth usage), and helps the ABR scheme achieve better streaming performance than it would by itself. Using CBF in conjunction with existing ABR adaptation schemes is also attractive from a practical incremental deployment perspective. CBF has no dependencies on and requires no changes to the complex ABR adaptation logic, and can be relatively easily inserted into the existing streaming workflow (§4.4.3).

- *Quality-aware ABR Adaptation.* From a performance and bandwidth-efficiency trade-off perspective, it is possible to do even better, if the ABR scheme itself can explicitly integrate the goal of approaching the target quality into its rate adaptation logic. To this end, we develop *QUality-Aware Data-efficient streaming (QUAD)*, a holistic rate adaptation algorithm that is designed ground up (§4.5). QUAD jointly considers three aspects when making rate adaptation decisions: pacing the selected chunks' bitrate to the estimated network bandwidth to prevent stalls, adapting to the target quality to reduce bandwidth consumption, and minimizing the inter-chunk quality change to enhance the playback smoothness. QUAD is robust and lightweight as it is developed upon solid control theoretic foundations.

We implemented CBF and QUAD (§4.6) in two popular state-of-the-art open source ABR video players: `dash.js` [53] and `ExoPlayer` [30]. Our evaluation of these two techniques uses a diverse set of real videos and different encoding schemes (VBR and CBR), under both emulated and real-world LTE networks (§4.6). The key evaluation results include the following.

- CBF significantly improves the performance of existing state-of-the-art ABR schemes (§4.7). Specifically, after employing CBF as a prefiltering step, the average deviation from the

target quality is reduced by 37-67%; the average quality variation is reduced by 7-31%; and the data usage is reduced by 34-67% even in challenging network conditions (in easier conditions with ample bandwidth, the reduction is even more). We further experimentally demonstrate that CBF is significantly more effective in steering existing ABR schemes to more desirable rate adaptation decisions than traditional service-based or network-based data saving approaches.

- Compared to existing schemes enhanced with CBF, QUAD achieves even better performance in approaching the target quality with low quality variations while still achieving good QoE (§4.8). For instance, our evaluation on `dash.js` shows that, compared to a state-of-the-art ABR scheme, BOLA-E [37] enhanced with CBF, QUAD leads to 37% fewer low-quality chunks and 12% reduction in quality variation. Compared to the default rate adaptation of ExoPlayer, QUAD reduces the deviation from the target quality by 64%, reduces the number of low-quality chunks by 81%, and reduces the quality variation by 43%. Compared to an optimized version of ExoPlayer’s algorithm enhanced with CBF, the corresponding reductions brought by QUAD are 40%, 46% and 22%, respectively.

4.2 Quality and Bitrate Tradeoffs

In this section, we describe the encoding characteristics of both VBR and CBR videos to motivate our proposed solutions.

4.2.1 Video Dataset

Our video dataset includes 18 VBR and 4 CBR videos. We consider both VBR and CBR videos because both are widely used in practice [24], with the trend of wider adoption of VBR videos thanks to their many advantages over CBR videos [22]. Each video is around 10 minutes long, and encoded at 6 tracks/levels¹ for ABR streaming,

¹ We use the terms *track* and *level* interchangeably in this chapter. Other equivalent terms include representation and rendition, which are also widely used in the literature.

with resolutions of 144p, 240p, 360p, 480p, 720p, and 1080p.

VBR Videos. All the 18 VBR videos were encoded by YouTube (YouTube has adopted VBR encoding [62]). Four videos, Elephant Dream (ED), Big Buck Bunny (BBB), Sintel, and Tears of Steel (ToS), were encoded from publicly available *raw* videos [58]. Specifically, we uploaded the raw videos to YouTube and downloaded the encoded videos using `youtube-dl` [61]. These four videos are in the categories of animation and science fiction. We further downloaded 14 other videos, in a wide range of categories, including sports, animal, nature, action movies, family drama, comedy, and documentary, using `youtube-dl`. All the above videos are encoded using the H.264 codec [31], with chunk duration of around 5 seconds, consistent with [62] (the encoding is multi-pass; readers can find the detailed encoding settings in [62]). Ten out of the aforementioned 14 videos were also available in another codec, VP9 [33], encoded by YouTube. In addition, we further use `FFmpeg` to encode the four publicly available videos using a more recent and efficient codec, H.265 [32], following the “three-pass” encoding in [57].

CBR Videos.

We also created CBR encodings for the four publicly available raw videos using `FFmpeg` [55], a popular open source encoder. Specifically, we used the one-pass CBR encoder, the default CBR encoder in `FFmpeg`, which is often used instead of multi-pass encoders due to latency considerations, particularly in live streaming. Each video is encoded using H.264 into six tracks (144p to 1080p), and each track is segmented into 5-sec chunks, consistent with the ABR track configurations of YouTube.²

² As an example, the command for encoding an input video into a 1080p track is `ffmpeg -i inputvideo -b:v 2500k -minrate 2500k -maxrate 2500k -bufsize 2500k -r 24 -profile:v high -x264-params nal-hrd=cbr:keyint=120 :min-keyint=120:scenecut=0 -vcodec libx264 -vf scale=1920:1080 -preset fast output.mp4`.

4.2.2 Video Quality Metrics

We use two quality metrics, Peak Signal-to-Noise Ratio (PSNR) and Video Multi-method Assessment Fusion (VMAF) [66]. PSNR is a traditional image quality metric. VMAF is a recently proposed perceptual quality metric that correlates quality strongly with subjective scores, and has been validated independently in [69]. VMAF provides different models tailored to various screen sizes, such as phone and TV. We focus on the VMAF phone model in this chapter since phones are the dominant platform for viewing videos over cellular networks. A VMAF score is between 0 and 100: a score of 0-20 is considered as unacceptable, 20-40 as poor, 40-60 as fair, 60-80 as good, and 80-100 as excellent [66]. Similarly, different ranges of PSNR values are used to categorize picture qualities [57]. The aggregate VMAF of a chunk is set as the median VMAF of all the frames in a chunk (using mean leads to similar values for videos in our dataset) [70]. The same approach is used for PSNR.

To calculate PSNR and VMAF for a video, we need a *reference video*, i.e., a pristine high quality copy of the video against which to compute these metrics. For the four VBR and CBR videos that were encoded using the publicly available raw videos, the corresponding raw videos are used as the reference videos. For the other VBR videos downloaded from YouTube, we do not have the raw video footage, and use the top track (1080p) as the reference track to measure the video quality of the lower tracks. To understand the impact of this approximation, we calculate the quality values for the four videos that we have raw videos under two options, one with the raw video and the other with the 1080p track as the reference video. We find empirically that the latter leads to lower variability across the chunks in the same track for both PSNR and VMAF, a point that we will return to in §4.2.3.

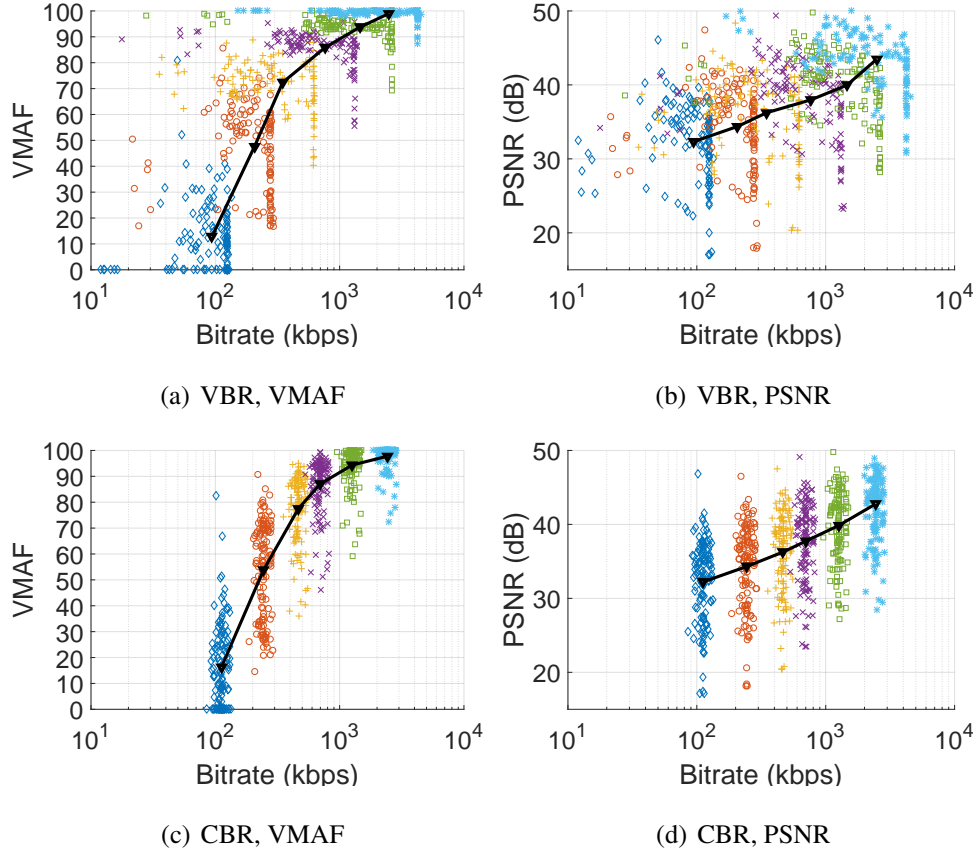


Fig. 4.1: Quality vs. bitrate for one video (ED).

4.2.3 Perceptual Quality vs. Encoding Bitrate

We first use an example video to illustrate the tradeoffs between quality and bitrate, and then describe the observations across the video dataset. Figures 4.1(a) and (b) plot quality versus bitrate for a VBR video (with 123 chunks, each of 5-sec duration, and 6 tracks), using VMAF and PSNR as the quality metric, respectively. In these figures, different colors represent the chunks in the different tracks; the black curve shows the average quality versus average bitrate for each track. We see a diminishing gain in increasing bitrate on quality (note the log scale in x-axis), consistent with the observations in [85]. Furthermore, even under VBR encoding, the chunks in the same track have significantly variable perceptual quality (a VMAF difference of 6 or more would

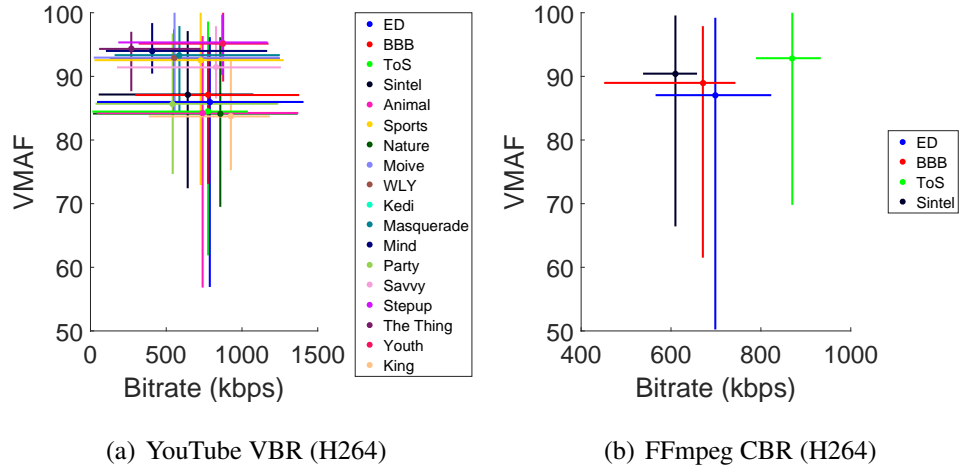


Fig. 4.2: Quality vs. bitrate for track 4 (480p).

be noticeable to a viewer [74, 85]). Specifically, for a track, the standard deviation of quality across the chunks varies from 2 to 14 for VMAF, 4.1 to 5.4 in PSNR (note PSNR values in log scale), with the middle tracks exhibiting more variability. We make similar observations for CBR video. Figures 4.1(c) and (d) plot VMAF quality versus bitrate for a CBR video, where all the chunks in same track have similar bitrates.

Fig. 4.2 plots the quality (in VMAF) and bitrate variations for track 4 for all the videos we consider (18 VBR videos in Fig. 4.2(a) and 4 CBR videos in Fig. 4.2(b)); the results under PSNR show a similar trend. Each video is represented by two error bars, representing the 1st and 99th percentile in quality and bitrate, respectively. We see the same two observations hold for all the videos we consider. Note that Fig. 4.2(a) includes the 14 VBR videos for which we use the 1080p tracks as the reference videos (due to unavailability of the raw videos), which tend to underestimate the quality variability across the chunks in the same track (see empirical observations in §4.2.2). We see significant variability even with the underestimation.

The above results are for H.264 [31] videos. To ensure that the above observations are general, we further investigate the quality and bitrate relationships for other encoders and content. Specifically, we examine (i) H.265 [32], a more recent and effi-

cient codec than H.264, using the four publicly available videos, (ii) VP9 [33], another widely used codec in YouTube, using ten VP9 videos downloaded from YouTube, and (iii) Twitch, another popular video streaming service, by selecting five popular videos in different genres based on the number of viewers. For all the three cases, our results confirm the same two quality and bitrate relationships observed earlier: (1) increasing bitrate leads to diminishing gain in quality improvement, and (2) the chunks in the same track have significantly variable quality. These two observations are consistent with the results of Netflix encoded videos [85, 86], indicating that they hold widely across encoding platforms and videos.

The property that chunks within the same track have highly variable quality holds obviously for CBR encodings, which encode the entire video at a relatively fixed bitrate, allocating the same bit budget to both *simple scenes* (i.e., low-motion or low-complexity scenes) and *complex scenes* (i.e., high-motion or high-complexity scenes). The fact that it also holds for VBR is somewhat counterintuitive since VBR allocates bits according to scene complexity to achieve a more consistent quality throughout a track. Part of the reason is the inherent complexity of encoding and the difficulty of handling scenes of diverse complexities [62, 85].

4.3 Reducing Data Usage

The diminishing gains in increasing bitrate on quality improvement demonstrated in the previous section indicate that an ABR logic that simply aims to maximize quality is not bandwidth efficient. In the following, we first describe the current data saving practices and show that they are inefficient. We then propose a quality-aware strategy for reducing data usage.

| Option | Top Track | Declared Bitrate | Resolution |
|------------|-----------|------------------|------------|
| Data saver | 3 | 120kbps | 288p |
| Good | 6 | 450kbps | 360p |
| Better | 7 | 650kbps | 396p |
| Best | 8 | 1000kbps | 480p |

Table 4.1: Data saving options in Amazon Prime video.

4.3.1 Current Data Saving Practices

Certain cellular network operators provide users with options to limit the network bandwidth for a streaming session (e.g., [87, 88]). The rationale is that the bandwidth cap may lead an ABR player to avoid bandwidth-consuming High-Definition (HD) tracks so as to save data.

Various commercial video streaming services have also provided users with options to save data. For instance, the YouTube phone app provides an option called “Play HD on Wi-Fi only”, i.e., only Standard Definition (SD) videos will be streamed over cellular networks. To understand the behavior of this option, we stream eight videos in different categories using the YouTube app over a commercial LTE network. We observe that, when the option is on, even if the network bandwidth is very high (over tens of Mbps), the 480p track is selected throughout the video. The fact that the selected tracks never exceed 480p despite significantly higher bandwidth indicates that the data saving is achieved by capping the top track to the 480p track. Henceforth, we refer to this practice as *Track-based Filtering (TBF)*. We find that data saving options in the Amazon Prime Video app are also achieved by capping the top track. Table 4.1 summarizes the measurement results, showing the top track for the four options varies from track 3 to 8.

The above two current practices both have drawbacks. The network-based approach forces an ABR scheme to choose lower tracks due to the network bandwidth limit. It provides no explicit control on what quality will be chosen for a particular chunk position, thus leading to highly variable quality across the rendered chunks

(§4.7.2). The practice of TBF does not account for the high quality variability across chunks within the same track. For example, the purple points in Fig.4.1(b) represent chunks encoded at track 4 (or 480p). When using TBF with 480p as top track, the quality for some chunk positions is lower than 60 (i.e., the threshold for good quality in VMAF [66]), *no matter what ABR scheme is being used and how much network bandwidth is available.*

4.3.2 Quality-aware Data Saving

To address the drawbacks of the current data saving practices, we propose a quality-aware strategy for reducing data usage. We assume that a user is provided with multiple viewing quality options (e.g., good, better, best), with the understanding that the saving is higher under a lower viewing quality option and vice versa. For an option chosen by a user, the player will map it to a particular quality value, referred to as *target quality*, and the goal of the ABR logic is to maintain the quality to be close to the target quality, subject to the network bandwidth constraints. In contrast to the current data saving practices, the above target quality based strategy provides data savings while directly controlling the quality level.

The target quality can be specified in terms of a wide range of perceptual quality metrics. While there is no single agreed-upon way of defining a good perceptual quality, existing literature has established certain metrics, e.g., through threshold values in VMAF and PSNR (see §4.2.2). As an example, VMAF values of 60 and 80 are the thresholds for “good” and “very good” quality, respectively [66]. The player can set the target quality in VMAF values based on the viewing quality option that a user chooses: when the “good”, “better”, “best” option is chosen, the target quality is set to VMAF 60, 70, 80, respectively. Users do not need to numerically specify the target quality. Instead, they only need to select a desired viewing quality option such as good/better/best—similar to the current practice in commercial streaming systems. For a given video, the quality metrics such as PSNR and VMAF can be calculated by the

server after the video is encoded, and then shared with the client. In addition, a video player can also automatically decide the target quality based on the user's cellular data plan, the cellular data budget, the video content type, and the user's historical preferences. Furthermore, the target quality can be changed over time during the playback; our schemes in §4.4 and §4.5 can be applied to dynamic target qualities.

4.4 Chunk-based Filtering (CBF)

We first describe the CBF approach, and then detail its deployment scenarios and how to leverage it in ABR streaming.

4.4.1 CBF Approach

CBF is motivated from the two video quality and bitrate tradeoffs in §4.2, i.e., (i) increasing bitrate leads to diminishing gain in improving quality, and (ii) the chunks in the same track exhibit significantly variable quality. Specifically, for a given target quality, Q_r , CBF filters the tracks that are undesirable on a *per-chunk basis* as follows. For the i -th chunk position, let $q_{i,\ell}$ denote the quality for track ℓ , which can be obtained right after the encoding process at the server. Then, for a given Q_r , CBF sets the top level for chunk position i to $\bar{\ell}_i$ so that the corresponding quality, $q_{i,\bar{\ell}_i}$, is closest to the target quality, Q_r , among all the tracks for chunk position i (i.e., $|q_{i,\bar{\ell}_i} - Q_r|$ is the smallest). In other words, for chunk position i , all the encodings (i.e., tracks) that are above $\bar{\ell}_i$ will not be considered in ABR streaming.

Fig. 4.3(a) illustrates CBF using an example. It plots the top track after filtering by CBF for each chunk position when the target quality is 80 (VMAF). The video has 6 tracks originally. We see that the top track after CBF varies from 1 to 6 for the different chunk positions (with 53% and 39% as track 3 and 4, respectively, and 6% above 4, and 2% below 3). As an example, for the 29th chunk, the lowest track (i.e., track 1) is sufficient to achieve the target quality 80. A manual inspection reveals that this chunk

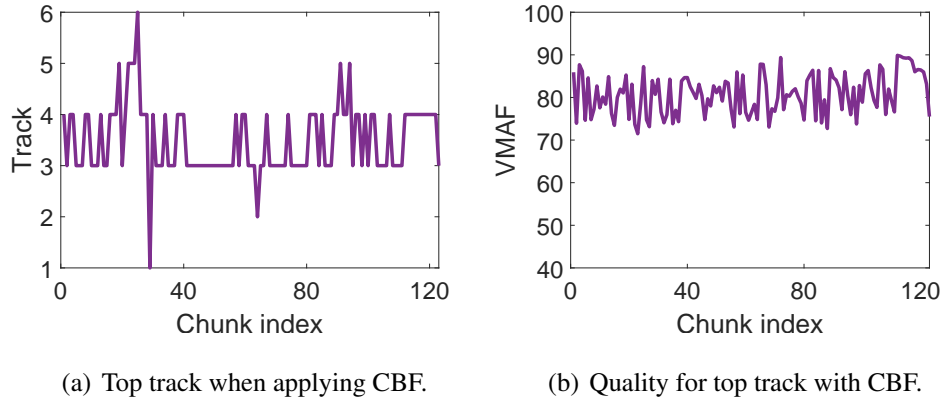


Fig. 4.3: Illustration of CBF (ED, $Q_r = 80$).

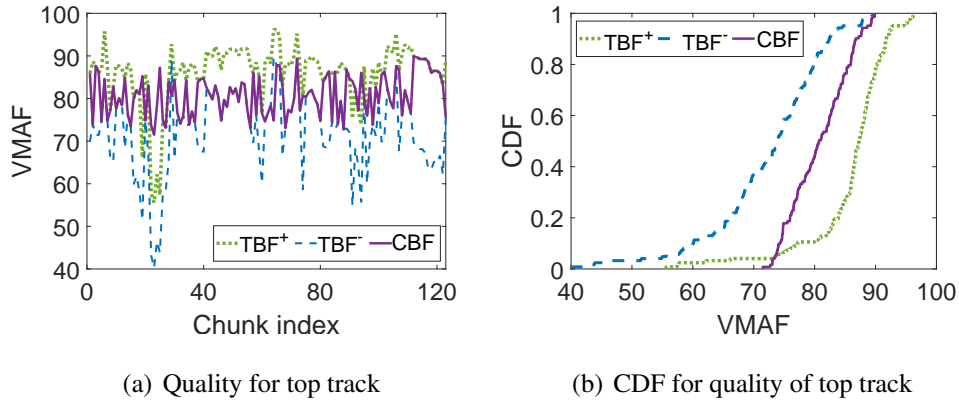


Fig. 4.4: CBF, TBF⁻, and TBF⁺ (ED, $Q_r = 80$).

contains very simple scenes that require less bits to encode. Fig. 4.3(b) plots the highest quality variant for each chunk position that CBF retains. We see that 95% of the chunk positions have top quality within 10% of the target quality (i.e., between 72 and 88).

4.4.2 CBF vs. TBF

We next compare CBF and TBF. Specifically, we consider two variants of TBF as follows. For a video, let $\tilde{Q}(\ell)$ represent the average quality of all the chunks in track ℓ . Let ℓ^- and ℓ^+ denote two adjacent tracks, $\ell^- = \ell^+ - 1$, satisfying that $\tilde{Q}(\ell^-) \leq Q_r$ and $\tilde{Q}(\ell^+) > Q_r$. The first variant of TBF, denoted as TBF⁻, caps the top track to ℓ^- , i.e., it removes all the tracks that are higher than ℓ^- . The second variant of TBF, denoted as TBF⁺, caps the top track to ℓ^+ . Clearly, TBF⁻ is more aggressive in filtering out tracks

than TBF^+ .

Fig. 4.4(a) plots the quality of the top track for each chunk position under CBF, TBF^- , and TBF^+ for one video when the target quality is 80. For this setting, $\ell^- = 3$ and $\ell^+ = 4$. In TBF^+ , all the tracks above track 4 (with resolution 480p) are removed, which coincides with YouTube’s data saving option (§4.3.1). In Fig. 4.4(a), the quality for a given chunk position represents the maximum achievable quality when the network bandwidth is sufficiently large. We see that the quality under CBF is overall much closer to the target quality than that under the two TBF variants. Fig. 4.4(b) shows the cumulative distribution function (CDF) corresponding to the quality values in Fig. 4.4(a). For TBF^- and TBF^+ , only 56% and 53% of the chunk positions have quality within 10% of the target quality, compared to 95% under CBF. We observe similar results as above for other videos and target quality investigated. It is easy to prove that, for any chunk position, the top quality under CBF is no farther away from the target quality than that under the two TBF variants.

4.4.3 Deployment Scenarios

From a practical perspective, a key advantage of CBF is that it can be *incrementally* deployed in the existing DASH and HLS streaming pipelines at either the server or client side. In both deployment scenarios, the server does not remove any chunk from its storage. Rather, it modifies or extends the manifest file that it transmits to the client. We next describe the two deployment scenarios, and end the section with a brief description of using CBF in ABR streaming.

Server Side Deployment. Two approaches, called *chunk variant trimming* and *chunk variant substitution*, can be used for server side deployment. In chunk variant trimming, the server simply modifies the manifest file so that, for each chunk position, it only lists the chunk variants that remain after CBF filtering. As an example, in Fig. 4.5(a), for chunk 1, only the three lowest track variants will be listed in the manifest file. In chunk variant substitution, the server makes the filtering completely transparent

to the client operation by substituting the information for certain chunk variants as follows. Consider the chunks at position i . Let $i.\ell$ represent the chunk at level ℓ . Let $\bar{\ell}$ denote the top track after the filtering by CBF. Then the server modifies the manifest file so that the information for chunk $i.\ell$, $\ell > \bar{\ell}$, is replaced with the information of chunk $i.\bar{\ell}$. In this way, each playback position still has the same number of levels, and the changes through CBF is transparent to the client. For example, in Fig. 4.5(a), for chunk 1, levels 4, 5 and 6 are filtered according to CBF; the server modifies the manifest file to replace the information for chunks 1.4, 1.5 and 1.6 with that of 1.3.

We have verified that the above two approaches work in the context of both DASH and HLS protocols and common packaging formats such as Fragmented MP4 and MPEG-2 TS [3, 4]. The chunk variant substitution approach clearly works when the media format does not include separate initialization segments (i.e., each chunk is self-initializing). It can also be realized for media formats where separate initialization segments (each containing information required to initialize the video decoder to decode a particular chunk) are included, as long as a proper initialization segment is specified for each chunk in the manifest file. We have confirmed through experiments that both DASH and HLS have ways to specify such associations, and that, when presented with the appropriately modified manifest file, the player was able to correctly decode and play the associated video. In DASH, this can be achieved using “Period” construct [4]. In HLS, this can be achieved through extra “EXT-X-MAP” tags [3].

Client Side Deployment. When CBF is deployed at the client, the server further needs to transmit the quality information for each chunk to the client, e.g., by including the information in the manifest file, as our prototype implementation of CBF in two ABR streaming platforms (§4.6). The client, when making rate adaptation decision for a chunk position, will exclude the levels that are above the top track for that chunk position (illustrate as shaded chunks in Fig. 4.5(b)). Note that while quality metrics can be carried in the media file, e.g., following the ISO standard [89], for rate adaptation purposes, the quality information needs to be known to the client beforehand to assist

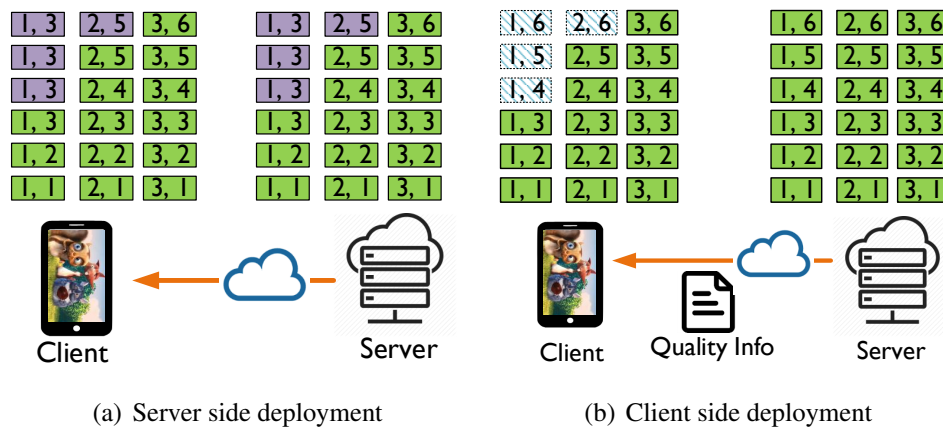


Fig. 4.5: Illustration of CBF deployment.

the decision making, instead of extracting after a chunk is downloaded. Therefore, our implementation embeds the quality information in the manifest file instead of the media file.

Leveraging CBF in ABR Streaming. CBF can be retrofitted to, and improve the performance and data efficiency of existing ABR schemes that may not be quality-aware themselves. This can be achieved either through server-side or client-side deployment of CBF. Specifically, under server-side deployment of CBF, an existing ABR scheme simply selects from the remaining levels for each chunk position. The scheme does not need to leverage or even be aware of any quality information. It can simply aim at maximizing the bitrate (as an indirect way of maximizing the quality) with other QoE considerations, as in most existing schemes. Under client-side deployment of CBF, the client can add a function that applies CBF, and then pass the information of the remaining tracks for a chunk position to an existing ABR algorithm.

4.5 Grounds-up Design: QUAD

Besides integrating CBF into existing ABR schemes, another approach to design target quality aware ABR adaptation schemes is to develop them from the ground up. Such schemes, since explicitly designed with the target quality in mind, have the potential to outperform existing schemes enhanced with CBF. To demonstrate this approach, we

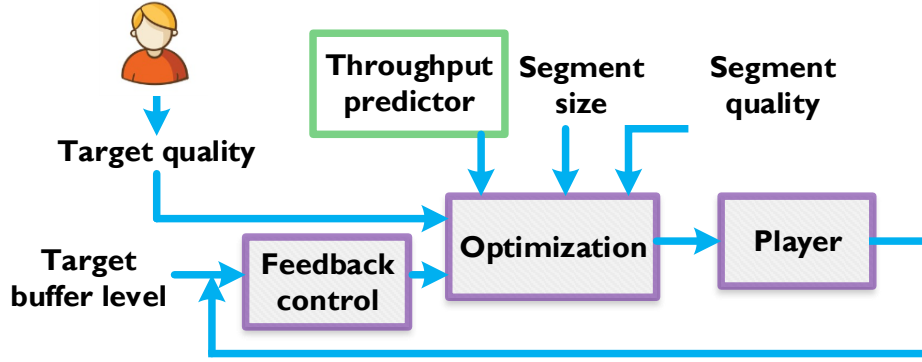


Fig. 4.6: Design diagram of QUAD.

propose one design, called QUAD (Quality Aware Data-efficient streaming), based on control theory. QUAD explicitly integrates the goal of approaching the target quality into its online optimization framework. As a result, it is more capable of maintaining the target quality, and more adaptive to the fluctuating network conditions compared to using CBF with existing schemes.

As shown in Fig. 4.6, QUAD takes a target quality as input, and leverages an optimization formulation and feedback control to optimize the QoE metrics while approaching the target quality.

Target Quality based Optimization. The optimization formulation below aims to make the chosen chunks' quality approach the target quality while minimizing re-buffering and quality changes. Let ℓ_t denote the track number selected at time t . Let $R_t(\ell_t)$ denote the corresponding bitrate of the selected chunk. We use $R_t(\ell_t)$ instead of $R(\ell_t)$ to accommodate VBR encoding whose bitrate is both a function of ℓ_t and time t since the bitrate can vary significantly even within a track. The client selects ℓ_t from the set of levels that remains after CBF. The optimization problem is to determine the track, ℓ_t , so that the following objective function is minimized:

$$J(\ell_t) = \max\left(0, u_t R_t(\ell_t) - \widehat{C}_t\right)^2 + \alpha Q_r - Q_t(\ell_t)^2 + \eta Q_t(\ell_t) - Q_{t-1}(\ell_{t-1})^2,$$

where u_t is the controller output and \widehat{C}_t is the estimated link bandwidth at time t , $\alpha > 0$ and $\eta > 0$ are parameters for the second and third terms, respectively, Q_r is the target

quality specified by the user, $Q_t(\ell_t)$ denotes the quality of the chunk at track ℓ_t for time t , and $Q_{t-1}(\ell_{t-1})$ represents the quality of the previous chunk (here we slightly abuse the notation by using t to represent the index of the chunk for time t and use $t - 1$ to represent the index of the previous chunk).

The formulation in Eq. (4.1) is a least-square optimization problem. In the first term, $u_t R_t(\ell_t)$ represents the bandwidth requirement of the selected track, derived from the feedback control that we will explain shortly. For now readers can regard it as a black box. The first term is zero if the bandwidth requirement of the selected track is no more than the estimated network bandwidth; otherwise, a stall may potentially occur, so it incurs a penalty that equals to the amount of bandwidth that is exceeded by the bandwidth requirement. The second term depends on how much the chosen quality for the chunk deviates from the target quality. The sum of the first and second terms allows the chosen track to be as close to the target quality as possible, while does not overly exceed the network bandwidth (to avoid stalls). The last term penalizes quality changes between two adjacent chunks, in order to maintain a more consistent quality and smooth playback.

We apply normalization in Eq. (4.1) since the first term is of a different unit from the second and third terms. Specifically, we normalize all the three terms to be unitless as follows. The first term is normalized by \widehat{C}_t , the estimated bandwidth, and the other two terms are normalized by Q_r (since QUAD selects from the tracks that remain after CBF, the maximum quality is approximately Q_r). In Eq. (4.1), α and η represent the weights for the second and third terms, respectively. We set both of them to 1 since all the three terms in Eq. (4.1) are important QoE metrics.

We see from Eq. (4.1) that choosing ℓ_t above the target quality Q_r is not beneficial in minimizing the objective function. Therefore, we may apply CBF before solving the optimization problem to reduce the problem space and improve the runtime efficiency. Let \mathcal{L}_t be the set of track levels for chunk t (retained after CBF). We can find the optimal solution to (4.1) by evaluating Eq. (4.1) using all possible values of \mathcal{L}_t , leading

to computational overhead $O(|\mathcal{L}_t|)$. In §4.8, we show that QUAD is very lightweight using our implementation.

Feedback Control Block. In the first term in (4.1), $u_t R_t(\ell_t)$, is derived from the feedback control block shown in Fig. 4.6. We use PID control [45] as the underlying control framework since it is simple and robust for ABR streaming [56]. Specifically, the PID control block works by continuously monitoring the difference between the target and current buffer levels of the video player, and adjusting the control signal to maintain the target buffer level, which helps to avoid stalls. We define the controller output, u_t , as:

$$u_t = \frac{C_t}{R_t(\ell_t)}, \quad (4.1)$$

where C_t denotes the network bandwidth at time t , and $R_t(\ell_t)$ denotes the bitrate of the chunk selected for time t . The control policy is defined as:

$$u_t = K_p(x_r - x_t) + K_i \int_0^t (x_r - x_\tau) d\tau + \mathbf{1}(x_t - \Delta) \quad (4.2)$$

where K_p and K_i denote respectively the parameters for proportional and integral control (two key parameters in PID control), x_r is the target buffer level, x_t is the current buffer level (in seconds) at time t , Δ denotes the playback duration of a chunk, and the last term, $\mathbf{1}(x_t - \Delta)$, is an indicator function (1 when $x_t \geq \Delta$ and 0 otherwise), which makes the feedback control system linear, and hence easier to control and analyze. From (4.1), we derive $C_t = u_t R_t(\ell_t)$ and plug it into (4.1).

Further Reducing Rebuffering. To avoid rebuffering when the current buffer level is low, we further use a heuristic. Specifically, if $x_t < 4\Delta$, i.e., there are less than four chunks in the buffer, then the track is selected as $\min(\ell_f, \widehat{C}_t/u_t)$, where ℓ_f is the lowest track with fair quality for that chunk position. In other words, when the current buffer level is low, we ignore the goals of achieving the target quality and reducing quality changes (i.e., the last two terms in (4.1)), and only consider the first term (to reduce the risk of stalls). In that case, we first select the track based on \widehat{C}_t/u_t . Since \widehat{C}_t can be an overestimate of the actual network bandwidth, we further bound the selected

track to be no more than level ℓ_f . For the videos that we use in our evaluation (see §4.6), we set ℓ_f to 2, which has significantly higher quality than track 1.

4.6 Implementation & Evaluation Setup

Implementation. We implemented client-based CBF and QUAD in two popular players, `dash.js` [53] and `ExoPlayer` [30]. We made a set of non-trivial changes. First, we included the quality information of each chunk in the manifest file. We then modified `dash.js` and `ExoPlayer` so that the chunk quality information can be passed to the ABR logic. We also implemented a new module `cbf.js` to realize CBF, and a new rate adaptation module `quad.js` to realize QUAD in `dash.js`. In `ExoPlayer`, we created two new classes, `cbf.java` and `quad.java`, for CBF and QUAD. The total number of LoC that is involved in the above changes is 336 in `dash.js` and 396 in `ExoPlayer`. In `dash.js`, we developed a bandwidth estimation module that responds to playback progress events and estimates network throughput using the harmonic mean of the last 5 chunks.

Evaluation Setup. Our evaluations use a combination of controlled lab experiments with our implementations in `dash.js` and `ExoPlayer`, as well as simulations, all driven by real-world network bandwidth traces collected from commercial cellular networks. This methodology allows repeatable experiments and to evaluate different schemes under identical settings. In §4.8.4, we also run in-the-wild tests using `ExoPlayer` on a phone over an LTE network.

Network Traces and Videos. We collected a total of 42 hours of network traces over two large commercial LTE networks in the U.S. Our traces consist of per-second network bandwidth measurements, which are collected on a phone, by recording the throughput of a large file downloading from a well-provisioned server. They cover a diverse set of scenarios, including different time of day, different locations, and different movement speeds (stationary, walking, local driving, and highway driving). We selected 50 *challenging* traces, each of 700 seconds, with the average network bandwidth

below 1 Mbps. The reason for choosing such traces is because even with target quality of 80 (in VMAF, regarded as very good quality [66], the highest quality we evaluate), the average bandwidth requirement is below 1 Mbps (varies from 500 to 800 kbps) for the videos we use. Using higher bandwidth traces will diminish the differences among different schemes; these low-bandwidth traces, measured from commercial cellular networks, represent challenging conditions that do occur in real networks, e.g., when the network is congested or the signal is poor. We use 4 VBR and 4 CBR videos in our evaluation. They are encoded using the four raw videos (ED, BBB, Sintel, ToS) that we have access to (see §4.2.1), and hence we can calculate the perceptual quality using raw videos as the reference. The results in §4.7 and §4.8 focus on VBR videos; the results for CBR videos are consistent and omitted due to space.

CBF with Existing ABR Schemes. We use CBF as a prefilter for the following state-of-the-art rate adaptation schemes: (i) **RobustMPC** [13], which is a well-known scheme based on model predictive control. (ii) **PANDA/CQ** [27], which directly incorporates video quality information in ABR streaming. It maximizes the minimum quality for the next N chunks, which achieves better fairness (in terms of quality) among multiple chunks. (iii) **BOLA-E** [11, 37], which selects the bitrate to maximize a utility function considering both rebuffering and delivered bitrate. (iv) **ExoPlayer**'s ABR adaptation [30], referred to as *Exo* henceforth, which is essentially a rate based logic, i.e., selecting the track based on bandwidth estimation. The results for RobustMPC and PANDA/CQ are obtained through trace-driven simulation; the evaluation involving BOLA-E and ExoPlayer ABR logic is done using open source implementation in `dash.js` and `ExoPlayer`, respectively.

Offline Optimal Scheme. We further use an offline optimal solution as a baseline to evaluate the performance of various schemes. This offline scheme assumes that the entire network bandwidth is known beforehand. It considers three QoE metrics related to target quality, quality changes, and stalls. Specifically, for a video with n chunks, it

selects tracks ℓ_1, \dots, ℓ_n to minimize

$$J(\ell_1, \dots, \ell_n) = \sum_{t=1}^n (Q_r - Q_t(\ell_t))^2 + \sum_{t=1}^{n-1} (Q_{t+1}(\ell_{t+1}) - Q_t(\ell_t))^2 + \gamma T_r(\ell_1, \dots, \ell_n)$$

where Q_r is the target quality, $Q_t(\ell_t)$ is the quality for ℓ_t , and $T_r(\ell_1, \dots, \ell_n)$ is the rebuffering duration, and γ is the weight for rebuffering. The results below use $\gamma = 100^2$, i.e., we penalize each second of rebuffering with square of the maximum VMAF quality.

ABR Configurations. Following practices in commercial production players [24], we set the player to start the playback when two chunks are downloaded into the buffer. The track for the first chunk is selected to be the middle track (i.e., track 3). Unless otherwise stated, we use the harmonic mean of the average download throughout for the past 5 chunks as the bandwidth prediction, as it has been shown to be robust to measurement outliers [13, 34]. For the results using ExoPlayer, the bandwidth prediction uses the built-in sliding percentile technique [30]. Unless otherwise stated, for all schemes, we set the maximum client-side buffer size to 120 seconds. This is reasonable for Video on Demand (VOD) streaming, and is consistent with existing practices that set the maximum buffer limit to hundreds of seconds [14, 24, 53]. An ABR scheme may use thresholds to control when to stop and resume downloading based on the buffer level. When comparing with another scheme, we ensure that our schemes use the same thresholds as used in that scheme. For QUAD, the controller parameters, K_p and K_i , are selected by adopting the methodology outlined in [56]. Specifically, we varied K_p and K_i , and confirmed that a wide range of K_p and K_i values lead to good performance.

Perceptual Quality Metric. We measure video quality using VMAF (§4.2). Specifically, we use VMAF phone model (instead of TV model) given our focus on cellular networks. In the testing, we assume that a user selects from three quality options, good/better/best. Correspondingly, the player maps these quality options to VMAF values of 60 (for “good”), 70 (for “better”), and 80 (for “best”).

Performance Metrics. We use five metrics: four for measuring different aspects of user QoE and one for measuring data usage. All metrics are computed with respect to the delivered video, i.e., considering the chunks that have been downloaded and played back. The metrics are listed as follows. (i) *Quality of all the chunks*: measures how the quality of each chunk differs from the target quality. (ii) *Low-quality chunk percentage*: measures the proportion of the chunks that were selected with low quality during a streaming session. The reason for using this metric is because human eyes are sensitive to bad quality chunks [70]. We identify VMAF values below 40 as low-quality based on [66]. (iii) *Rebuffering duration*: measures the total rebuffering/stall time in a streaming session. (iv) *Average quality change per chunk*: defined as the average quality difference of two consecutive chunks in playback order for a streaming session (since human eyes are more sensitive to level changes in adjacent chunks). (v) *Data usage*: measures the total amount of data downloaded for a streaming session. For metrics (ii)-(v), a lower value is preferable; for (i), we measure how close it is to the target quality. In addition to the above metrics, we further explored the number of stalls during a session in various cases. Our results show that using CBF in existing schemes reduces the number of stalls, and QUAD leads to fewer stalls compared to existing scheme enhanced with CBF in almost all the cases.

4.7 Evaluation Existing ABR Schemes Enhanced with CBF

We evaluate the performance of adding CBF to existing ABR schemes. We focus on two existing schemes, RobustMPC and PANDA/CQ. The performance of other schemes with CBF is deferred to §4.8.

4.7.1 Benefits of CBF

Fig. 4.7 shows the performance of RobustMPC and PANDA/CQ with and without CBF for one video across the network traces when the target quality is 80. The results for the five performance metrics are shown in the five subplots in the figure: the first subplot

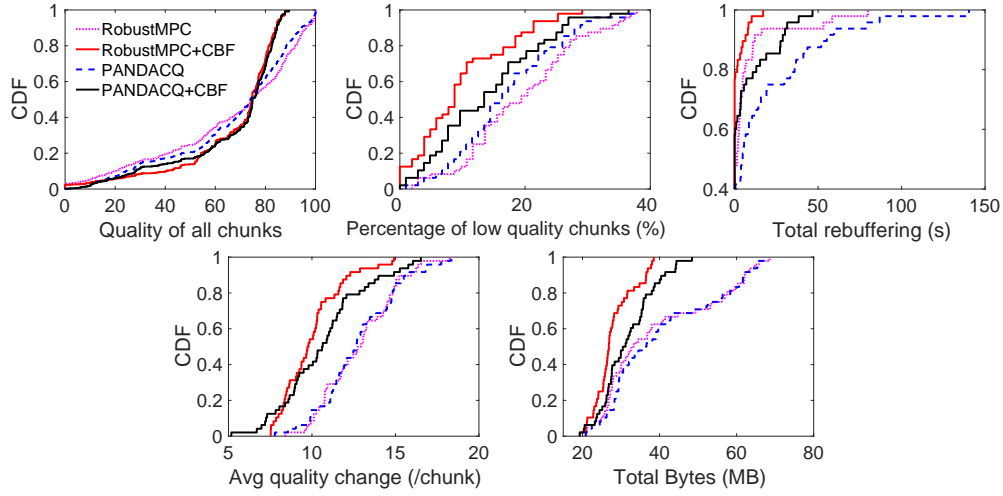


Fig. 4.7: Two existing ABR schemes with and without CBF (ED, YouTube encoded, target quality 80).

is the CDF across individual chunks across all runs; the rest four are CDFs across runs, with each run corresponding to a different network trace. We observe that CBF improves performance for both ABR schemes, across all metrics. Specifically, compared to the original schemes, adding CBF leads the quality to be closer to the target quality, and reduces the percentage of low-quality chunks, the quality changes, rebuffering, and data usage.

Table 4.2 summarizes the results for four VBR videos for RobustMPC with and without CBF for target quality of 60 and 80, respectively. The first column is the average deviation from the target quality across all the network traces; the value for one trace is $(\sum |q_i - Q_r|)/n$, where q_i is the quality of chunk i in the rendered video, Q_r is the target quality, and n is the number of chunks in the video. The second column shows the percentage of the traces that have more than 20% of low-quality chunks. The third column shows the average rebuffering duration for the traces where either case (i.e., with or without CBF) has rebuffering. The last two columns show the average quality changes and the data usage, averaged across the network traces. We see that CBF reduces the deviation from the target quality by 37-67%, reduces the number of traces with frequent low-quality chunks by 6-42%, and reduces the average quality

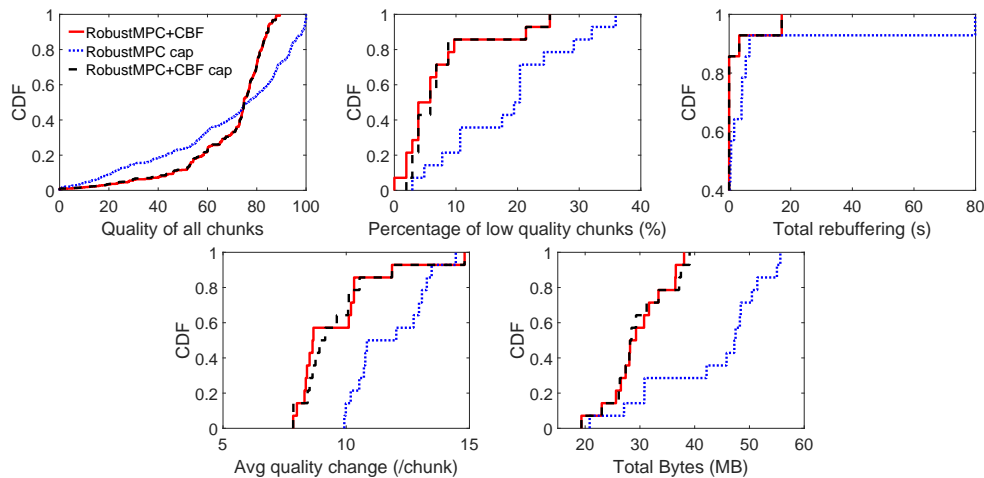


Fig. 4.8: CBF versus capping network bandwidth (ED, YouTube encoded, target quality 80).

change by 7-31%. For many videos, across all network traces, using CBF leads to no stalls compared to substantial amount of stalls without CBF. The data usage with CBF is 34-67% lower than that without CBF. In the extreme case when the bandwidth is sufficiently high, RobustMPC without CBF will choose the highest track (i.e., track 6). The data usage for the four videos will be 203, 179, 240, and 209 MB respectively, 5.6-7.5 times higher than the corresponding values with CBF under target quality 80 (the ratios are even higher for target quality 60).

We see similar results for PANDA/CQ with and without CBF. The above results demonstrate that CBF can significantly improve the performance of existing ABR schemes by prefiltering the chunks whose qualities are higher than the target quality, and hence steering the schemes to the set of more desirable choices.

4.7.2 CBF vs. Network Bandwidth Cap

We now compare CBF with an existing practice for saving data by capping network bandwidth (§4.3.1). Specifically, for an existing ABR scheme, we consider three cases: (i) we assume that the cellular network provider caps the network bandwidth to 1.5 Mbps; (ii) there is no cap on the network bandwidth, while the scheme is used together

Table 4.2: RobustMPC vs. RobustMPC+CBF.

| | Video | Avg. dev. from target quality | % of traces w/ > 20% low-qual. chunks | Avg. stall dura. (s) | Avg. quality change | Data usage (MB) |
|---------|--------|--|--|-------------------------------|---------------------------|-----------------------|
| VBR, 60 | ED | 25, 9 | 48%, 10% | 8, 0 | 13, 9 | 39, 19 |
| | BBB | 27, 9 | 37%, 8% | 6, 0 | 14, 11 | 36, 14 |
| | Sintel | 28, 11 | 6%, 0% | 8, 0 | 10, 12 | 55, 18 |
| | ToS | 26, 14 | 56%, 40% | 5, 0 | 13, 12 | 46, 22 |
| VBR, 80 | ED | 23, 15 | 48%, 12% | 8, 2 | 13, 10 | 39, 28 |
| | BBB | 22, 14 | 37%, 8% | 6, 1 | 14, 13 | 36, 21 |
| | Sintel | 19, 9 | 6%, 0% | 8, 0 | 10, 9 | 55, 29 |
| | ToS | 24, 16 | 56%, 21% | 5, 2 | 13, 10 | 46, 35 |

* The two numbers in each cell are the results for RobustMPC and RobustMPC+CBF, respectively.

with CBF; and (iii) there is a bandwidth cap and the scheme is used with CBF. Since the network bandwidth of some traces is low and imposing the constraint of 1.5 Mbps leads to little impact, we choose a subset of network traces where the cap meaningfully changes the available bandwidth. Specifically, a network trace is chosen if the bandwidth estimated using a window of 1 second is larger than 1.5 Mbps for at least 10% of the time. The results below are obtained from 20 traces selected as above.

Fig. 4.8 shows the results for RobustMPC with target quality 80; the results for PANDA/CQ show a similar trend. We see that the two variants with CBF achieve similar performance. Both of them significantly outperform the other variant (i.e., with bandwidth cap but no CBF) in all performance metrics. The results demonstrate the effectiveness of CBF compared to the network bandwidth capping approach. They also indicate that CBF can co-exist with the network bandwidth capping approach. The above results are for one video with target quality 80. We observe similar results for

other videos and target qualities. For lower target qualities (i.e., 60 and 70), we observe that CBF achieves even better performance.

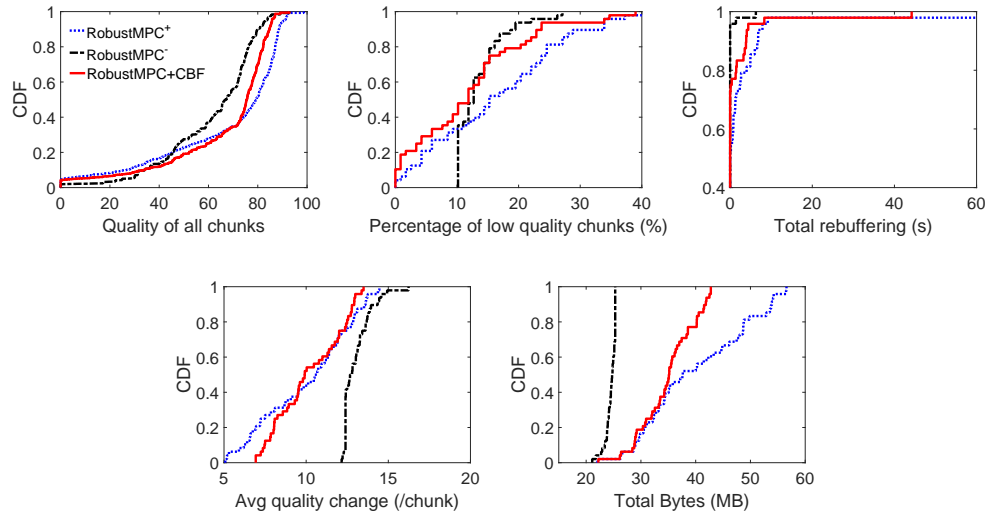


Fig. 4.9: RobustMPC with CBF vs TBF (ToS, YouTube encoded, target quality 80).

4.7.3 CBF vs. TBF

We now compare CBF with TBF, which is used by commercial streaming services such as YouTube and Amazon for reducing data usage (see §4.3.1). Specifically, we consider two variants of TBF, i.e., TBF⁻ and TBF⁺ (see §4.4.2).

Fig. 4.9 plots the performance of RobustMPC with CBF, and with the two TBF variants, referred to as RobustMPC⁻ and RobustMPC⁺. The results are for one VBR video when the target quality is 80. For this setting, the top track in RobustMPC⁻ and RobustMPC⁺ is track 3 and 4, respectively. We make the following observations. (i) RobustMPC⁻ is quite conservative. It provides low rebuffering time. However, the negative side is that it undershoots the target quality (its average deviation from the target quality is 20 VMAF points across the chunks, compared to 15 under RobustMPC⁺+CBF), and leads to a higher percentage of low-quality chunks (it has at least 10% low-quality chunks for 100% of the traces, compared to 58% and 68% of the traces under RobustMPC⁺+CBF and RobustMPC⁺, respectively). (ii) RobustMPC⁺,

on the other hand, is too aggressive. It overshoots the target quality (it exceeds the target quality in 50% of the chunks, compared to 30% under RobustMPC+CBF), incurs the highest rebuffering time, and consumes the highest network bandwidth among the three schemes. Also, it results in highly variable quality by choosing high quality for some chunks while leaving a higher percentage of chunks with low quality. (iii) RobustMPC+CBF strikes a better balance among the aforementioned factors. It also achieves a quality that is closest to the target quality. We observe similar results for other videos and target qualities. We further compare the three variants of PANDA/CQ and observe that PANDA/CQ+CBF achieves better performance than the others. The reason, as explained in §4.4.2, is that compared to TBF, CBF filters out chunks at a finer granularity (on the basis of chunks instead of tracks), thus allowing it to make better choices.

4.8 Evaluation of QUAD

In this section, we compare QUAD and existing schemes enhanced with CBF. We also evaluate them in `dash.js` and `ExoPlayer`.

4.8.1 QUAD vs. CBF

Fig. 4.11 plots the performance of QUAD and two existing schemes (RobustMPC and PANDA/CQ) with CBF for two videos, based on trace-driven simulations. It also plots the results of the offline optimal scheme (see §4.6). We observe that for all five metrics except the data usage, QUAD achieves performance closest to that of the offline optimal; for data usage, the offline optimal uses more data than other schemes, consistent with the best quality that it achieves. QUAD outperforms RobustMPC+CBF and PANDA/CQ+CBF for both videos in Fig. 4.11. For video BBB (Fig. 4.11 bottom row), while RobustMPC+CBF has similar rebuffering as QUAD, it leads to a noticeably worse quality (the average deviation from the target quality is 14 VMAF points across the runs under RobustMPC+CBF, and 10 under QUAD). For video ED (Fig. 4.11 top

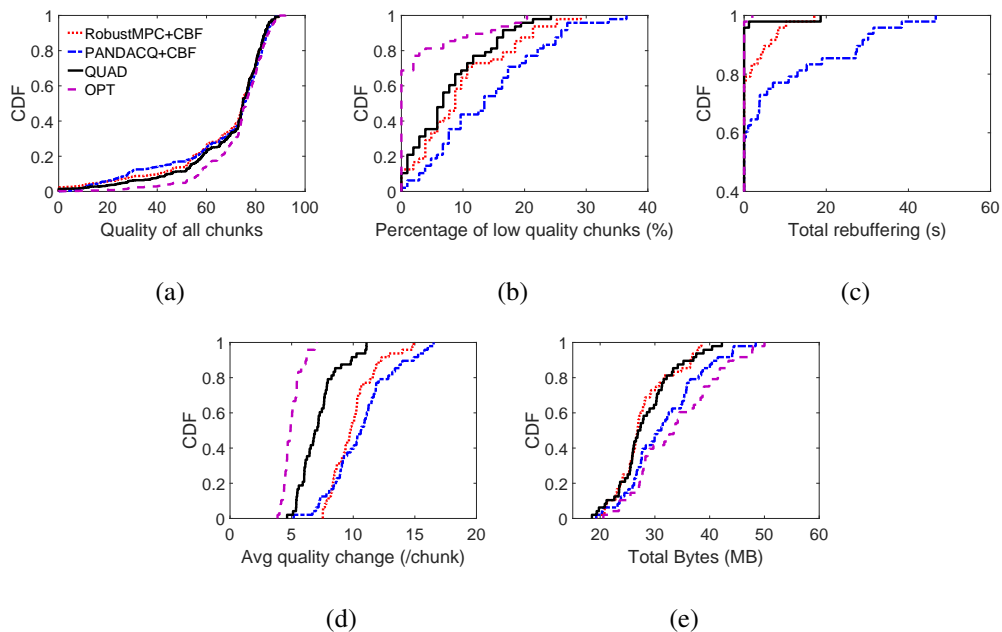


Fig. 4.10: QUAD vs. two existing schemes with CBF (ED, YouTube encoded, target quality 80).

row), the overall quality of the two schemes is similar, while RobustMPC+CBF has more rebuffering than QUAD (it has rebuffering in 23% of the runs, compared to only 4% in QUAD). For both videos, the average quality change per chunk under QUAD is much lower compared to RobustMPC+CBF: 7 under QUAD for both videos, compared to 10 and 13 under RobustMPC+CBF. The overall quality of PANDA/CQ+CBF is comparable to that of QUAD for both videos, but has significantly more rebuffering, higher quality changes, and uses more data.

4.8.2 dash.js based Evaluation

Using our developed QUAD in dash.js (version 2.4.1), we compare its performance with BOLA-E [11] and BOLA-E+CBF. The original BOLA-E design takes a single bitrate rate for each track, which is suitable for CBR videos; for VBR videos, we improved the design by using the actual chunk sizes in the ABR logic based on [11]. Our evaluation below uses two computers (Ubuntu 12.04 LTS, CPU Intel Core 2 Duo,

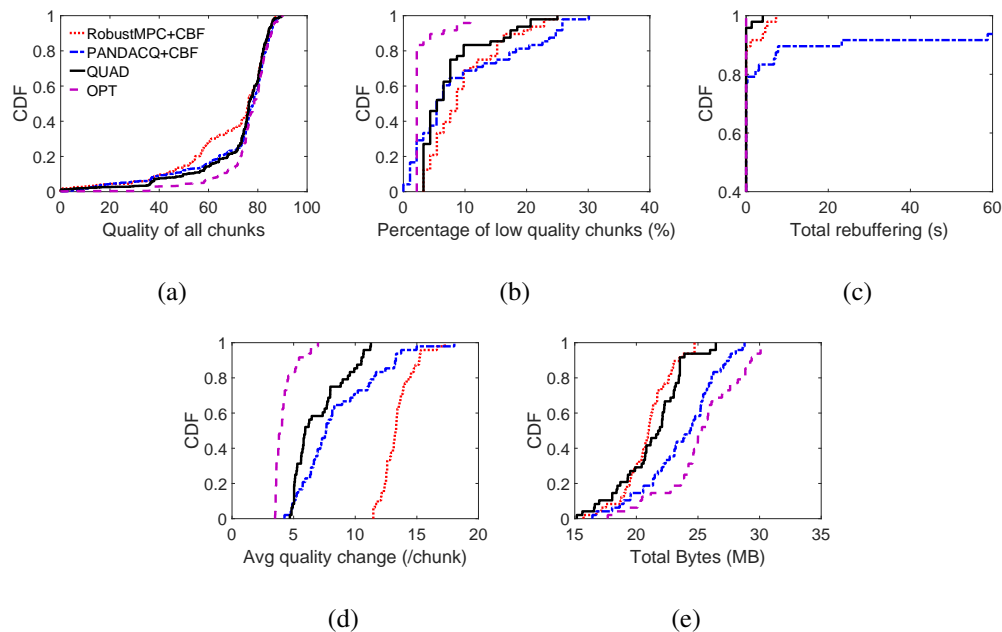


Fig. 4.11: QUAD vs. two existing schemes with CBF (ED, BBB, YouTube encoded, target quality 80).

4GB memory) with a 100 Mbps direct network connection to emulate the video server (Apache httpd) and client. At the client, we use `selenium` [75] to run a Google Chrome web browser and use `dash.js` APIs to collect the streaming performance data. We use `tc` to emulate real-world variable mobile network conditions by “replaying” the network traces (§4.6). We find QUAD is very light-weight. With the current prototype, the total execution time of QUAD is only about 10ms for a 10mins video.

Fig. 4.12 shows the performance of QUAD, BOLA-E, and BOLA-E+CBF for one video with target quality 80. We observe that BOLA-E+CBF significantly outperforms BOLA-E in all performance metrics. QUAD further outperforms BOLA-E+CBF in achieving 37% reduction in average percentage of low-quality chunks and 12% reduction in average quality changes across the runs. QUAD has rebuffering in 8% of the runs, compared to 15% under BOLA-E+CBF. The chunk quality of BOLA-E+CBF is close to that of QUAD, with data usage close to than that of QUAD. The results for other videos and target qualities show a similar trend.

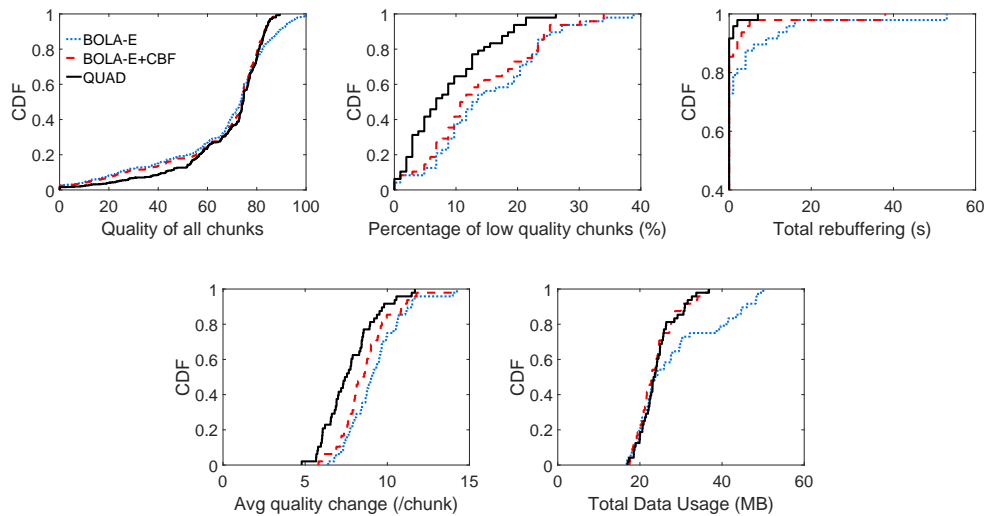


Fig. 4.12: QUAD vs. BOLA-E with and without CBF in dash.js (ED, YouTube encoded, target quality 80).

4.8.3 ExoPlayer based Evaluation

We compare the performance of QUAD (using our implementation) with Exo (the default ABR algorithm, see §4.6, with and without CBF) in ExoPlayer (version 2.4.4). The client is an LG V20 phone (Qualcomm Snapdragon 820, 64GB storage and 4 GB RAM) with Android 7.0. The experiments are conducted over a WiFi network (with consistent tens of Mbps bandwidth). We again emulate the 50 challenging cellular network traces (§4.6) by “replaying” the traces.

Fig. 4.13 shows the results for two variants of Exo: the first using the default parameters, and the second (referred to as *ExoTuned*) using tuned parameters to improve its quality. In the first variant (i.e., the default ABR logic), the downloading stops when the buffer level reaches 30 seconds and resumes when the buffer is less than 15 seconds. In ExoTuned, the parameters are set so that the player stops downloading when the buffer reaches 120 seconds (the value we have used for other schemes, see §4.6), and resumes downloading when the buffer level drops to 105 seconds. Correspondingly, the two parameters for QUAD are set to 120 and 105 seconds as well. We see

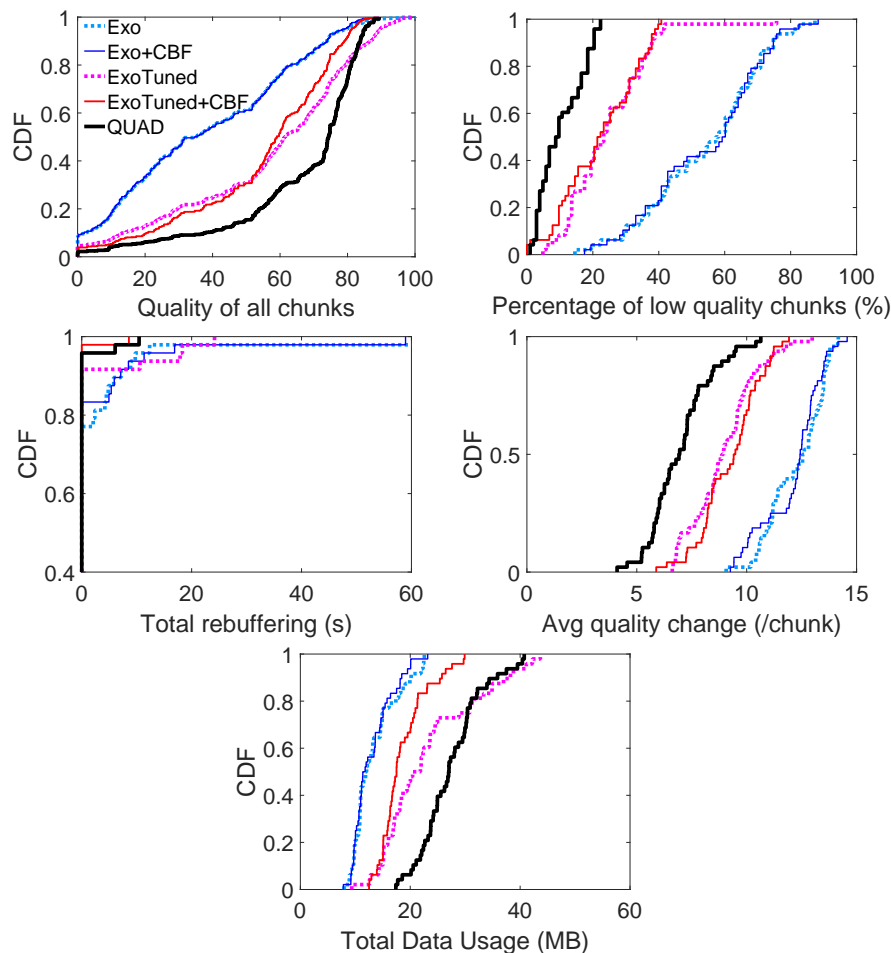


Fig. 4.13: QUAD vs. Exo with and without CBF in ExoPlayer (ED, YouTube encoded, target quality 80).

that ExoTuned indeed achieves better performance compared to Exo since the larger buffer allows the player to download and store more content in the buffer. For both Exo and ExoTuned, adding CBF avoids downloading chunks with excessively high quality, which reduces rebuffering and the data usage (for these two schemes, adding CBF does not lead to much improvement in quality since their quality selections are already quite conservative). We further see that QUAD significantly outperforms all Exo variants. Compared to Exo, QUAD reduces the average deviation from the target quality by 64%, reduces the average percentage of low-quality chunks across all runs by 81%,

Table 4.3: In-the-wild tests using ExoPlayer.

| | Avg. dev. from target quality | Avg. % of low quality chunks | Avg. stall dura. (s) | Avg. quality change | Data usage (MB) |
|-------------|--|---------------------------------------|-------------------------------|---------------------------|-----------------------|
| Low bw. | 19.5±6.1 | 17.3±10.2 | 2.4±4.6 | 7.8±0.9 | 26.1±6.5 |
| | 20.0±6.2 | 14.2±8.5 | 0 | 8.5±1.1 | 21.0±4.3 |
| | 11.9±2.9 | 6.5±3.7 | 0 | 5.6±1.2 | 28.8± 3.7 |
| High bw. | 17.9±0.6 | 0 | 0 | 1.5±0.3 | 181.0±9.9 |
| | 3.9±0.1 | 0 | 0 | 5.0±0.1 | 47.7±0.6 |
| | 4.2±0.1 | 0 | 0 | 4.6±0.1 | 45.2±0.1 |

* The three rows in each cell are the results for ExoTuned,
ExoTuned+CBF, and QUAD, respectively.

reduces the average rebuffering (over of the subset of runs where either algorithm has rebuffering) by 86%, and reduces the average quality change across the runs by 43%. Compared to ExoTuned+CBF, the corresponding reductions in the deviation from the target quality, the average percentage of low-quality chunks, and the quality changes are 40%, 46%, and 22%, respectively, albeit QUAD uses more data.

4.8.4 In-the-wild Tests

So far, our evaluation has been through large-scale trace-driven simulation and experimentation using real systems. We next present in-the-wild test results, by running QUAD and ExoTuned (which outperforms Exo) over a commercial LTE network. The video we use is ED (YouTube encoded). We consider two settings, one with poor signal conditions and hence low bandwidth (consistently less than 1Mbps and unstable), and the other with good signal conditions and hence high bandwidth. The first setting is in a residential home, and the second one is in an office building. For each setting, we make 10 runs, each consisting of three schemes (QUAD, ExoTuned and ExoTuned+CBF, in

a random order). The results are shown in Table 4.3, which lists the mean and standard deviation across the runs for each case. Under high bandwidth conditions, compared to ExoTuned alone, we see significant benefits of CBF and QUAD in reducing data usage and achieving quality close to the target quality. Under low bandwidth conditions, the results exhibit more variations due to the fluctuating network bandwidth caused by the poor signal strength. Despite that, compared to ExoTuned, we still observe that CBF significantly reduces the percentage of low-quality chunks, and QUAD achieves the best QoE overall. ExoTuned+CBF and QUAD have no rebuffering, while ExoTuned shows non-negligible rebuffering duration for the 10-minute video.

4.9 Related work

Improving Video QoE. In addition to the schemes already described in §4.6, QDASH [90] tries to reduce quality switches during adaptation. BBA [14] proposes adaptation schemes based on client-side buffer information. PIA [56] designs a PID-based framework to account for various requirements of ABR streaming. Pensieve [35] proposes a system that generates ABR algorithms using reinforcement learning. Oboe [36] pre-computes the best possible ABR parameters for different network conditions and dynamically adapts the parameters at run-time. CAVA [91] proposes design principles for VBR-based ABR streaming and a concrete scheme that instantiates these design principles. PANDA/CQ [27] directly incorporates video quality information in ABR streaming and maximizing QoE by dynamic programming. The study in [92] outlines the challenges and open issues in consistent-quality streaming such as the scheme in [27]. None of the above studies explicitly considers data efficiency.

Reducing Data Usage. A number of studies have proposed techniques for reducing data in the content encoding process. Chen et al. [71] propose an optimization framework to identify the optimal encoding bitrates that minimize the average streaming bitrate, subject to a given lower bound on delivered quality. De Cock et al. [86] present a constant-slope rate allocation approach to improve the Bitrate-Distortion rate.

Aaron et al. [59] propose per-title encoding, i.e., each title should receive a bitrate ladder, tailored to its complexity characteristics. Katsavounidis et al. [93] develop a dynamic optimizer framework that searches for optimized encoding parameters. Toni et al. [94] determine the optimal selection of tracks for encoding. Our work differs from the above by jointly improving video QoE and reducing data usage in the streaming process. Therefore, our work is orthogonal to those on reducing data in the encoding process, and can complement those efforts.

The study in [95] manages the tradeoff between monthly data usage and video quality by leveraging the compressibility of videos and predicting consumer usage behavior throughout a billing cycle. Our study differs from it in that we consider the data usage and quality tradeoffs when streaming a video. The study in [96] observes that, for some chunks, lower bitrate tracks may be of similar perceptual quality as higher bitrate tracks. Given a set of encoded ABR tracks, it proposes to perform a server-side chunk replacement (within the same resolution) so that a higher bitrate chunk can be replaced by a lower bitrate chunk with a perceptually similar quality. Unlike our work, this study does not perform an in-depth exploration of how their approach interacts with existing ABR rate adaptation algorithms. QBR [97] aims to improve the efficiency of existing ABR schemes by reducing the data usage while potentially increasing QoE. Specifically, a QBR server provides additional metadata hints to a client, allowing the client to request a reduced bitrate for chunks of low complexity. QBR is not designed to achieve a target quality based on a user-specified option. In addition, it does not provide a grounds-up design as QUAD.

4.10 Summary

Existing data saving practices for ABR videos often incur undesired and highly variable video quality, without making the most effective use of the available network bandwidth. In this chapter, we identify underlying causes for this behavior and design two novel approaches, CBF and QUAD, to achieve better tradeoffs among video quality,

rebuffering, quality variations, and cellular data usage. Evaluations demonstrate that compared to the state of the art, these two schemes achieve quality closer to desired levels, lower stalls, and more efficient data usage. Specifically, using CBF with existing schemes leads to significant benefits in all performance metrics, and QUAD achieves even better QoE compared to existing schemes enhanced with CBF.

Aligned with this work, we further propose a novel framework for quality-aware Adaptive Bitrate (ABR) streaming involving a per-session data budget constraint. Under the framework, we develop two planning based strategies, one for the case where fine-grained perceptual quality information is known to the planning scheme, and another for the case where such information is not available. More details can be found at [98].

Chapter 5

ABR Streaming with Separate Audio and Video Tracks: Measurements and Best Practices

5.1 Introduction

Little is known on how best to mesh together audio and video rate adaptation in ABR streaming. In this chapter, we first examine the current practice in the predominant DASH [4] and HLS [3] protocols and three popular players, ExoPlayer [30], Shaka Player [99], and `dash.js` player [53] (see §5.2). Using a combination of code inspection and experiments, we identify a number of limitations in existing practices both in the protocols and the player implementations (see §5.3). We identify the root causes of these limitations, and present a set of best practices and guidelines (see §5.4). Our work makes the following contributions:

- We find that all three players have various issues in handling demuxed audio and video tracks (§5.3). These issues are not simple implementation bugs, but rather arise due to a confluence of sometimes subtle interacting factors, ranging from a lack of sufficient insights, design/engineering inadequacies to architectural deficiencies. Specifically, these issues include (i) limitations in how DASH/HLS handles demuxed content, (ii) player designs to circumvent the limitations in DASH/HLS, (iii) little understood differences between HLS and DASH with important implications, (iv) attempts in applying the same player logic designed for one protocol (DASH/HLS) to the other, and (v) inadequate attention to synchronizing a player’s video and audio downloading.
- Our findings demonstrate that meshing together audio and video rate adaptation is

a very challenging problem – it involves many pieces (in ABR protocols, server and player designs) and needs a holistic solution. As a starting point in addressing the challenges, we provide a set of best practices and guidelines (§5.4) for the ABR protocol level (manifest file specification enhancements), the server side (appropriately using manifest to convey needed information to the client), and the player side (audio/video prefetching, and joint adaptation for audio and video).

Note that in this work we consider coordinated ABR rate adaptation for streaming demuxed video and audio to the *same user* to maximize QoE. The demuxed video and audio tracks may be located at different servers and hence may not necessarily share the same bottleneck link. This problem is very different from the multi-user rate adaptation problem where videos are streamed to *multiple users* while sharing the same bottleneck link [34, 100, 101, 102].

We hope that our study brings the problem of ABR streaming with demuxed audio and video tracks to the community’s attention. With coordinated efforts, we hope that the community can come up with effective solutions soon.

5.2 Motivation and Methodology

5.2.1 Motivation

One way of treating demuxed audio and video tracks is determining their rate adaptation independently, and combining the audio and video chunks at playback time. While this approach is easy to implement, it has two major drawbacks. First, it can lead to some audio and video combinations that are clearly undesirable (e.g., lowest quality audio with highest quality video, or vice versa). Second, it can cause the prefetched audio and video streams to be severely unbalanced, e.g., audio (resp. video) buffer underruns and hence leads to stalls, while there is a lot of prefetched data for the corresponding video content (resp. audio).

Although the audio/video rate adaptation is decided by the player at the client, we argue that the server needs to provide sufficient information to facilitate the deci-

sion. Determining a good set of audio and video combinations is not a trivial task. It depends on the nature of the specific content, device characteristics (e.g., screen size, sound system), and the business rules encoding the content provider’s preferences for that content. For instance, for music shows, the sound quality may be relatively more important than video quality, and hence it might be more desirable to combine high audio tracks with low/medium video tracks; while for an action movie, the desirable combinations may be the opposite. The origin server knows the content information, client device types, and the business rules, and hence is at a better position for deciding the combinations. Ideally, the server can determine a good set of audio and video combinations beforehand, and pass the information to the player through the manifest file or other out-of-the-band mechanisms.

5.2.2 High-level Methodology

To understand the current practice for handling demuxed audio and video tracks, we examine both predominant ABR streaming protocols (DASH and HLS) and the treatment in three open-source popular players, specifically, ExoPlayer [30] and Shaka [99] that are widely used in industry, and `dash.js` [53] that showcases the DASH standard. For each player, our focus is on understanding the interaction between audio and video rate adaptation and their impact on each other. Specifically, we use a combination of source code analysis (all the three players are open-source players) and controlled experiments (with additional instrumentation in the source code when necessary). The combined approach is necessary because as a large-scale often multithreaded software system, the player source code contains a large number of interlocking components with complex interactions, and just code analysis by itself may not be sufficient to understand the behavior of the system. The controlled experiments therefore play a crucial role in profiling the overall behavior and also help us to confirm our understanding. While our study focuses on these three players, our findings of specific issues (§5.3) in these players have wide applicability to the services that use these players. Our best practice

recommendations (§5.4) are not player specific; we expect them to be widely applicable to any ABR streaming service.

5.2.3 ABR Streaming Protocols

DASH [4] and HLS [3] are the two predominant ABR streaming protocols. Both of them now support demuxed audio and video tracks. The DASH protocol defines an Adaptation Set as a set of interchangeable encoded versions of one or several media content components. For demuxed audio and video tracks, it defines one Adaptation Set for video tracks and another set for audio tracks. A `bandwidth` attribute is associated with each track (termed *Representation* in DASH) to declare the required bandwidth (which is close to the peak bitrate; see one example in Table 5.1). In HLS, a top-level master playlist uses the EXT-X-STREAM-INF tag to specify an audio and video track combination (termed *Variant* in HLS). With HLS, one can specify all possible combinations or a subset thereof. A `BANDWIDTH` attribute is associated with a video and audio track combination to declare the aggregate bandwidth requirement of the combination (which is the sum of the peak bitrates of the audio and video tracks in the combination). In the rest of the chapter, depending on the context, the phrase *bandwidth requirement* refers to the `bandwidth` attribute in DASH or `BANDWIDTH` attribute in HLS.

There are some key differences between DASH and HLS specifications in terms of how they treat demuxed audio and video tracks. These differences have important implications for both player ABR logic design and the resulting QoE. One key difference is that DASH does not provide a mechanism for a content provider to specify only the desired subset of audio and video track combinations, while HLS provides an explicit mechanism to do so. *Therefore, DASH provides a player more freedom to select combinations from the available audio and video tracks, potentially making it more vulnerable to choosing undesirable combinations (see §5.3).*

Another key difference between DASH and HLS is that DASH specifies the band-

width requirements of individual audio and video tracks, while HLS top-level manifest only supports specifying the aggregate bandwidth requirement of each audio and video track combination. This difference should be recognized by the player to avoid undesirable behaviors, as we shall see later.

5.2.4 Players

We focus on three widely used and open-source players, ExoPlayer (v2.10.2) [30], Shaka Player (v2.5.1) [99], and `dash.js` player (v2.9.3) [53], and try to understand their behaviors towards audio and video rate adaptation using their latest versions. ExoPlayer is a widely used application level media player for Android platforms. More than 140,000 applications in Google Play Store use ExoPlayer to play media [103]. Shaka Player is an open-source JavaScript library for adaptive media, and has been used by more than 1,600 websites [104]. `dash.js` is an open-source JavaScript based player and is the reference player maintained by the DASH Industry Forum. ExoPlayer and Shaka Player support both DASH and HLS streaming; `dash.js` only supports DASH.

5.3 Practice of Popular Players

5.3.1 Experimental Setup

In the experiments below, we use a drama show downloaded from YouTube using `youtube-dl` [61]. It is around 5 minutes long, containing 6 video tracks and 3 audio tracks. Table 5.1 lists the average and peak bitrates of the video and audio tracks, as well as other key characteristics. The bitrate ladder in Table 5.1 is commonly used by YouTube [105]; the issues we point out below are related to the bitrate ladder (not particular to the specific content), and hence are broadly applicable.

We use the Bento4 toolkit [106] to create two sets of manifest files, complying respectively with DASH and HLS standards. For DASH, we create one manifest file, with the six video tracks and three audio tracks specified in two Adaptation Sets. The

Table 5.1: Video and audio of a YouTube drama show.

| Audio/ Video Track | Average Bitrate (Kbps) | Peak Bitrate (Kbps) | Declared Bitrate for DASH (Kbps) | Audio channels, sampling rate Video resolution |
|--------------------------|------------------------------|---------------------------|--|--|
| A1 | 128 | 134 | 128 | 2 channels, 44 kHz |
| A2 | 196 | 199 | 196 | 6 channels, 48 kHz |
| A3 | 384 | 391 | 384 | 6 channels, 48 kHz |
| V1 | 111 | 119 | 111 | 144p |
| V2 | 246 | 261 | 246 | 240p |
| V3 | 362 | 641 | 473 | 360p |
| V4 | 734 | 1190 | 914 | 480p |
| V5 | 1421 | 2382 | 1852 | 720p |
| V6 | 2728 | 4447 | 3746 | 1080p |

declared bitrate for each audio/video track is shown in Table 5.1. For HLS, we create two manifest files. The first, H_{all} , specifies all 18 combinations of video and audio tracks¹; the second, H_{sub} , specifies a subset of 6 combinations, i.e., V1+A1, V2+A1, V3+A2, V4+A2, V5+A3, V6+A3, where high quality video tracks are associated with high audio quality tracks, and vice versa. The bitrates (both peak and average bitrates) for the combinations contained in these two manifest files are listed in Tables 5.2 and 5.3.

Table 5.2 lists the full set of the 18 audio and video combinations for the drama show in Table 5.1. They are the combinations listed in the HLS manifest file H_{all} . For each combination, the peak bitrate is the sum of the peak bitrates of the audio and video tracks; the average bitrate is sum of their average bitrates. The combinations are placed

¹ While HLS provides a mechanism to specify a subset of video and audio combinations, it does not have an explicit recommendation that only carefully curated combinations should be specified. A content provider may choose to list all the combinations; we use H_{all} to illustrate the issues that may arise from such practices.

in increasing order of the peak bitrate.

Table 5.3 lists a subset of 6 audio and video combinations for the drama show in Table 5.1. They are the combinations listed in the HLS manifest file H_{sub} . For each combination, both the peak and average bitrates are listed in the table.

For controlled experiments, we set up a HTTP server as the origin server. The network bandwidths from the server to client are controlled by using `tc` [76] at the server. Our goal here is to identify demuxed audio-video related performance problems for each player, not to compare the performance across the multiple players. Therefore, we choose the experimental settings targeting the different issues of the different players. Whenever appropriate, we choose fixed network bandwidths, since the behavior of a player is more easily understood under such bandwidth profiles.

5.3.2 ExoPlayer

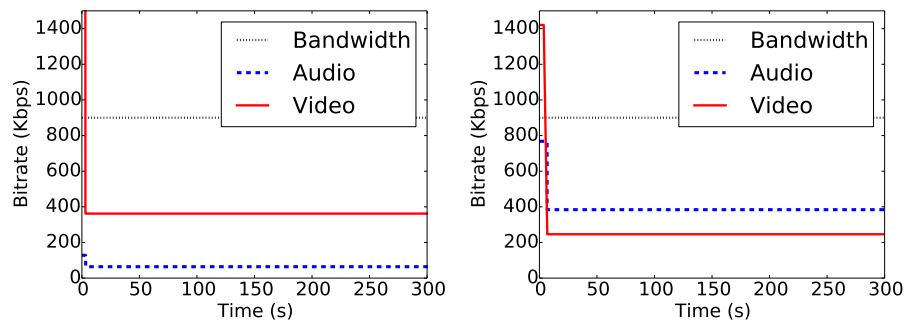
ExoPlayer adopted joint audio and video rate adaptation only very recently (starting from version v2.10.0, released in May 2019). Prior to that, it did not support simultaneous audio and video rate adaptation. Specifically, for multiple demuxed video and audio tracks, it selected a fixed audio track and used it throughout the session without any audio rate adaptation. In the following, we use ExoPlayer version v2.10.2, the latest version that is publicly available.

DASH. Since a DASH manifest file does not restrict the combinations of audio and video tracks that can be selected, ExoPlayer designs a specific logic that uses the per-track declared bitrate in the manifest file to determine a subset of combinations that combines higher bitrate/quality audio tracks with higher bitrate/quality video tracks. Specifically, for the audio and video tracks listed in Table 5.1, the resultant combinations, in increasing order of bandwidth requirement, are V1+A1, V2+A1, V2+A2, V3+A2, V4+A2, V4+A3, V5+A3, and V6+A3, where two adjacent combinations have either the same video or audio track. We refer to these combinations as the *predetermined* combinations by ExoPlayer. The subsequent rate adaptation process *only* consid-

ers these predetermined combinations. Specifically, during rate adaptation, the player estimates the available network bandwidth by considering both video and audio downloading, and conservatively assumes that the actual network bandwidth is 75% of the estimated bandwidth. It then selects an audio and video combination out of the predetermined combinations (based on the bitrate of each of the combinations, network bandwidth estimate, and the buffer status).

The above treatment has the following limitation. The predetermined combinations by ExoPlayer, while may be reasonable for some bitrate ladder or content types, may not be suitable for others. As an example, for the above drama show, it may be desirable to allow V5+A2 (i.e., high quality video with medium quality audio), which is, however, not in the predetermined combinations, and hence will not be selected by ExoPlayer.

We next further illustrate the above point using two experiments. In the first experiment, we create an audio adaptation set with three audio tracks B1, B2 and B3 with the declared bitrate as 32, 64 and 128 Kbps, respectively. The video tracks are the same as listed in Table 5.1. In this case, the predetermined combinations are V1+B1, V2+B1, V2+B2, V3+B2, V4+B2, V5+B2, V5+B3, and V6+B3. The network bandwidth is fixed at 900 Kbps. Fig. 5.1(a) plots the average bitrate of the selected tracks. We see that V3+B2 is selected, while V3+B3 would be a better choice, since it has higher audio quality, and its bandwidth requirement (601 Kbps) is below the available network bandwidth. This more desirable combination (V3+B3) is, however, not in the predetermined combinations, and hence will not be selected. In the second experiment, we switch the audio adaptation set to three audio tracks with relatively higher bitrate, referred to as C1, C2 and C2 with the declared bitrate as 196, 384 and 768 Kbps, respectively. In this case, the predetermined combinations are V1+C1, V2+C1, V2+C2, V3+C2, V4+C2, V5+C2, V5+C3, and V6+C3. Fig. 5.1(b) shows that ExoPlayer selects V2+C2, resulting in very low video quality and high audio quality. The combination V3+C1 would be a better choice (V3+C1 has declared video and audio



(a) Selected bitrates (experiment 1).

(b) Selected bitrates (experiment 2).

Fig. 5.1: ExoPlayer results (DASH).

bitrates as 473 and 196 Kbps, respectively, versus 246 and 384 Kbps in V2+A2), which is however not in the predetermined combinations.

While clearly undesirable, the root cause of the above problem flows from a limitation in the DASH standard. As we mentioned in §5.2, the server is better placed to specify the desirable set of video and audio combinations. However, the DASH standard lacks such specifications. The DASH client, typically lacks detailed domain knowledge of the content being streamed, and therefore is forced to either (i) consider all possible combinations of video and audio track variants, or (ii) apply its own policy to determine a subset of combinations (as in ExoPlayer). Both approaches have drawbacks. The former can lead to a player selecting an unsuitable combination for a certain type of content, while the latter can potentially exclude desirable combinations of audio and video tracks for a content.

HLS. ExoPlayer uses the same rate adaptation code for both DASH and HLS. In contrast to the behavior with DASH, for HLS, this unfortunately leads to selecting a fixed audio track. In the following, we first illustrate this behavior using experiments and then explain the root cause.

In the first experiment, we specify a subset of audio and video combinations, H_{sub} , in the top-level master playlist; the first audio track in the manifest file is A3 (i.e., the highest bitrate/quality audio track). The network bandwidth is set to be time-

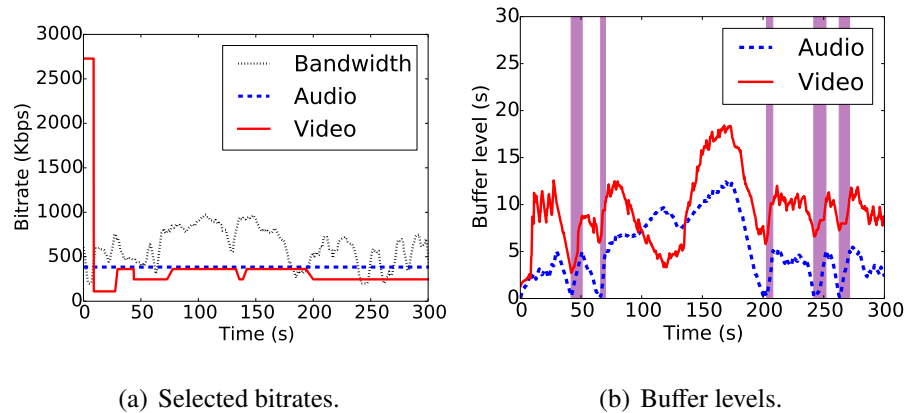
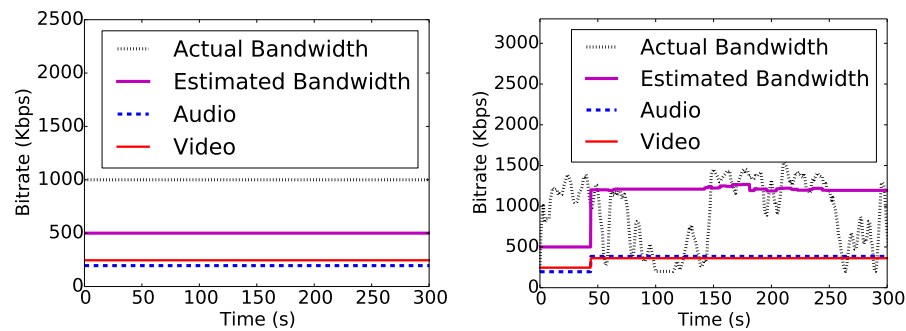


Fig. 5.2: ExoPlayer results (HLS).

varying, with the average as 600 Kbps. The evolution of the selected audio and video tracks is shown in Fig. 5.2(a); the audio and video buffer levels over time are shown in Fig. 5.2(b). We note that ExoPlayer selects A3 throughout the playback, resulting in 5 *stall events and 36.9 seconds of rebuffering (marked as the shaded regions)*. In addition, the ABR selection has the effect of *disobeying the subset of audio and video combinations specified in the HLS manifest* as it selects some combinations (e.g., V1+A3) that are not in the specified subset. In the second experiment, we modify the manifest file so that A1 (the lowest quality audio track) is listed as the first audio track and fix the network bandwidth to 5 Mbps. ExoPlayer selects A1 throughout the playback despite plenty of available network bandwidth (figures omitted), leading to unnecessarily poor audio QoE.

What causes such behavior? Inspecting the ExoPlayer source code, we find that it is due to the lack of specification of the individual audio and video track's bitrate information in the top-level manifest file, which is needed by ExoPlayer to predetermine a subset of audio and video combinations. To accommodate the lack of this information, ExoPlayer simply assumes that all the audio tracks have the same quality, thereby leading to a fixed audio track selection. For a video track, it uses the aggregate bitrate of the first variant in the top-level manifest file that contains this video track as its bitrate, which is clearly an overestimation. The overestimation will be even more severe when the order of the variants is not specified properly (i.e., the first variant for a video



(a) Selected bitrates (experiment 1).

(b) Selected bitrates (experiment 2).

Fig. 5.3: Shaka Player results (HLS).

track contains the video track and the highest bitrate audio track). In §5.4.1, we outline practical solutions to this problem.

5.3.3 Shaka Player

HLS. We use two experiments with the HLS manifest file H_{all} to understand the behavior of Shaka Player. In the first experiment, the network bandwidth is set to a constant 1 Mbps. Fig. 5.3(a) shows that the bandwidth estimated by Shaka is a constant 500 Kbps, only half of the actual specified network bandwidth. As a result, V2+A2 (with aggregate peak bitrate of only 460 Kbps) is selected. In the second experiment, the specified network bandwidth is dynamic (with the average as 600 Kbps, see Fig. 5.3(b)). In this case, Shaka first underestimates the network bandwidth, and then overestimates the bandwidth starting around 50 s. Correspondingly, the selected video and audio tracks are initially low (V2+A2), and then overly high (V3+A3), leading to a total rebuffering of 39 s. Inspecting the player code, we find that the above undesirable behaviors are due to Shaka’s network bandwidth estimation algorithm. Specifically, Shaka uses past video and audio downloading throughputs as samples to estimate the bandwidth. It treats video and audio downloading separately. While downloading a video track (the same applies to audio downloading), Shaka considers each interval ($\delta = 0.125$ s), calculates the amount of data d downloaded in that interval, and only counts the resultant

throughput as a valid sample if $d \geq 16$ KB. To estimate the overall available network bandwidth, it considers a set of samples $\{c_1, \dots, c_n\}$, where c_i is the throughput from either video or audio downloading, and sets the estimated bandwidth as an exponential weighted average of these samples. For time intervals when the audio and video streams are being concurrently downloaded over a shared network bottleneck link, the above strategy will severely underestimate the available network bandwidth. In addition, the filtering rule (i.e., only consider samples with $d \geq 16$ KB) itself can lead to bandwidth underestimation or overestimation, depending on the network conditions. In the first experiment above, none of the throughput samples satisfies the filtering rule, and hence the default bandwidth estimation of 500 Kbps is used throughout the streaming session. In the second experiment, only the throughput samples under high network bandwidth satisfy the rule, while those under low network bandwidth are discarded, leading to significant bandwidth overestimation.

Another issue is that Shaka uses a simple rate based adaptation scheme (i.e., selects the combination with the bandwidth requirement closest to the estimated bandwidth), which can cause the selected audio and video tracks to fluctuate frequently even if the bandwidth estimation is accurate. The above fluctuation problem is more severe for the case of demuxed audio and video since a large number of audio and video combinations may have close bandwidth requirements. For example, suppose manifest file H_{all} is used and the estimated network bandwidth varies between 300 to 700 Kbps. Then the selected combinations can fluctuate among V1+A2, V2+A1, V2+A2, V1+A3 and V2+A3, with bandwidth requirements as 318, 395, 460, 510 and 652 Kbps, respectively.

DASH. Under DASH, since no combinations of audio and video tracks are specified in the manifest file, the player creates all the combinations of video and audio tracks when parsing the DASH manifest file. Therefore, the result is the same as that for HLS when using manifest file H_{all} .

5.3.4 dash.js Player

The default ABR algorithm used in dash.js is DYNAMIC [37], which switches between two schemes, THROUGHPUT and BOLA. THROUGHPUT is a rate based approach that chooses tracks whose declared peak bitrates are close to the estimated bandwidth. BOLA is a buffer based approach that optimizes a utility function [11]. DYNAMIC starts by using THROUGHPUT rule. It switches to BOLA when the buffer level is above 12 s and BOLA selects a bitrate at least as high as that selected by THROUGHPUT; it switches back to THROUGHPUT if the buffer is less than 6 s and BOLA selects a bitrate lower than that selected by THROUGHPUT.

Examination of the source code of dash.js shows that it utilizes DYNAMIC strategy for both audio and video, and performs rate adaptation for audio and video separately. In addition, the bandwidth estimation for audio (video) is based on past audio (video) downloading only. Fig. 5.4 plots the results when using a fixed network bandwidth of 700 Kbps. We see that the selected video and audio combinations includes V2+A3, V2+A2, V2+A3 and V3+A3. Some of these combinations are clearly undesirable, e.g., V2+A3. The combination, V3+A2, fits the network bandwidth profile (it actually has lower bandwidth requirement than V2+A3), while it has higher video quality and slightly lower audio quality than V2+A3, which might be more preferable from the user perspective for the drama show. We further see from Fig. 5.4(b) that the buffer levels for audio and video can be unbalanced, which is undesirable since when one of them underruns, stalls will happen, even if there is a lot of content in the other buffer.

5.3.5 Summary of Findings

In summary, we observe the following problems with current ABR streaming protocols and player implementations.

- When a player does not perform rate adaptation for audio (e.g., ExoPlayer for HLS), it can lead to poor performance (e.g., a large amount of rebuffering). Therefore, it is

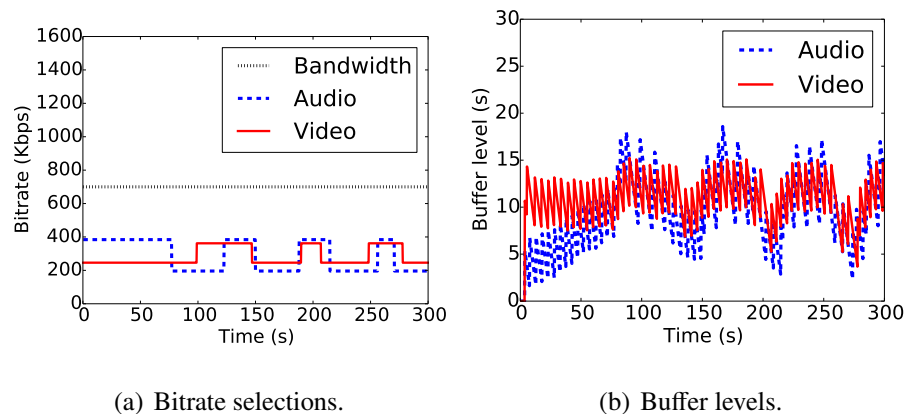


Fig. 5.4: dash.js results (DASH).

desirable to perform rate adaptation for both audio and video.

- Some players select undesirable audio and video combinations, which can lead to poor viewing quality (e.g., the lowest video and highest audio tracks). The problem is more severe for DASH, which does not provide a mechanism to specify a subset of desirable audio and video combinations, making the player more vulnerable to selecting bad combinations.
- Some players make the rate adaptation decisions for audio and video completely independently (e.g., dash.js). Considering audio and video jointly is better than considering them independently. But considering them jointly in an overly simplistic way is also not desirable (e.g., the practice in Shaka player can lead to frequent audio/video track changes).
- Some players do not synchronize audio and video downloading explicitly (e.g., dash.js). This can lead to unbalanced content in video and audio buffers. Since we need both video and audio in the playback, having a lot more content in video/audio is not helpful. Instead, it is more desirable to synchronize them on a finer granularity (e.g., on per chunk level as in ExoPlayer).
- An HLS manifest can specify a subset of audio and video combinations, but some players do not conform to the manifest file. For example, ExoPlayer may select some bad combinations that are not in the manifest file.

5.4 Suggested Best Practices

Based on the analysis in §5.3, we suggest the following best practices for demuxed audio and video tracks for the server side as well as the player side.

5.4.1 Server Side Manifest Specifications

Audio and video combinations. *The content provider should identify desirable combinations of audio and video tracks based on content type and domain expertise, and specify these combinations in the manifest file. A player should only select chunks from the allowed combinations.* This practice provides the following advantages: (i) allows the content owner to specify combinations that are suitable for the specific content (e.g., music video v.s. action movie) and devices (considering screen size, connected sound system, e.g., speaker or headphone), and (ii) simplifies the rate adaptation task for the player. HLS already supports this capability to include specific combinations in the manifest file. However it is important for the content provider to utilize and leverage this capability appropriately, and not specify all possible combinations unless they are all desirable. Unlike HLS, DASH at present does not offer a way to list only specific allowed combinations in the manifest. A practical short term workaround would be for the client to get this additional information from the server using HTTP. In the longer term, the DASH specification can be expanded to support this feature.

Audio and video bandwidth declaration. *In the manifest file, it would be good to specify sufficient information about the aggregate bandwidth requirements of audio and video combinations, as well as the bandwidth requirements of individual audio/video tracks.* This is particularly important when audio and video are fetched over different network paths that have different network characteristics (e.g., when they are stored at different servers). Currently, DASH specifies the bandwidth for each audio and video track, and the aggregate bandwidth requirement for audio and video combinations (if provided following the earlier suggestion) can be calculated from the individual tracks.

In HLS, the top-level master playlist *only* specifies the aggregate bitrate for each specified audio and video combination. The bitrate of each individual audio/video track is not in the top-level master playlist, but can be obtained from the second-level media playlists as follows (commercial players only use the information to identify the content address for an already selected chunk): (i) When all the video/audio chunks are packaged into a single file, the media playlists specify the EXT-X-BYTERANGE information (i.e., the start and end byte positions), which can be used to obtain the audio/video bitrate, as pointed out in [107]. (ii) When each video/audio chunk is packaged into an individual file, no byte range information is provided in the media playlists. However, HLS recently added an optional EXT-X-BITRATE tag that can be used to obtain per-chunk bitrate. We recommend that this option should be made mandatory. In addition, for both of the above two cases in HLS, since the information required for computing the per-track bitrates is in the second-level manifest files, we suggest that the player should download these files and read the information before making rate adaptation decisions². A more robust longer term solution is to enhance the HLS specification so that the top-level master playlist directly provides per-track audio and per-track video bitrate information.

5.4.2 Player Side ABR Logic

Adopt audio rate adaptation. *For dynamic network bandwidth scenarios, it is important to perform audio rate adaptation.* High quality audio tracks can have similar or even higher bitrates than lower-rung video tracks. Audio rate adaptation is just as important as video rate adaptation to avoid adverse impact on QoE (e.g., rebuffering as observed in §5.3.2 or low audio quality).

Select only from allowed audio and video combinations. *The ABR logic should only*

² We suggest avoiding the practice of “lazy” fetching, which only fetches the playlist manifest file for a track when a chunk from that track has been selected, at which point the player needs to know the address of that chunk.

select from the set of allowed audio and video combinations if provided by the server (e.g., via manifest file or certain out-of-band mechanism). As mentioned in §5.4.1, the allowed combinations reflect the desirable combinations between audio and video based on the content. Therefore, it is important for the client to select only from those combinations.

Joint adaptation of audio and video. *We suggest that the selection of the audio and video tracks for each chunk position (in playback order) be considered jointly.* For both video and audio rate adaptation, it is desirable to satisfy conflicting goals in maximizing quality, minimizing stalls and minimizing quality variation. Since the selection of audio and video is inherently coupled (so that good combinations of audio and video tracks are chosen), we recommend considering the combinations of audio and video (i.e., those specified in the manifest file if provided) while making rate adaptation decisions, instead of considering audio and video individually. The rate adaptation should be done carefully to avoid frequent changes in either audio or video tracks.

Maintain balance between audio and video prefetching. *It is desirable to keep the audio and video buffer levels (in seconds) balanced.* This is because either empty audio or video buffer leads to stalls. The balance can be achieved by synchronizing the duration of prefetched audio and video content at a fine granularity, e.g., at the chunk level or in terms of a small number of chunks.

5.5 Summary

In this chapter, we examined the handling of ABR adaptation for demuxed video and audio tracks in predominant ABR streaming protocols (DASH and HLS), and in three popular ABR players. We identified a number of limitations in existing practices that can adversely impact user QoE, and traced their root causes. We then proposed a number of best practices and principles for the server, ABR streaming protocols and client. We hope these findings will encourage further studies on this important topic.

Table 5.2: Bitrates of the full set of audio and video combinations (used in HLS manifest file H_{all}).

| Video/Audio Combination | Average Bitrate (Kbps) | Peak Bitrate (Kbps) |
|----------------------------|---------------------------|------------------------|
| V1 + A1 | 239 | 253 |
| V1 + A2 | 307 | 318 |
| V2 + A1 | 374 | 395 |
| V2 + A2 | 442 | 460 |
| V1 + A3 | 495 | 510 |
| V2 + A3 | 630 | 652 |
| V3 + A1 | 490 | 775 |
| V3 + A2 | 558 | 840 |
| V3 + A3 | 746 | 1032 |
| V4 + A1 | 862 | 1324 |
| V4 + A2 | 930 | 1389 |
| V4 + A3 | 1118 | 1581 |
| V5 + A1 | 1549 | 2516 |
| V5 + A2 | 1617 | 2581 |
| V5 + A3 | 1805 | 2773 |
| V6 + A1 | 2856 | 4581 |
| V6 + A2 | 2924 | 4646 |
| V6 + A3 | 3112 | 4838 |

Table 5.3: Bitrates of a subset of audio and video combinations (used in HLS manifest file H_{sub}).

| Video/Audio Combination | Average Bitrate (Kbps) | Peak Bitrate (Kbps) |
|----------------------------|---------------------------|------------------------|
| V1+A1 | 239 | 253 |
| V2+A1 | 374 | 395 |
| V3+A2 | 558 | 840 |
| V4+A2 | 930 | 1389 |
| V5+A3 | 1805 | 2773 |
| V6+A3 | 3112 | 4838 |

Chapter 6

Conclusion and Future Work

In this dissertation, we first take a fresh look at PID-based bit rate adaptation and design a framework called PIA (PID-control based ABR streaming) that strategically leverages PID control concepts and incorporates several novel strategies to account for the various requirements of ABR streaming. The evaluation results demonstrate that PIA outperforms state-of-the-art schemes in providing high average bitrate with significantly lower bitrate changes and stalls, while incurring very small runtime overhead. We further design PIA-E (PIA Enhanced), which improves the performance of PIA in the important initial playback phase.

As streaming providers have been moving towards using Variable Bitrate (VBR) encodings for the video content, we identify distinguishing characteristics of VBR encodings that impact user QoE and should be factored in any ABR adaptation decision and find that traditional ABR adaptation strategies designed for the CBR case are not adequate for VBR. We develop novel best practice design principles to guide ABR rate adaptation for VBR encodings. As a proof of concept, we design a novel and practical control-theoretic rate adaptation scheme, CAVA (Control-theoretic Adaption for VBR-based ABR streaming), incorporating these concepts. Extensive evaluations show that CAVA substantially outperforms existing state-of-the-art adaptation techniques.

We also explore quality-aware strategies for optimizing QoE while saving data. We analyze the underlying causes for suboptimal existing data saving practices and propose novel approaches to achieve better tradeoffs between video quality and data

usage. The first approach is Chunk-Based Filtering (CBF), which can be retrofitted to any existing ABR scheme. The second approach is QUality-Aware Data-efficient streaming (QUAD), a holistic rate adaptation algorithm that is designed ground up. Our evaluations demonstrate that compared to the state of the art, the two proposed schemes achieve consistent video quality that is much closer to the user-specified target, lead to far more efficient data usage, and incur lower stalls.

We further examine the state of the art in the handling of demuxed audio and video tracks in predominant ABR protocols (DASH and HLS), as well as in real ABR client implementations in three popular players covering both browsers and mobile platforms. Combining experimental insights with code analysis, we shed light on a number of limitations in existing practices both in the protocols and the player implementations, which can cause undesirable behaviors such as stalls, selection of potentially undesirable combinations such as very low quality video with very high quality audio, etc. Based on our gained insights, we identify the underlying root causes of these issues, and propose a number of practical design best practices and principles whose collective adoption will help avoid these issues and lead to better QoE.

As future work, we plan to explore extending CAVA and its concepts to ABR streaming of live VBR encoded videos, develop data saving strategies that directly take account of a user's data budget in ABR decisions. Another direction is to further refine the suggested practices for ABR streaming with separate audio and video tracks, and design and implement rate adaptation schemes following the suggested practices. As cellular network infrastructure are upgrading from 4G/LTE to 5G, exploring video streaming over 5G is a promising research direction based on our work. Finally, some of my previous works in SDN, quantum internet, quantum encryption and cybersecurity [108, 109, 110, 111, 112, 113, 114, 115, 116, 117, 118, 119, 120, 121] inspire me that there might be a way to apply new approaches from other fields to video streaming study.

Chapter 7

List of Publications during My PhD Study

1. Y. Qin, C. Shende, C. Park, S. Sen, and B. Wang. “DataPlanner: Data-budget Driven Approach to Resource-efficient ABR Streaming,” Proceedings of ACM MMSys, 2021.
2. Y. Qin, R. Jin, S. Hao, K. R. Pattipati, F. Qian, S. Sen, B. Wang, and C. Yue. “A Control Theoretic Approach to ABR Video Streaming: A Fresh Look at PID-based Rate Adaptation,” IEEE Transactions on Mobile Computing, vol. 19, no. 11, pp. 2505-2519, 1 Nov. 2020.
3. Y. Qin, S. Sen, and B. Wang. “ABR Streaming with Separate Audio and Video Tracks: Measurements and Best Practices,” Proceedings of ACM CoNEXT, December 2019.
4. Y. Qin, R. Jin, S. Hao, K. R. Pattipati, F. Qian, S. Sen, B. Wang, and C. Yue. “Quality-aware Strategies for Optimizing ABR Video Streaming QoE and Reducing Data Usage,” Proceedings of ACM MMSys, June 2019.
5. Y. Qin, R. Jin, S. Hao, K. R. Pattipati, F. Qian, S. Sen, B. Wang, and C. Yue. “ABR Streaming of VBR-encoded Videos: Characterization, Challenges, and Solutions,” Proceedings of ACM CoNEXT, December 2018. (Best Paper Award)
6. Y. Qin, R. Jin, S. Hao, K. R. Pattipati, F. Qian, S. Sen, B. Wang, and C. Yue. “A Control Theoretic Approach to ABR Video Streaming: A Fresh Look at PID-

- based Rate Adaptation,” Proceedings of IEEE INFOCOM, May 2017.
7. C. Yue, S. Sen, B. Wang, Y. Qin, and F. Qian, “Energy Considerations for ABR Video Streaming to Smartphones: Measurements, Models and Insights,” Proceedings of ACM MMSys, June 2020.
 8. C. Yue, R. Jin, K. Suh, Y. Qin, B. Wang, and W. Wei. “LinkForecast: Cellular Link Bandwidth Prediction in LTE Networks,” IEEE Transactions on Mobile Computing, vol. 17, no. 7, pp. 1582-1594, July 2018.
 9. S. Chen, R. Morillo, Y. Qin, A. Russell, R. Jin, B. Wang, and S. Vasudevan, “Asynchronous Neighbor Discovery on Duty-Cycled Mobile Devices: Models and Schedules,” in IEEE Transactions on Wireless Communications, vol. 19, no. 8, pp. 5204-5217, Aug. 2020
 10. S. Chen, A. Russell, R. Jin, Y. Qin, B. Wang, and S. Vasudevan. “Asynchronous Neighbor Discovery on Duty-cycled Mobile Devices: Integer and Non-Integer Schedules,” Proceedings of ACM MobiHoc, June 2015.
 11. Z. Jiang, Z. Tang, Y. Qin, C. Kang, and P. Zhang, “Quantum Internet for Resilient Electric Grids,” International Transactions on Electrical Energy Systems (2021): e12911.
 12. Z. Jiang, Z. Tang, Y. Qin, and P. Zhang, “Programmable adaptive security scanning for networked microgrids”. Engineering, 2021.
 13. Z. Tang, Y. Qin, Z. Jiang, W.O. Krawec, and P. Zhang, “Quantum-Secure Networked Microgrid”, IEEE Power & Energy Society General Meeting, August 2020. (Best Paper Award)
 14. Z. Tang, Y. Qin, Z. Jiang, W. Krawec, and P. Zhang, “Quantum-Secure Microgrids,” IEEE Transactions on Power Systems, July, 2020.

15. W. Wan, M. A. Bragin, B. Yan, Y. Qin, J. Philhower, P. Zhang, and P. B. Luh, "Distributed and Asynchronous Active Fault Management for Networked Microgrids," *IEEE Transactions on Power System*, vol. 35, no. 5, pp. 3857-3868, Sept. 2020.
16. L. Wang, Y. Qin, Z. Tang, and P. Zhang, "Software-defined microgrid control," *IEEE Open Access Journal of Power and Energy*, vol. 7, pp. 173-182, 2020.
17. J. Wang, Y. Qin, Z. Tang, and P. Zhang, "Software-defined Cyber-Energy Secure Underwater Wireless Power Transfer," *IEEE Journal of Emerging and Selected Topics in Industrial Electronics*, Oct. 2020.
18. Y. Qin. "Resilient Networked Microgrids through Software Defined Networking," *Networked Microgrids*, Cambridge University Press, 2021. (Book chapter)
19. Y. Li, Y. Qin, P. Zhang, and A. Herzberg. "SDN-Enabled Cyber-Physical Security in Networked Microgrids," *IEEE Transactions on Sustainable Energy*, vol. 10, no. 3, pp. 1613-1622, 2018.
20. L. Ren, Y. Qin, Y. Li, P. Zhang, B. Wang, P. B. Luh, S. Han, T. Orekan, and T. Gong. "Enabling Resilient Distributed Power Sharing in Networked Microgrids through Software Defined Networking," *Applied Energy*, vol. 56, no. 1, pp. 237-244, January 2018.
21. G. Wang, and Y. Qin. "MAC Protocols for Wireless Mesh Networks with Multi-beam Antennas: A Survey." In *Future of Information and Communication Conference*, pp. 117-142. Springer, Cham, 2019.
22. G. Wang, Y. Qin, and C. Chang, "Communication with Partial Noisy Feedback," *IEEE Symposium on Computers and Communications (ISCC)*, Heraklion, 2017, pp. 602-607.

23. L. Ren, Y. Qin, B. Wang, P. Zhang, P. B. Luh, and R. Jin. "Enabling Resilient Microgrid through Programmable Network," IEEE Transactions on Smart Grid, vol. 8, no. 6, November 2017.
24. L. Ren, Y. Qin, B. Wang, P. Zhang, P. B. Luh and R. Jin, "Enabling Resilient Microgrid Through Programmable Network," IEEE Power & Energy Society General Meeting, Chicago, IL, 2017.
25. Y. Qin, L. Ren, B. Wang, P. Zhang and P. Luh, "SDN-enabled Highly Resilient and Efficient Microgrids," GENI Engineering Conference 23, UIUC, June 15-18, 2015.
26. Y. Qin, L. Ren, B. Wang, P. Zhang and P. Luh, "Enabling Highly Resilient and Efficient Microgrids through Ultra-fast Programmable Networks," US Ignite GENI Engineering Conference 22/, DC, March 23-26, 2015.
27. S. Sen, S. Hao, Y. Qin, K.R. Pattipati, and B. Wang, "Chunk-based filtering to optimize video streaming quality and data usage ," US Patent App. 16/560,721, 2021.
28. S. Sen, K.R. Pattipati, B. Wang and Y. Qin, "Perceptual visual quality video chunk selection," US Patent 10917667, 2021.
29. S. Sen, S. Hao, Y. Qin, K.R. Pattipati, and B. Wang, "Differential Adaptive Bitrate Streaming Based on Scene Complexity," US Patent 10827181, 2020.
30. S. Sen, S. Hao, Y. Qin, B. Wang, and K. R. Pattipati, "Methods, Systems, and Devices for Video Streaming Adaptation using Control Theoretic Approach," US Patent 10362080, 2019.
31. S. Sen, S. Hao, Y. Qin, B. Wang, K. R. Pattipati, and R. Jin, "Apparatus, Storage Medium and Method for Adaptive Bitrate Streaming Adaptation of Variable Bitrate Encodings", US Patent 10728180, 2020.

32. P. Zhang, B. Wang, P. Luh, L. Ren, Y. Qin. “Enabling Resilient Microgrid Through Ultra-Fast Programmable Network,” US Patent 10257100, 2019.

Bibliography

- [1] Cisco Networks. Cisco VNI: Global Mobile Data Traffic Forecast Update, 2016-2021. <https://goo.gl/64zqTT>, 2016.
- [2] Citrix Mobile Analytics Report, 2014. <https://www.citrix.com/products/bytemobile-adaptive-traffic-management/tech-info.html#reports>.
- [3] Apple. Apple's HTTP Live Streaming. <https://developer.apple.com/streaming/>, 2017.
- [4] International Organization for Standardization. ISO/IEC DIS 23009-1.2 Dynamic adaptive streaming over HTTP (DASH), 2012.
- [5] Florin Dobrian, Vyas Sekar, Asad Awan, Ion Stoica, Dilip Joseph, Aditya Ganjam, Jibin Zhan, and Hui Zhang. Understanding the impact of video quality on user engagement. In *Proc. of ACM SIGCOMM*, 2011.
- [6] S Shunmuga Krishnan and Ramesh K Sitaraman. Video stream quality impacts viewer behavior: inferring causality using quasi-experimental designs. *IEEE/ACM Transactions on Networking*, 21(6):2001–2014, 2013.
- [7] Yao Liu, Sujit Dey, Fatih Ulupinar, Michael Luby, and Yinan Mao. Deriving and validating user experience model for DASH video streaming. *IEEE Transactions on Broadcasting*, 61(4), December 2015.
- [8] Pengpeng Ni, Ragnhild Eg, Alexander Eichhorn, Carsten Griwodz, and Pål Halvorsen. Flicker effects in adaptive video streaming to handheld devices. In *Proc. of ACM Multimedia*, 2011.
- [9] L. De Cicco, S. Mascolo, and V. Palmisano. Feedback control for adaptive live video streaming. In *Proc. of ACM MMSys*, 2011.
- [10] Luca De Cicco, Vito Caldaralo, Vittorio Palmisano, and Saverio Mascolo. ELASTIC: a client-side controller for dynamic adaptive streaming over HTTP (DASH). In *Proc. of Packet Video Workshop (PV)*. IEEE, 2013.

- [11] Kevin Spiteri, Rahul Uргаonkar, and Ramesh K Sitaraman. BOLA: near-optimal bitrate adaptation for online videos. In *Proc. of IEEE INFOCOM*, 2016.
- [12] Guibin Tian and Yong Liu. Towards agile and smooth video adaptation in dynamic HTTP streaming. In *Proc. of ACM CoNEXT*, 2012.
- [13] Xiaoqi Yin, Abhishek Jindal, Vyas Sekar, and Bruno Sinopoli. A control-theoretic approach for dynamic adaptive video streaming over HTTP. In *Proc. of ACM SIGCOMM*, 2015.
- [14] Te-Yuan Huang, Ramesh Johari, Nick McKeown, Matthew Trunnell, and Mark Watson. A buffer-based approach to rate adaptation: Evidence from a large video streaming service. In *Proc. of ACM SIGCOMM*, 2014.
- [15] Kevin Spiteri, Ramesh Sitaraman, and Daniel Sparacio. From theory to practice: Improving bitrate adaptation in the dash reference player. In *Proc. of ACM MMSys*. ACM, 2018.
- [16] Federico Chiariotti, Stefano D’Aronco, Laura Toni, and Pascal Frossard. Online learning adaptation strategy for dash clients. In *ACM MMSys*, 2016.
- [17] Hongzi Mao, Netravali Ravi, and Alizadeh. Mohammad. Neural adaptive video streaming with pensieve. In *Proc. of ACM SIGCOMM*, 2017.
- [18] Zahaib Akhtar, Yun Seong Nam, Ramesh Govindan, Sanjay Rao, Jessica Chen, Ethan Katz-Bassett, Bruno Ribeiro, Jibin Zhan, and Hui Zhang. Oboe: auto-tuning video abr algorithms to network conditions. In *Proc. of ACM SIGCOMM*, 2018.
- [19] Yanyuan Qin, Shuai Hao, Krishna R Pattipati, Feng Qian, Subhabrata Sen, Bing Wang, and Chaoqun Yue. Abr streaming of vbr-encoded videos: characterization, challenges, and solutions. In *Proc. of ACM CoNEXT*. ACM, 2018.
- [20] Y. Qin, R. Jin, S. Hao, K. R. Pattipati, F. Qian, S. Sen, C. Yue, and B. Wang. A control theoretic approach to abr video streaming: A fresh look at pid-based rate adaptation. *IEEE Transactions on Mobile Computing*, 19(11):2505–2519, 2020.
- [21] Subhabrata Sen, HAO Shuai, Yanyuan Qin, JIN Ruofan, Krishna R Pattipati, and Bing Wang. Methods, systems, and devices for video streaming adaptation using control theoretic approach, July 23 2019. US Patent 10,362,080.
- [22] TV Lakshman, Antonio Ortega, and Amy R Reibman. VBR video: Tradeoffs and potentials. *Proceedings of the IEEE*, 1998.

- [23] Andrew Reed and Benjamin Klimkowski. Leaky streams: Identifying variable bitrate DASH videos streamed over encrypted 802.11n connections. In *Consumer Communications & Networking Conference*. IEEE, 2016.
- [24] Shichang Xu, Z. Morley Mao, Subhabrata Sen, and Yunhan Jia. Dissecting VOD services for cellular: Performance, root causes and best practices. In *Proc. of IMC*, 2017.
- [25] Subhabrata Sen, HAO Shuai, Yanyuan Qin, Bing Wang, and Krishna R Pattipati. Apparatus, storage medium and method for adaptive bitrate streaming adaptation of variable bitrate encodings, July 28 2020. US Patent 10,728,180.
- [26] Subhabrata Sen, HAO Shuai, Krishna Pattipati, Yanyuan Qin, and Bing Wang. Differential adaptive bitrate streaming based on scene complexity, November 3 2020. US Patent 10,827,181.
- [27] Zhi Li, Ali Begen, Joshua Gahm, Yufeng Shan, Bruce Osler, and David Oran. Streaming video over HTTP with consistent quality. In *ACM MMSys*, 2014.
- [28] Tong Zhang, Fengyuan Ren, Wenxue Cheng, Xiaohui Luo, Ran Shu, and Xiaolan Liu. Modeling and analyzing the influence of chunk size variation on bitrate adaptation in DASH. In *INFOCOM*. IEEE, 2017.
- [29] Ericsson. Ericsson Mobility Report. <https://goo.gl/mjkwSH>, 2017.
- [30] Google. ExoPlayer. <https://github.com/google/ExoPlayer>, 2016.
- [31] ITU. H.264 : Advanced video coding for generic audiovisual services. <https://www.itu.int/rec/T-REC-H.264>, 2017.
- [32] MulticoreWare Inc. H.265 Video Codec. <http://x265.org/hevc-h265/>, 2018.
- [33] The WebM Project. VP9 Video Codec. <https://www.webmproject.org/vp9>, 2017.
- [34] Junchen Jiang, Vyas Sekar, and Hui Zhang. Improving fairness, efficiency, and stability in HTTP-based adaptive video streaming with FESTIVE. In *Proc. of ACM CoNEXT*, 2012.
- [35] Hongzi Mao, Ravi Netravali, and Mohammad Alizadeh. Neural adaptive video streaming with Pensieve. In *Proc. of ACM SIGCOMM*, 2017.
- [36] Zahaib Akhtar, Yun Seong Nam, Ramesh Govindan, Sanjay Rao, Jessica Chen, Ethan Katz-Bassett, Bruno Ribeiro, Jibin Zhan, and Hui Zhang. Oboe: Auto-tuning video abr algorithms to network conditions. In *Proc. of ACM SIGCOMM*, 2018.

- [37] Kevin Spiteri, Ramesh Sitaraman, and Daniel Sparacio. From theory to practice: Improving bitrate adaptation in the dash reference player. In *Proc. of ACM MMSys*, 2018.
- [38] Apple. HLS Authoring Specification for Apple Devices, 2017.
- [39] Dolby. The dolby atmos difference. <https://www.dolby.com/us/en/brands/dolby-atmos.html>, 2018.
- [40] Netflix. Bringing Studio Quality Sound to Netflix, 2019.
- [41] Netflix. Engineering a studio quality experience with high-quality audio at netflix. shorturl.at/cfhx5, 2019.
- [42] Yanyuan Qin, Subhabrata Sen, and Bing Wang. Abr streaming with separate audio and video tracks: Measurements and best practices. In *Proceedings of the 15th International Conference on Emerging Networking Experiments And Technologies*, CoNEXT '19, page 158–164, New York, NY, USA, 2019. Association for Computing Machinery.
- [43] C. Yue, R. Jin, K. Suh, Y. Qin, B. Wang, and W. Wei. Linkforecast: Cellular link bandwidth prediction in lte networks. *IEEE Transactions on Mobile Computing*, 17(7):1582–1594, 2018.
- [44] Yanyuan Qin, Shuai Hao, Krishna R. Pattipati, Feng Qian, Subhabrata Sen, Bing Wang, and Chaoqun Yue. Quality-aware strategies for optimizing abr video streaming qoe and reducing data usage. In *Proceedings of the 10th ACM Multimedia Systems Conference*, MMSys '19, page 189–200, New York, NY, USA, 2019. Association for Computing Machinery.
- [45] Karl Johan Åström and Richard M. Murray. *Feedback Systems: An Introduction for Scientists and Engineers*. Princeton University Press, 2008.
- [46] Microsoft Smooth Streaming Protocol. <https://goo.gl/Z8fDX6>.
- [47] Adobe HTTP Dynamic Streaming. <http://goo.gl/fgPXdH>.
- [48] Raymond T. Stefani, Bahram Shahian, and Gene Hostetter. *Design of Feedback Control Systems*. Oxford University Press, 4th edition, 2002.
- [49] Katsuhiko Ogata. *Modern Control Engineering*. Prentice Hall, 2010.
- [50] YouTube live encoder settings, bitrates and resolutions. <https://support.google.com/youtube/answer/2853702?hl=en>.

- [51] Best Practices for Creating and Deploying HTTP Live Streaming Media for Apple Devices (Apple Technical Note TN2224). https://developer.apple.com/library/content/technotes/tn2224/_index.html.
- [52] N. H. McClamroch. *State Models of Dynamic Systems: A Case Study Approach*. Springer, 1980.
- [53] DASH Industry Forum. DASH if reference client 2.9.3. <https://github.com/Dash-Industry-Forum/dash.js>, 2019.
- [54] Iraj Sodagar. The MPEG-DASH standard for multimedia streaming over the internet. *IEEE Multimedia*, (4):62–67, 2011.
- [55] FFmpeg. FFmpeg Project. <https://www.ffmpeg.org/>, 2017.
- [56] Yanyuan Qin, Ruofan Jin, Shuai Hao, Krishna R Pattipati, Feng Qian, Subhabrata Sen, Bing Wang, and Chaoqun Yue. A control theoretic approach to ABR video streaming: A fresh look at PID-based rate adaptation. In *INFOCOM*, 2017.
- [57] Jan De Cock, Aditya Mavlankar, Anush Moorthy, and Anne Aaron. A large-scale video codec comparison of x264, x265 and libvpx for practical VOD applications. In *SPIE, Applications of Digital Image Processing*, 2016.
- [58] Xiph.Org. Xiph.org Video Test Media. <https://media.xiph.org/video/derf/>, 2016.
- [59] Netflix. Per-title encode optimization. <https://medium.com/netflix-techblog/per-title-encode-optimization-7e99442b62a2>, 2015.
- [60] Werner Robitza. CRF guide (constant rate factor in x264 and x265). <http://slhck.info/video/2017/02/24/crf-guide.html>, February 2017.
- [61] youtube-dl developers. youtube-dl. <https://goo.gl/mgghW8>, 2018.
- [62] Yao-Chung Lin, Hugh Denman, and Anil Kokaram. Multipass encoding for reducing pulsing artifacts in cloud based video transcoding. In *Image Processing (ICIP), 2015 IEEE International Conference on*, pages 907–911. IEEE, 2015.
- [63] ITU-T P. 910. Subjective video quality assessment methods for multimedia applications, 2008.
- [64] Wolfgang Effelsberg, Otto Spaniol, André Danthine, and Domenico Ferrari. *High-speed networking for multimedia applications*. Springer, 1996.

- [65] Z. Wang, A. C. Bovik, H. R. Sheikh, and E. P. Simoncelli. Image quality assessment: from error visibility to structural similarity. *IEEE Transactions on Image Processing*, 13(4), 2004.
- [66] Li Zhi, Aaron Anne, Katsavounidis Ioannis, Moorthy Anush, and Manohara Megha. Toward A Practical Perceptual Video Quality Metric, 2016.
- [67] T.-J. Liu, J. Y. Lin, W. Lin, and C.-C. J. Kuo. Visual quality assessment: Recent developments, coding applications and future trends. *APSIPA Transactions on Signal and Information Processing*, 2013.
- [68] J. Y. Lin, T.-J. Liu, E. C.-H. Wu, and C.-C. J. Kuo. A fusion-based video quality assessment (FVQA) index. *APSIPA Transactions on Signal and Information Processing*, 2014.
- [69] Reza Rassool. VMAF reproducibility: Validating a perceptual practical video quality metric. In *IEEE International Symposium on Broadband Multimedia Systems and Broadcasting (BMSB)*, 2017.
- [70] Netflix. Vmaf score aggregation. <https://github.com/Netflix/vmaf/issues/20>, 2016.
- [71] Chao Chen, Yao-Chung Lin, Anil Kokaram, and Steve Benting. Encoding bitrate optimization using playback statistics for http-based adaptive video streaming. *arXiv preprint arXiv:1709.08763*, 2017.
- [72] Kiyotsugu Takaba. A tutorial on preview control systems. In *SICE*, 2003.
- [73] Measuring fixed broadband report - 2016. <https://www.fcc.gov/reports-research/reports/measuring-broadband-america/measuring-fixed-broadband-report-2016>, December 2016.
- [74] Finding the Just Noticeable Difference with Netflix VMAF. <https://goo.gl/TGWCGV>, September 2017.
- [75] Selenium Projects. Selenium Web Browser Automation. <http://www.seleniumhq.org>, 2017.
- [76] Linux. tc. <https://linux.die.net/man/8/tc>, 2014.
- [77] Xiufeng Xie, Xinyu Zhang, Swarun Kumar, and Li Erran Li. piStream: physical layer informed adaptive video streaming over LTE. In *Proc. of ACM MobiCom*, 2015.
- [78] J. Chen, R. Mahindra, M. A. Khojastepour, S. Rangarajan, and M. Chiang. A scheduling framework for adaptive video delivery over cellular networks. In *Proc. of ACM MobiCom*, 2013.

- [79] Xuan Kelvin Zou, Jeffrey Erman, Vijay Gopalakrishnan, Emir Halepovic, Ritwik Jana, Xin Jin, Jennifer Rexford, and Rakesh K. Sinha. Can accurate predictions improve video streaming in cellular networks? In *Proc. of HotMobile*, 2015.
- [80] Yi Sun, Xiaoqi Yin, Junchen Jiang, Vyas Sekar, Fuyuan Lin, Nanshu Wang, Tao Liu, and Bruno Sinopoli. Cs2p: Improving video bitrate selection and adaptation with data-driven throughput prediction. In *Proceedings of the 2016 ACM SIGCOMM Conference*, SIGCOMM '16, page 272–285, New York, NY, USA, 2016. Association for Computing Machinery.
- [81] Robert Kuschnig, Ingo Kofler, and Hermann Hellwagner. An evaluation of TCP-based rate-control algorithms for adaptive internet streaming of H.264/SVC. In *Proc. ACM Multimedia systems*, 2010.
- [82] Chaoqun Yue, Subhabrata Sen, Bing Wang, Yanyuan Qin, and Feng Qian. Energy considerations for abr video streaming to smartphones: Measurements, models and insights. In *Proceedings of the 11th ACM Multimedia Systems Conference*, MMSys '20, page 153–165, New York, NY, USA, 2020. Association for Computing Machinery.
- [83] Subhabrata Sen, HAO Shuai, Yanyuan Qin, Bing Wang, and Krishna R Pattipati. Chunk-based filtering to optimize video streaming quality and data usage, March 4 2021. US Patent App. 16/560,721.
- [84] Subhabrata Sen, Krishna Pattipati, Yanyuan Qin, and Bing Wang. Perceptual visual quality video chunk selection, November 3 2021. US Patent 10,917,667.
- [85] Jan De Cock, Zhi Li, Megha Manohara, and Anne Aaron. Complexity-based consistent-quality encoding in the cloud. In *Image Processing (ICIP), 2016 IEEE International Conference on*, pages 1484–1488. IEEE, 2016.
- [86] Jan De Cock and Anne Aaron. Constant-slope rate allocation for distributed real-world encoding. In *Picture Coding Symposium (PCS), 2016*, pages 1–5. IEEE, 2016.
- [87] AT&T. AT&T Stream Saver, 2018.
- [88] T-mobile. T-mobile Binge On, 2018.
- [89] International Organization for Standardization. ISO/IEC 23001-10:2015 carriage of timed metadata metrics of media in iso base media file format, 2015.
- [90] Ricky KP Mok, Xiapu Luo, Edmond WW Chan, and Rocky KC Chang. Qdash: a qoe-aware dash system. In *Proceedings of the 3rd Multimedia Systems Conference*, pages 11–22. ACM, 2012.

- [91] Yanyuan Qin, Shuai Hao, K. R. Pattipati, Feng Qian, Subhabrata Sen, Bing Wang, and Chaoqun Yue. Abr streaming of vbr-encoded videos: Characterization, challenges, and solutions. In *ACM CoNEXT*, 2018.
- [92] Ali Begen. Spending "quality" time with the web video. *IEEE Internet Computing*, 2016.
- [93] Ioannis Katsavounidis. Dynamic optimizer a perceptual video encoding optimization framework. <https://goo.gl/zHdium>, 2018.
- [94] Laura Toni, Ramon Aparicio, Telecom Bretagne, Karine Pires, Gwendal Simon, Alberto Blanc, and Pascal Frossard. Optimal selection of adaptive streaming representations. *ACM Trans. Multimedia Comput. Commun. Appl.*, 2015.
- [95] Jiasi Chen, Amitabha Ghosh, Josphat Magutt, and Mung Chiang. Qava: Quota aware video adaptation. In *Proc. of ACM CoNEXT*, pages 121–132, 2012.
- [96] Benjamin Rainer, Stefan Petschornig, Christian Timmerer, and Hermann Hellwagner. Statistically indifferent quality variation: An approach for reducing multimedia distribution cost for adaptive video streaming services. *IEEE Transactions on Multimedia*, 19(4):849–860, 2017.
- [97] William Cooper, Sue Farrell, and Kumar Subramanian. QBR metadata to improve streaming efficiency and quality. In *SMPTE 2017 Annual Technical Conference and Exhibition*. SMPTE, 2017.
- [98] Yanyuan Qin, Chinmaey Shende, Cheonjin Park, Subhabrata Sen, and Bing . Wang. Dataplanner: Data-budget driven approach to resource-efficient abr streaming. In *Proceedings of the 10th ACM Multimedia Systems Conference, MMSys '21*, New York, NY, USA, 2021. Association for Computing Machinery.
- [99] Google. Shaka Player. <https://github.com/google/shaka-player>, 2019.
- [100] Saamer Akhshabi, Lakshmi Anantakrishnan, Ali C Begen, and Constantine Dovrolis. What happens when http adaptive streaming players compete for bandwidth? In *Proceedings of International Workshop on Network and Operating System Support for Digital Audio and Video (NOSSDAV)*, pages 9–14. ACM, 2012.
- [101] Te-Yuan Huang, Nikhil Handigol, Brandon Heller, Nick McKeown, and Ramesh Johari. Confused, timid, and unstable: picking a video streaming rate is hard. In *Proc. of IMC*. ACM, 2012.

- [102] Z. Li, X. Zhu, J. Gahm, R. Pan, H. Hu, A. Begen, and D. Oran. Probe and adapt: Rate adaptation for HTTP video streaming at scale. *IEEE JSAC*, 32(4):719–733, 2014.
- [103] Google. ExoPlayer: Flexible Media Playback for Android (Google I/O ’17). <https://youtu.be/jAZn-J1I8Eg?t=552>, 2017.
- [104] SimilarTech Ltd. Facebook Video vs Shaka Player, 2019.
- [105] YouTube. Recommended upload encoding settings. <https://support.google.com/youtube/answer/1722171?hl=en>, 2019.
- [106] Axiomatic Systems LLC. Bento4 MP4 and DASH Class Library, SDK and Tools, 2016.
- [107] Yanyuan Qin, Shuai Hao, K. R. Pattipati, Feng Qian, Subhabrata Sen, Bing Wang, and Chaoqun Yue. Abr streaming of vbr-encoded videos: Characterization, challenges, and solutions. In *Proc. of ACM CoNEXT*, 2018.
- [108] L. Ren, Y. Qin, B. Wang, P. Zhang, P. B. Luh, and R. Jin. Enabling resilient microgrid through programmable network. *IEEE Transactions on Smart Grid*, 8(6):2826–2836, 2017.
- [109] L. Ren, Y. Qin, B. Wang, P. Zhang, P. B. Luh, S. Han, T. Orekan, and T. Gong. Enabling resilient distributed power sharing in networked microgrids through software defined networking. *Applied Energy*, 210:1251 – 1265, 2018.
- [110] Y. Li, Y. Qin, P. Zhang, and A. Herzberg. Sdn-enabled cyber-physical security in networked microgrids. *IEEE Transactions on Sustainable Energy*, 10(3):1613–1622, 2019.
- [111] L. Wang, Y. Qin, Z. Tang, and P. Zhang. Software-defined microgrid control: The genesis of decoupled cyber-physical microgrids. *IEEE Open Access Journal of Power and Energy*, 7:173–182, 2020.
- [112] J. Wang, Y. Qin, Z. Tang, and P. Zhang. Software-defined cyber-energy secure underwater wireless power transfer. *IEEE Journal of Emerging and Selected Topics in Industrial Electronics*, pages 1–1, 2020.
- [113] W. Wan, M. A. Bragin, B. Yan, Y. Qin, J. Philhower, P. Zhang, and P. B. Luh. Distributed and asynchronous active fault management for networked microgrids. *IEEE Transactions on Power Systems*, 35(5):3857–3868, 2020.
- [114] Peng Zhang, Bing Wang, Peter B Luh, Lingyu Ren, and Yanyuan Qin. Enabling resilient microgrid through ultra-fast programmable network, April 9 2019. US Patent 10,257,100.

- [115] Zefan Tang, Yanyuan Qin, Zimin Jiang, Walter O Krawec, and Peng Zhang. Quantum-secure microgrid. *arXiv preprint arXiv:2001.02301*, 2020.
- [116] G. Wang, Yanyuan Qin, and Chengjuan Chang. Communication with partial noisy feedback. In *2017 IEEE Symposium on Computers and Communications (ISCC)*, pages 602–607, 2017.
- [117] Gang Wang and Yanyuan Qin. Mac protocols for wireless mesh networks with multi-beam antennas: A survey. In *Advances in Information and Communication*, pages 117–142, Cham, 2020. Springer International Publishing.
- [118] Sixia Chen, Alexander Russell, Ruofan Jin, Yanyuan Qin, Bing Wang, and Sudarshan Vasudevan. Asynchronous neighbor discovery on duty-cycled mobile devices: Integer and non-integer schedules. In *Proceedings of the 16th ACM International Symposium on Mobile Ad Hoc Networking and Computing, Mobi-Hoc '15*, page 47–56, New York, NY, USA, 2015. Association for Computing Machinery.
- [119] S. Chen, R. Morillo, Y. Qin, A. Russell, R. Jin, B. Wang, and S. Vasudevan. Asynchronous neighbor discovery on duty-cycled mobile devices: Models and schedules. *IEEE Transactions on Wireless Communications*, 19(8):5204–5217, 2020.
- [120] Zimin Jiang, Zefan Tang, Yanyuan Qin, and Peng Zhang. Programmable adaptive security scanning for networked microgrids. *Engineering*, 2021.
- [121] Zimin Jiang, Zefan Tang, Yanyuan Qin, Chongqing Kang, and Peng Zhang. Quantum internet for resilient electric grids. *International Transactions on Electrical Energy Systems*, page e12911, 2021.